Department of Precision and Microsystems Engineering

Correlation and Error Localization; Analytical versus Experimental Dynamics of a Large Structural Assembly

Herman Marquart

Report no	:	EM 2013.024
Coach	:	dr.ir. D. de Klerk
Professor	:	prof.ir. R.H. Munnig Schmidt
Specialization	:	Engineering Mechanics
Type of report	:	Master Thesis
Date	:	7 August 2013

MASTER THESIS
HERMAN MARQUART

CORRELATION AND ERROR LOCALIZATION

ANALYTICAL VERSUS EXPERIMENTAL DYNAMICS OF A LARGE STRUCTURAL ASSEMBLY

SPECIFICALLY

HIGHLY INCORRECTLY PARAMETERIZED STIFFNESSES

DELFT UNIVERSITY OF TECHNOLOGY
Prof.ir. R.H. MUNNIG SCHMIDT
Dr.ir. D. DE KLERK

ASML
Dr.ir. R. RUIMERMAN

TU Delft

ASML

ACKNOWLEDGEMENT

Above all I would like to thank prof.ir. Robert H. Munnig Schmidt for the opportunity to graduate under his supervision. I would also like to express my gratitude to my supervisors dr.ir. Ronald Ruimerman and dr.ir. Dennis de Klerk for their useful comments, remarks and engagement through the learning process of this master thesis. Furthermore I would like to thank ir. Jacob Jan Velten and ir. Patrick Limpens for introducing me to the topic as well for the support on the way. Finally, I would like to thank my loved ones, who have supported me throughout the entire process. I will be grateful forever for your love.

ABSTRACT

In the high tech industry the performance of a system generally depends heavily on the system's structural dynamic behaviour. Relatively small resonating components can alter the dynamics of the assembly significantly. Due to the presence of many small components and limited test resources it is often difficult to find the disruptor.

In this report a procedure is proposed to trace a relatively small resonating component of a large structural assembly. It is based on correlation of analytical, finite element method (FEM), and experimental modal analysis data, specifically by using objective functions. No additional measurements are required; the entire procedure is performed with FEM calculations.

The proposed localization procedure is applied to different configurations of a specially designed and manufactured structural assembly.

The test results illustrate a successful localization of the resonating component for the investigated configurations. The complexity of the investigated structural assembly could be increased in further researches, since the procedure proved to be robust.

NOCLAMENTURE

$\mathbf{M}$	Mass matrix
$\mathbf{C}$	Damping matrix
$\mathbf{K}$	Stiffness matrix
$\mathbf{q}$	Degrees of freedom
$\mathbf{f}$	Forces
$\mathbf{g}$	Boundary forces
$\boldsymbol{\zeta}$	Intensity parameters
$\boldsymbol{\varphi}$	Modeshape
$\boldsymbol{\Phi}$	Modal matrix
$\boldsymbol{\Lambda}$	Spectral matrix
$\boldsymbol{\Omega}$	Diagonal squared frequency matrix
$\mathbf{H}$	Receptance matrix
$\mathbf{A}$	Accelerance matrix
λ	Eigenvalue
ω	Frequency
$o^{(s)}$	Substructure
$\overline{o}$	Block-diagonal assembled
$\hat{o}$	Reduced
$\tilde{o}$	Analytical
$\underset{\sim}{o}$	Experimental
o^{+}	Pseudo inverse
o^{*}	Complex conjugate
n	# Degrees of freedom
m	# Observed modes

TABLE OF CONTENTS

1 INTRODUCTION

ASML manufactures lithography systems for the semiconductor industry (Figure 1). These are critical to the production of integrated circuits or chips. The machines are expected to meet high requirements of the wafer production, regarding the:

- throughput (speed)
- overlay (accuracy)
- imaging performance (quality)

These requirements force engineers to model the systems accurately and precisely, both analytically and experimentally. These days those high tech developments are realized due to extensive use of virtual prototyping and analysis software.

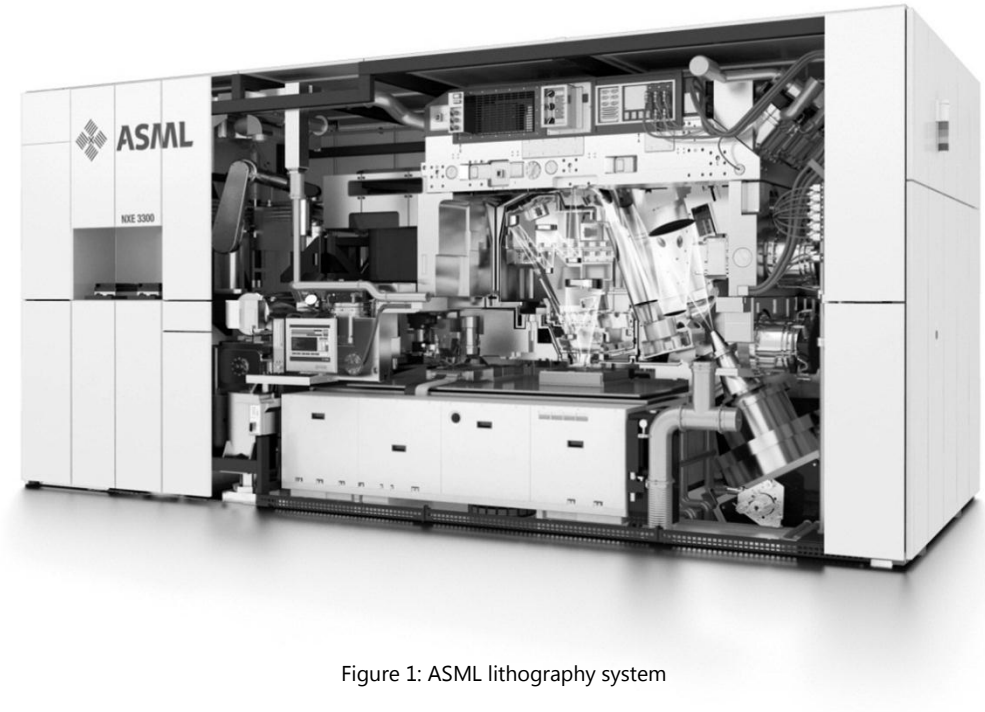

Figure 1: ASML lithography system

1.1 RESEARCH FIELD

In general, unacceptable differences may be found between model predictions and measurements. They could be the result of one or multiple causes. The challenge is to find these causes to get a better understanding of the system's behaviour.

In this study contemporary challenges of the field of structural dynamics are discussed, specifically for large assembled systems; systems composed of many components. This is a comprehensive and complex engineering field, when high precision and accuracy of the analyses are demanded. Especially in this field engineers continuously thrive for the right balance between minimization of modelling and solution time, versus maximization of precision and accuracy of analysis results.

Due to the continuous demand for improved machine performance and the increasing possibilities for virtual prototyping, in recent years engineers have been building more and more detailed and comprehensive structural dynamic models. These days, in many high tech industries, like the lithography machine industry, assemblies are constructed from a dozen to hundreds of components. In addition, many levels of assembly may be present. In this study, for relative simplicity, the building blocks of a structural assembly are limited to one assembly level, thus a:

- Master structure
- Slave structure(s)

Two reasons: firstly in many applications only degrees of freedom of the master structure are measured during the execution of an experimental modal analysis. Secondly, it limits the complexity of the investigated assembly since connections are in general difficult to model, let alone a chain of connections. [1]

1.2 RESEARCH OUTLINE

It is assumed that the reader has a basic education in structural dynamics. He knows how the equations of motion are set up and solved, and he is able to explain the experimental modal analysis approach in a few lines. For recapitulation of the theoretical basics I would recommend to have a look at literature from D.J. Ewins [2] and at the well condensed reports of Brüel and Kjær [3], [4].

This study presents a literature review on structural assembly dynamics for large systems together with the applicable post analysis techniques. Unanswered questions and shortcomings in current literature lead finally to the problem formulation. The review is presented in section 2.

The research question will be approached in the methodology, section 3. Here is tried to stay as close as possible to existing techniques to make the implementation of the proposed procedure accessible. After an extensive simulation, the procedure is eventually applied to a real structure, assembled in two different configurations. The results of the latter are subsequently presented and discussed.

The last section will include the discussion of the complete research (section 4). It will highlight the advantages and drawbacks of the proposed procedure, concluded by recommendations for further researches.

The literature review will discuss the following topics:

- Model domains
- Analytical model
  - Full model
  - Substructures
  - Reduced substructures
  - Assembly of reduced substructures
- Experimental model
- Post analysis
- Discussion

For each model type the most important steps are described, supplemented with the associated mathematical equations. The current status of the model will be illustrated with a representative example figure. The concept behind substructuring and reduction techniques will be introduced to allow:

- Concurrent engineering
- Relatively simple and efficient application of local modifications
- Possibility to transfer condensed data

The experimental analysis will cover the general single input single output (SISO) roving hammer method. All the signal analysis steps are not explained in detail; instead they are summarized into an overview, since the methodology is of primary importance. For detailed formulas see the well condensed presentations of Brüel and Kjær [3], [4].

The post analysis, or also frequently referred to as the validation process, assembles the results of both modelling approaches in a subjective as well as a mathematical way. The following steps are generally less known and will therefore receive relatively much attention in this study: [2]

- Comparison
- Correlation
- Verification
- Reconciliation
- Localization
- Correction

In the last subsection of the literature review, both modelling approaches and the post analysis steps are reflected in the way of working at the high tech industries. Typical properties, assumptions and simplifications of structural dynamic assemblies are highlighted; modelling errors occur on finite element, component and/or assembly level. The application of the available techniques is namely far from trivial. Ewins and Imregun have shown that the solution of one problem could lead to significantly different results when performed by independent engineers [5]. The discussion will eventually result in the formulation of the research question.

1.2.1 RESEARCH QUESTION

Further investigation is necessary despite all the methods that already exist to control the structural dynamic modelling process, as unfortunately these will never cover all possible mistakes; they only help to minimize previously investigated error types. Therefore the literature discussion leads to the following research question.

What is the influence of a relatively lightweight resonating slave structure on the global structural dynamic behaviour of the master structure? How could you find the location of an unmeasured resonating slave structure with existing correlation tools and validation procedures, when multiple components are suspicious?

Until now, no standard procedures exist for solving such a problem, opening up a new research direction with opportunities for innovation.

1.2.2 RESEARCH TYPE

This research could be categorized as an applied research which is investigated by using existing analytical theories and tools. A conceptual approach will be set up with these tools to solve the research problem with a quantitative or mathematically robust process and as less as possible subjective interventions of the engineer. The intention is to validate the conceptual method with an illustrative simplified example structure and an experiment. The type of research conducted could be summarized by the following properties:

- Applied
- Analytical
- Conceptual
- Quantitative
- Experimental

The methodology will cover the design of the simplified structure used, the development of the analytical and experimental model and the elaboration on the post analysis procedure to locate the resonating mass. It will be concluded with a discussion of the research results and an overall discussion of the research content. Finally recommendations for further improvement of the proposed procedure and for follow up researches are given.

2 LITERATURE REVIEW: THEORY OF STRUCTURAL DYNAMICS

The field of structural dynamics could be divided into analytical and experimental structural dynamics. For many applications both approaches are used. Engineers build analytical models with aiming to understand the system. Therewith they can execute an efficient, economical and targeted search to system improvements. Eventually, the precision and accuracy of an analytical model could be determined through correlation with an experimentally built model.

The theory behind engineering analytical and experimental structural dynamics models, specifically for large assembled structures, will be explained in this section, 2.2 and 2.3. As an introduction to both approaches, the different model domains and their interrelations are explained first in section 2.1, since both modelling approaches result into a structural dynamics model built in a different domain.

Section 2.4 will highlight the post-analysis tools that engineers have at their disposal to determine the accuracy of the performed analyses. At first, attention will be paid to making both models compatible. This means that the modal results from both models have to be expressed in similar degrees of freedom. Hereafter the post-analysis will continue by introducing the general procedure of model validation and subsequently discuss the applicable correlation tools.

The theoretical methods of section 2.1 to 2.4 will be criticized in section 2.5 by practical limits encountered in the industry. Also additional practical restraints, assumptions and complexities are mentioned in the discussion. Finally several topics are listed for which little attention is paid in literature yet. According to these topics a composite formulation will be taken as research question.

2.1 MODEL DOMAINS

The dynamic behaviour of a structure could be mathematically described in three different types of domains: the spatial domain, the response domain or the modal domain. The models can be transformed into an equivalent model of a different domain, either by a calculation or approximation. The latter is often called the identification of system parameters.

2.1.1 SPATIAL DOMAIN

The analytical modelling approach in structural dynamics starts with engineering the equations of motion. Nowadays this is often done by using the finite element method (FEM). In short, this procedure could be described as: a subdivision of a structure into a finite number of spatially distributed elements of simple geometry with well-identified structural behaviour. The resulting mathematical model is therefore said to be in the spatial domain. The general equations of motion in matrix notation are often assumed to be:

$$\mathbf{M}\ddot{\mathbf{q}} + \mathbf{C}\dot{\mathbf{q}} + \mathbf{K}\mathbf{q} = \mathbf{f} \tag{1}$$

M	Mass matrix
C	Damping matrix
K	Stiffness matrix
q	Degrees of freedom
f	Forces

2.1.2 RESPONSE DOMAIN

The experimental modelling approach in structural dynamics starts with performing dynamic input (force) and output (acceleration) measurements to eventually obtain frequency response functions. The resulting model, typically represented by a frequency response function (FRF) matrix, is therefore said to be in the response domain. In many measurement setups, the forces are either applied through a hammer, a shaker or operational forces. Load cells and accelerometers are commonly used sensors for measuring forces and accelerations respectively. The frequency response function matrix (accelerance matrix) is defined as:

$$A_{ij}(\omega) = \frac{\ddot{q}_i(\omega)}{f_j(\omega)} = -\omega^2 \frac{q_i(\omega)}{f_j(\omega)} = -\omega^2 H_{ij}(\omega) \tag{2}$$

A	Accelerance matrix
H	Receptance matrix
q	Degrees of freedom
f	Forces
ω	Frequency

2.1.3 MODAL DOMAIN

A modal model is obtained by either the calculation of the eigensolutions of a spatial model or by the approximate identification of the modal parameters from a response model. The latter is done by applying a curve fitting method on the measured frequency response functions. The modal domain is often presented with mode shape figures and a list of corresponding eigenfrequencies. The modal and spectral matrix are defined for $r = 1,\ldots,m$ observed mass normalized modes as

$$\boldsymbol{\Phi} = \left[\boldsymbol{\varphi}_1 \,,\ldots,\, \boldsymbol{\varphi}_m\right] \tag{3}$$

$$\boldsymbol{\Lambda} = diag\left(\lambda_1 \,,\ldots,\, \lambda_m\right) \tag{4}$$

$$\lambda_r = \omega_r^2 \tag{5}$$

$\boldsymbol{\varphi}_r$	Mode shape
$\boldsymbol{\Phi}$	Modal matrix
$\boldsymbol{\Lambda}$	Spectral matrix
λ_r	Eigenvalue
ω_r	Eigenfrequency

2.1.4 RELATION BETWEEN DOMAINS

The necessary calculations or approximations to transform a model from one domain into another are illustrated in Figure 2 for both approaches, analytically and experimentally [6]. Note that these transformations are significantly simplified, thus mostly the real transformations are more complex than represented here. More details about these relations will be presented in the next two consecutive sections.

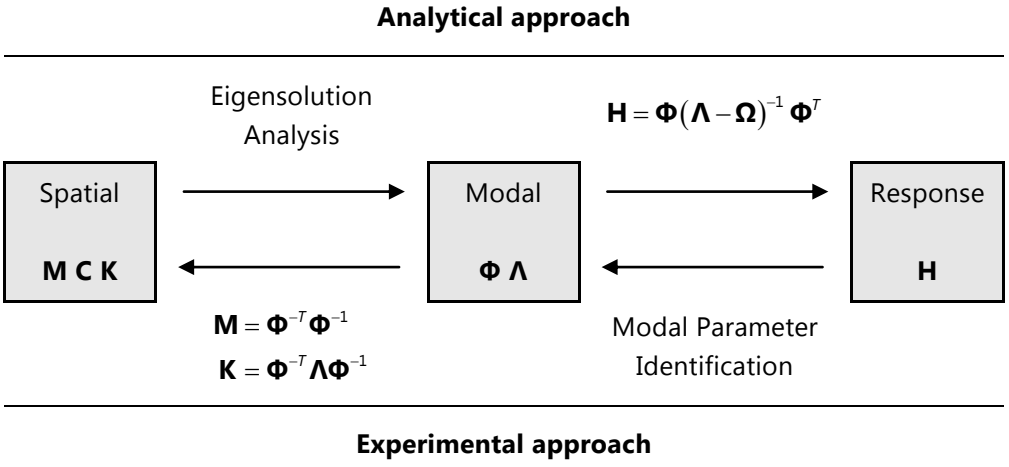

Figure 2: Relation between model domains;
Here the matrix $\boldsymbol{\Omega}$ is defined as a diagonal squared frequency matrix.

2.1.4.1 ANALYTICAL APPROACH

Here the relations of an analytical spatial model with its equivalent models from the other two domains are illustrated in more detail. The explanation of the methodology is the primary focus of this section. Hence, the general equations of motions are:

$$\mathbf{M}\ddot{\mathbf{q}} + \mathbf{C}\dot{\mathbf{q}} + \mathbf{K}\mathbf{q} = \mathbf{f} \tag{6}$$

These equations can be simplified towards undamped free vibration equations of motion by neglecting structural damping and applying no forces. (Solutions of forced and/or damped systems will not be discussed in this report.)

$$\mathbf{M}\ddot{\mathbf{q}} + \mathbf{K}\mathbf{q} = \mathbf{0} \tag{7}$$

The solution on this system of equations is assumed to be a synchronous free vibration motion with a harmonic time history with the amplitude $\boldsymbol{\varphi}$ being the time independent shape of the motion.

$$\mathbf{q} = \boldsymbol{\varphi}\left[\alpha\cos(\omega t) + \beta\sin(\omega t)\right] \tag{8}$$

After differentiating this equation twice with respect to time and substituting these results into the equations of motion of the free undamped system, you end up with n characteristic equations. Because in many applications engineers are only interested in the modes of a predefined frequency bandwidth, often not all but only m modes are of interest. This reduction of required solutions also shortens the computation time significantly for large models. Engineers should always be aware when using reduced or truncated models. The results are only valid for a certain frequency bandwidth. The characteristic equation to be solved for observed mode $r = 1,\ldots,m$ is defined as:

$$(\mathbf{K} - \lambda_r\mathbf{M})\boldsymbol{\varphi}_r = \mathbf{0} \tag{9}$$

By solving this equation the eigenfrequency λ_r and mode shape $\boldsymbol{\varphi}_r$ are obtained. Iterative solvers like the Block Lanczos method were developed for this purpose. By assembling these results into two matrices, the mass normalized modal model with its modal and spectral matrix are defined as:

$$\boldsymbol{\Phi} = \left[\boldsymbol{\varphi}_1\ ,\ldots,\ \boldsymbol{\varphi}_m\right] \tag{10}$$

$$\boldsymbol{\Lambda} = diag\left(\lambda_1\ ,\ldots,\ \lambda_m\right) \tag{11}$$

Mass normalized modes are scaled such that:

$$\boldsymbol{\Phi}^T\mathbf{M}\boldsymbol{\Phi} = \mathbf{I} \tag{12}$$

$$\boldsymbol{\Phi}^T\mathbf{K}\boldsymbol{\Phi} = \boldsymbol{\Lambda} \tag{13}$$

The eigenvalues λ_r are related to the eigenfrequencies ω_r using the formula:

$$\lambda_r = \omega_r^2 \tag{14}$$

To describe the structure in the response domain, the frequency response function matrix (here defined as the receptance matrix) has to be calculated. This could either be done directly from the spatial domain or from the modal domain. Both calculations are illustrated here, together with the individual frequency response functions for the degrees of freedom *i* and *j*.

$$\mathbf{H}(\omega) = \left(\mathbf{K} - \omega^2\mathbf{M}\right)^{-1} = \mathbf{\Phi}\left[(\mathbf{\Lambda} - \mathbf{\Omega})\right]^{-1}\mathbf{\Phi}^T \tag{15}$$

$$\mathbf{\Omega} = diag\left(\omega^2\right) \tag{16}$$

$$H_{ij}(\omega) = \sum_{r=1}^{n} \frac{\varphi_{ir}\varphi_{jr}}{\omega_r^2 - \omega^2} \tag{17}$$

2.1.4.2 EXPERIMENTAL APPROACH

This section will explain the experimental approach towards structural dynamics in more detail. The explanation is focussed on the single-input-single-output (SISO) roving hammer method, as this method is a widely used approach by engineers. First the methodology is described, followed through a short and general introduction of all the equipment and the test setup used. The section will be concluded by summing up the advantages and disadvantages of the experimental approach, specifically for this method. The end result will be a description in physical degrees of freedom in the response domain.

Firstly, both a driving point measurement and all the corresponding transfer measurements have to be performed in order to be able to build an experimental response model. The filtered signals are measured by a high sampling frequency to minimize aliasing effects and obtain a fine resolution of the time data respectively. The time block (duration of each individual measurement) determines eventually the frequency resolution of the measurement.

Secondly, an exponential window and the average of multiple measurements are used to prepare the acceleration data for the transformation to the frequency domain. The same has been done with a transient window for the measured force. Windowing prevents truncation of the time data because the latter leads to more leakage; an unwanted effect that smears out the resonance frequency over a range of frequencies. The transformation to the frequency domain is done by applying the so-called discrete Fast Fourier Transformation (FFT) on each signal. [4]

The coherence function provides us with a means of assessing the degree of linearity between the input and output signals. A good coherence of the repeated measurements is required for accurate results. It is based on the cross and auto spectral density of both signals as in:

$$\gamma(\omega)^2 \equiv \frac{\left|G_{f\ddot{q}}(\omega)\right|^2}{G_{\ddot{q}\ddot{q}}(\omega)\cdot G_{ff}(\omega)} \tag{18}$$

The cross and auto spectral density function are defined as: [3]

$$G_{f\ddot{q}}(\omega) = \sum f^*(\omega)\cdot q(\omega) \tag{19}$$

$$G_{ff}(\omega) = \sum f^*(\omega)\cdot f(\omega) \tag{20}$$

The coherence function value is bounded from:

$$0 \leq \gamma(\omega)^2 \leq 1 \tag{21}$$

The bounds for the coherence function are: 'one' for no noise and 'zero' for pure noise in the measurements. For each frequency ω it shows the degree of linear relationship between the measured input signals and output signals.

Theoretically, the accelerance matrix could be determined by:

$$A_{ij}(\omega) = \frac{\ddot{q}_i(\omega)}{f_j(\omega)} \tag{22}$$

However to reduce the noise on the output, the following estimator is used:

$$A_{ij}(\omega) \equiv \frac{G_{f_j \ddot{q}_i}(\omega)}{G_{f_j f_j}(\omega)} \tag{23}$$

The measured responses in the following accelerance matrix of a typical SISO roving hammer procedure are highlighted in black. Here the accelerometer is mounted at location number two. On paper all the grey parameters can be calculated after the experiment due to the consistency properties of the matrix. Unfortunately, the evaluation of unmeasured FRFs based on a single column (or row) of the FRF matrix is not as straightforward as it seems. It is inaccurate due to the incompleteness of the model in terms of frequency range. [6]

$$\begin{bmatrix} \ddot{\underset{\sim}{q}}_1 \\ \ddot{\underset{\sim}{q}}_2 \\ \vdots \\ \ddot{\underset{\sim}{q}}_n \end{bmatrix} = \begin{bmatrix} \underset{\sim}{A}_{11} & \underset{\sim}{A}_{12} & \cdots & \underset{\sim}{A}_{1n} \\ \underset{\sim}{A}_{21} & \underset{\sim}{A}_{22} & \cdots & \underset{\sim}{A}_{2n} \\ \vdots & \vdots & \ddots & \vdots \\ \underset{\sim}{A}_{n1} & \underset{\sim}{A}_{n2} & \cdots & \underset{\sim}{A}_{nn} \end{bmatrix} \begin{bmatrix} \underset{\sim}{f}_1 \\ \underset{\sim}{f}_2 \\ \vdots \\ \underset{\sim}{f}_n \end{bmatrix} \tag{24}$$

Fortunately, the measurement of only one row or column is enough to transform the experimental response model to a modal model. The modes and frequencies are obtained by using a mode shape fitting procedure. This procedure fits a resonance peak of a single (or multiple) mass spring system(s) onto one (or multiple) resonance peak(s) of the measured responses. The results of the mode shape fitting process could be assembled in a similar way as the analytical results. Here, the experimental modal and spectral matrix is illustrated:

$$\underset{\sim}{\boldsymbol{\Phi}} = \left[\underset{\sim}{\boldsymbol{\varphi}}_1 , \ldots , \underset{\sim}{\boldsymbol{\varphi}}_m \right] \tag{25}$$

$$\underset{\sim}{\boldsymbol{\Lambda}} = diag\left(\underset{\sim}{\lambda}_1 , \ldots , \underset{\sim}{\lambda}_m \right) \tag{26}$$

Due to often spatial and model incompleteness of the experimental model, the transformation towards a spatial model is hardly ever done and so not further explained here.

2.1.4.2.1 EQUIPEMENT

Here, the equipment used for a roving hammer procedure is listed:

- Hammer + tip (hard or soft)
- Accelerometers (unidirectional or tri-directional)
- Amplifiers
- Data acquisition module
- USB connection to computer
- Software package like ME'scopeVES

2.1.4.2.2 SETUP

Here, the setup used for a roving hammer procedure is listed:

- Free-free simulation
- Support modelled as foam or springs
- Sensor location
- Measurement location(s)
- Typical photo, see Figure 3

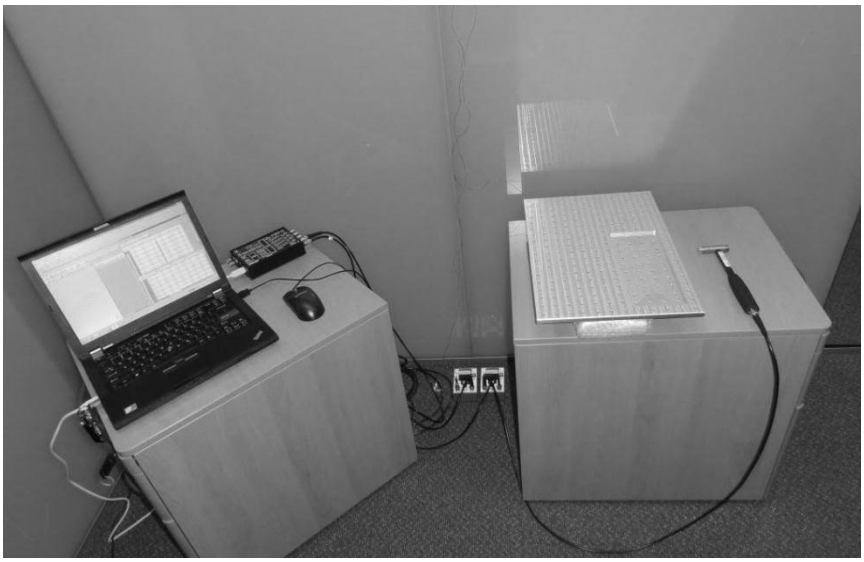

Figure 3: Experimental setup; structure, suspension (bubble foil), hammer, amplifiers, acquisition module and computer are visible. The accelerometer is not visible, since it is mounted at the bottom of the plate.

2.1.4.3 ADVANTAGES

Here, the advantages of the roving hammer method are listed: (i.a. from [7], [8])

- No elaborate fixtures are required
- Speed, only a few averages are needed
- Portable and very suitable for measurements in the field
- Relatively inexpensive
- There is no variable mass loading of the structure. This is of particular advantage with light structures, since changing the mass loading from point to point can cause shifts in modal frequencies from one measurement to another

2.1.4.3.1 DISADVANTAGES

Here, the disadvantages of the roving hammer method are listed: (i.a. from [4], [7], [8], [9])

- Possible occurrence of double impacts, especially with a hard hammer tip
- High potential for signal overload and underload of analogue to digital converter, therefore also not suitable for linear approximation of nonlinear systems
- Excitation location varies with each excitation
- The spectrum can only be controlled at the upper frequency limit by choosing a different hammer tip, which means that the technique is not suitable for a zoom analysis.
- The high crest factor makes the technique unsuitable for testing systems with non-linear properties, since the non-linear behaviour will be provoked by high peak forces
- Very high peak forces might be required for sufficient energy supply, and the structure may become damaged locally
- Due to the deterministic nature of the signal, the coherence function cannot show either leakage or non-linear behaviour

2.2 ANALYTICAL MODEL

The purpose of building an analytical model is to describe, but above all, to understand the physics of a system's behaviour. In structural dynamics this model is often built with the help of the finite element method (FEM). This method helps engineers to discretize a system into many easy to solve structures. Specialized software, like ANSYS, is developed to apply this method. Although the program is relatively accessible, insufficient models can be made with it as well. Therefore here follows a list of issues requiring serious attention when interpreting the solutions of the models:

- Geometry
- Material
- Discretization (mesh)
- Boundary conditions
- Loads
- Algorithm

All these elements introduce errors in the mass matrix, damping matrix and stiffness matrix. The magnitude of error of each issue could be minimized by the engineer, but never prevented. Simplifications and assumptions are done when the engineer assumes that their influence on the results is neglectable. Over simplification causes invalid model behaviour thus wrong conclusions could be formulated. However, engineers will sometimes take the risk because it is economically efficient when the simplification is allowable.

By creating a measurement report, the geometry of a model could be controlled relatively easily, in comparison with all the other issues. Besides that, the influence of the geometry deviations on the system's dynamic behaviour is often well interpretable and it is neglectable in many situations.

On the other hand, parameter values and their uniformity over the material from which the geometry is made are not always so simple to control and thus often stay an assumption. The values are mostly averages of many tests, acquired via material suppliers and frequently assumed to be constant when the system's performance is simulated. Fortunately, for some materials the property deviations are small and therefore often neglectable.

Discretization errors could be minimized by using a converged mesh. However this is not always done because engineers use rules of thumb for the mesh size, in order to save time. These rules are mostly based on experience of many similar systems. Though, the effect of not converged meshes could be significant.

The larger the system, the more issues it may contain, especially when it is an assembly. This increases the chance for modelling errors. When building a model for such a system, another issue is emerging. The computation time of the results of the model becomes significant. This invites to reduce and simplify the model even more; again increasing the chance for modelling errors.

2.2.1 APPROACH FOR LARGE ASSEMBLED STRUCTURES

The size of an analytical structural dynamics model increases when the complexity of the system increases. For example, typical features of large and complex structures are: many sides, interfaces, holes, pockets, thin walls and mounting positions. At such locations, the mesh has to be refined in order to describe the dynamic behaviour with an acceptable accuracy. A refined mesh means more degrees of freedom and thus a larger model.

In contrast to finite element models, experimentally derived models hardly increase in size, maybe just a few additional measuring points. The observed number of modes depends on the interesting frequency bandwidth. As long as the additional modes of the assembly are outside the interesting frequency range, due to increasing complexity, there is no need to increase the number of measurement degrees of freedom.

In this study, the typical analysis for a large assembled structure is of interest; a system assembled of many components. As mentioned, the finite element method will be applied to such a large assembled structure. This full structure FEM model, obtained by means of a converged mesh, is taken as a reference for all consecutive models.

The latter are obtained by using a substructuring and reduction technique. [10] These techniques make the model more flexible and also solvable in a significantly less time; [11] very comfortable for assembly design iterations, model updating and multiple load cases. The combination of these techniques is already applied in the high tech industry nowadays, to reduce development time and support concurrent engineering. Hence the discussed model types are:

- Full structure
- Substructures
- Reduced substructures
- Assembly of reduced substructures

Additional simplifications and assumptions made in the industry have been discussed in section 2.5 to show their contribution to the process. Therefore what will be explained next is the theoretical background on modelling structural assemblies. How these assemblies could be prepared for validation purposes and which post analysis tools are applicable, is explained in section 2.4. As a guiding example for this section, the following geometry is taken, illustrated in Figure 4.

Figure 4: Solid structure

2.2.2 FULL STRUCTURE

The equation of motion of a system, designed as one structure, hence one solid geometry, could be described in matrix notation as:

$$\mathbf{M}\ddot{\mathbf{q}} + \mathbf{C}\dot{\mathbf{q}} + \mathbf{K}\mathbf{q} = \mathbf{f} \tag{27}$$

$$\mathbf{M}, \mathbf{C}, \mathbf{K} \in \mathbb{R}^{n \times n}$$
$$\mathbf{q}, \mathbf{f} \in \mathbb{R}^{n}$$

For a large structure the number of degrees of freedom (DOF) n could be of the order of millions degrees of freedom. In Figure 5 the full model of the example geometry is illustrated. Many nodes and many elements are visible.

The model is assumed to be too large and inflexible to solve and manage respectively. The latter problem could be solved by dividing the structure into several smaller structures; a technique called substructuring. This is explained in the next section. The problem concerning the size of the system could be tackled by reducing the number of degrees of freedom of the substructures. This technique is often used in situations where multiple calculations have to be done with the same model. More about this reduction technique follows after the substructuring technique.

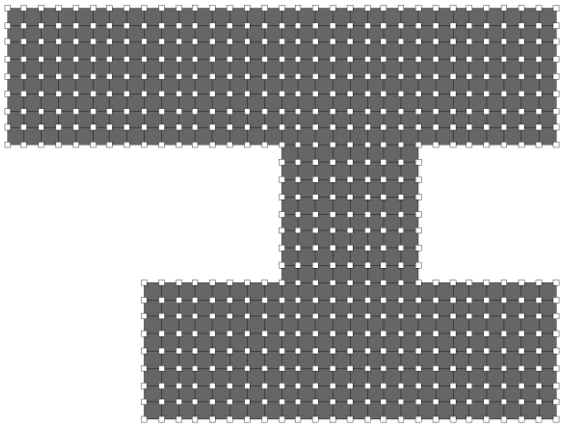

Figure 5: FEM model of example structure

2.2.3 SUBSTRUCTURES

The system could be divided into several components. This means that the full structure could be divided into N_s substructures. The equations of motion of a substructure s is:

$$\mathbf{M}^{(s)}\ddot{\mathbf{q}}^{(s)} + \mathbf{C}^{(s)}\dot{\mathbf{q}}^{(s)} + \mathbf{K}^{(s)}\mathbf{q}^{(s)} = \mathbf{f}^{(s)} + \mathbf{g}^{(s)} \tag{28}$$

$$\mathbf{q}^{(s)} = \left[\mathbf{q}_b^{(s)T} \ \mathbf{q}_i^{(s)T} \right]^T \tag{29}$$

$$\mathbf{M}^{(s)}, \mathbf{C}^{(s)}, \mathbf{K}^{(s)} \in \mathbb{R}^{n^{(s)} \times n^{(s)}}$$
$$\mathbf{q}^{(s)}, \mathbf{f}^{(s)}, \mathbf{g}^{(s)} \in \mathbb{R}^{n^{(s)}}$$

These equations have introduced a new categorization of forces and degrees of freedom, namely:

g	Boundary forces
b	Boundary DOF
i	Internal DOF

Here, the total number of degrees of freedom has become larger, since the number of boundary degrees of freedom has doubled. (The boundary degrees of freedom are the ones on the cut interfaces of the substructures.)

Figure 6 illustrates the status of the example geometry after applying the substructuring technique. To set an example: the structure is divided into two substructures. Here, the top one is called the master structure; the lower one is called the slave structure.

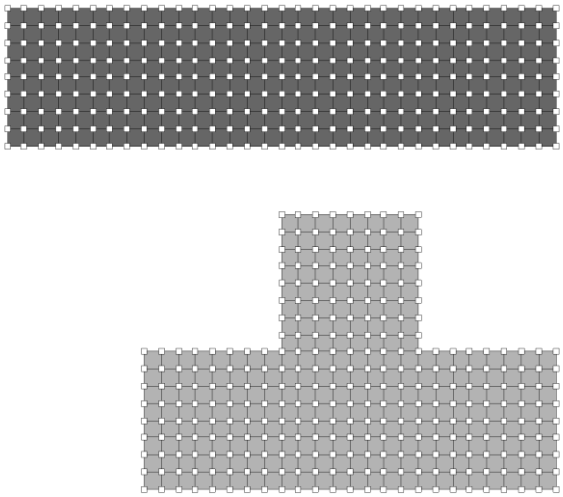

Figure 6: Substructured FEM model of example structure

Advantages of the substructuring technique are listed below: (i.a. from [1], [31])

- Allows parallel engineering to increase development speed
- Natural approach if model already decomposed
- Allows evaluating dynamic behaviour of structures that are too large or complex to be analysed as a whole
- By analysing substructures local dynamic behaviour can be recognized more easily than when the entire structure is analysed
- Gives the possibility of combining analytical and experimental models in an assembly
- During model updating, the technique enables the possibility of correcting the model parameters of an assembly locally
- Allows combining analytical and experimental substructures

2.2.3.1 BLOCK-DIAGONAL ASSEMBLED SUBSTRUCTURES

As already mentioned, the total number of degrees of freedom of the structure $\bar{n}$ has become larger and could be determined with a summation over all the substructures, mathematically:

$$\bar{n} = \sum_{s=1}^{N_s} n^{(s)} \tag{30}$$

Since, in this case, the concern is with the full system: the substructures need to be assembled to get the full structure back. First this is done block-diagonally. Then the double degrees of freedom, recalling the ones on boundary of the substructures, are constrained with a displacement and force equilibrium. The resulting equations are:

$$\bar{\mathbf{M}}\ddot{\bar{\mathbf{q}}} + \bar{\mathbf{C}}\dot{\bar{\mathbf{q}}} + \bar{\mathbf{K}}\bar{\mathbf{q}} = \bar{\mathbf{f}} + \bar{\mathbf{g}} \tag{31}$$

$$\mathbf{B}\bar{\mathbf{q}} = \mathbf{0} \tag{32}$$

$$\mathbf{L}^T\bar{\mathbf{g}} = \mathbf{0} \tag{33}$$

$\mathbf{B} \in \mathbb{R}^{n_b \times \bar{n}}$ Signed Boolean matrix

$\mathbf{L} \in \mathbb{R}^{\bar{n} \times n}$ Localization matrix

On the one hand, equation 27 is nothing more than the definition of displacement equality at each interface degree of freedom, written in matrix form. This results in a signed Boolean matrix.

Equation 28, on the other hand is nothing else than the definition of the force equilibrium at each interface degree of freedom, written in matrix form. The resulting localization matrix is therefore a Boolean matrix. Here, the details about establishing the Boolean and the Localization matrix of the constraint equations are not explained [10]; this is too detailed for the discussion. For more details about these matrices, I refer to appendix 5.1. Hence, the newly introduced matrices of the equation of motion are block-diagonally assembled as:

$$\bar{\mathbf{M}} = diag\left(\mathbf{M}^{(1)}, \ldots, \mathbf{M}^{(N_s)}\right) \in \mathbb{R}^{\bar{n} \times \bar{n}} \tag{34}$$

$$\bar{\mathbf{C}} = diag\left(\mathbf{C}^{(1)}, \ldots, \mathbf{C}^{(N_s)}\right) \in \mathbb{R}^{\bar{n} \times \bar{n}} \tag{35}$$

$$\bar{\mathbf{K}} = diag\left(\mathbf{K}^{(1)}, \ldots, \mathbf{K}^{(N_s)}\right) \in \mathbb{R}^{\bar{n} \times \bar{n}} \tag{36}$$

$$\bar{\mathbf{q}} = \left[\mathbf{q}^{(1)T} \ \ldots \ \mathbf{q}^{(N_s)T}\right]^T \in \mathbb{R}^{\bar{n}} \tag{37}$$

$$\bar{\mathbf{f}} = \left[\mathbf{f}^{(1)T} \ \ldots \ \mathbf{f}^{(N_s)T}\right]^T \in \mathbb{R}^{\bar{n}} \tag{38}$$

$$\bar{\mathbf{q}} = \left[\mathbf{g}^{(1)T} \ \ldots \ \mathbf{g}^{(N_s)T}\right]^T \in \mathbb{R}^{\bar{n}} \tag{39}$$

The status of the block-diagonally assembled example structure is illustrated in Figure 7. The black nodes are indicating the locations of the double nodes.

Still this stage is not yet similar to the full structure as before. In order to re-establish the full structure back, the constraints have to be substituted into the block-diagonal equations of motion. This is called the primal assembled formulation of substructures [1]; the classical finite element method assembly procedure.

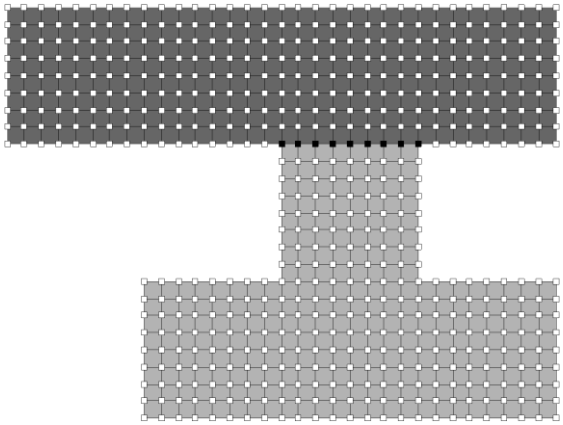

Figure 7: Block-diagonally assembled FEM model of example structure

2.2.3.2 PRIMAL ASSEMBLED SUBSTRUCTURES

The equations of motion of the primal assembled substructures are similar to the reference finite element model (Eq. (27)), hence:

$$\mathbf{M}\ddot{\mathbf{q}} + \mathbf{C}\dot{\mathbf{q}} + \mathbf{K}\mathbf{q} = \mathbf{f} \tag{40}$$

However, here these matrices have their origin in the previously defined substructures. They are transformed with the following operations:

$$\mathbf{M} = \mathbf{L}^T\bar{\mathbf{M}}\mathbf{L} \tag{41}$$
$$\mathbf{C} = \mathbf{L}^T\bar{\mathbf{C}}\mathbf{L} \tag{42}$$
$$\mathbf{K} = \mathbf{L}^T\bar{\mathbf{K}}\mathbf{L} \tag{43}$$
$$\mathbf{f} = \mathbf{L}^T\bar{\mathbf{f}} \tag{44}$$

The number of degrees of freedom of this structure is equal to *n* again. The status of the structure could now be visualized as illustrated in Figure 8.

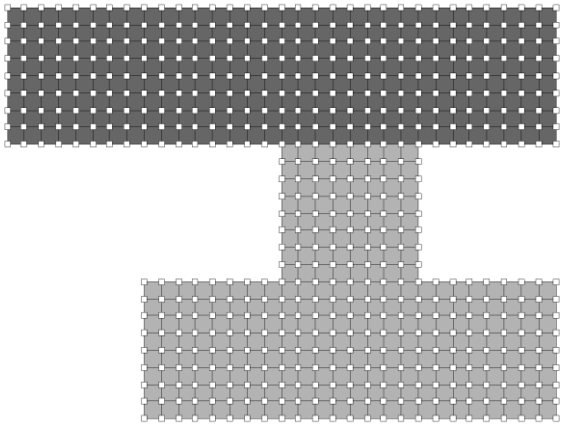

Figure 8: Primal assembled FEM model of example structure

So far, the sole use of substructuring has been explained and it seems to be a useful technique looking at the advantages. However, it becomes an even more powerful technique when it comes with a reduction technique. This combination is explained in the following section.

2.2.4 REDUCED SUBSTRUCTURES

The substructuring technique has solved the two issues partially: calculation time and manageability of the model. Together with a reduction technique, both issues could be solved almost completely. However, a sacrifice has to be made, namely: the reduced and substructured FEM model will be an approximation of the full FEM (in dynamics perspective). But in the end, when the techniques are properly used (the reduced substructures are sufficiently truncated; enough fixed interface modes are included [5]), it is possible to identify good approximations of the exact modes. The reduced equations of motion for a substructure could be written in matrix notation as:

$$\hat{\mathbf{M}}^{(s)}\ddot{\hat{\mathbf{q}}}^{(s)} + \hat{\mathbf{C}}^{(s)}\dot{\hat{\mathbf{q}}}^{(s)} + \hat{\mathbf{K}}^{(s)}\hat{\mathbf{q}}^{(s)} = \hat{\mathbf{f}}^{(s)} + \hat{\mathbf{g}}^{(s)} \tag{45}$$

$$\mathbf{q}^{(s)} \simeq \mathbf{R}^{(s)}\hat{\mathbf{q}}^{(s)} = \mathbf{R}^{(s)}\left[\mathbf{q}_r^{(s)T}\ \boldsymbol{\zeta}_m^{(s)T}\right]^T \tag{46}$$

$\mathbf{R}$	Reduction matrix
$\mathbf{q}_r$	Retained DOFs
$\boldsymbol{\zeta}$	Intensity parameters

The retained physical degrees of freedom (boundary and arbitrarily selected internal DOFs) are supplemented by generalized modal degrees of freedom. The latter are also called intensity parameters of the substructure internal vibration modes. The introduced reduced matrices can be formed through multiplication with the reduction matrix of the substructure, hence:

$$\hat{\mathbf{M}}^{(s)} = \mathbf{R}^{(s)T}\mathbf{M}^{(s)}\mathbf{R}^{(s)} \in \mathbb{R}^{\hat{n}^{(s)}\times\hat{n}^{(s)}} \tag{47}$$

$$\hat{\mathbf{C}}^{(s)} = \mathbf{R}^{(s)T}\mathbf{C}^{(s)}\mathbf{R}^{(s)} \in \mathbb{R}^{\hat{n}^{(s)}\times\hat{n}^{(s)}} \tag{48}$$

$$\hat{\mathbf{K}}^{(s)} = \mathbf{R}^{(s)T}\mathbf{K}^{(s)}\mathbf{R}^{(s)} \in \mathbb{R}^{\hat{n}^{(s)}\times\hat{n}^{(s)}} \tag{49}$$

$$\hat{\mathbf{f}}^{(s)} = \mathbf{R}^{(s)T}\mathbf{f}^{(s)} \in \mathbb{R}^{\hat{n}^{(s)}} \tag{50}$$

$$\hat{\mathbf{g}}^{(s)} = \mathbf{R}^{(s)T}\mathbf{g}^{(s)} \in \mathbb{R}^{\hat{n}^{(s)}} \tag{51}$$

The reduction matrix of the substructure could be created by applying a Craig-Bampton component mode synthesis on the substructure. This is one of the most used reduction techniques in structural dynamics. In the next subsection, a short summary of the synthesis is given. For a more detailed explanation of this method, please have a look at the specific literature. [12] Figure 9 illustrates the typical status of the system after using both substructuring and reduction.

Figure 9: Reduced substructured FEM model of example structure

Advantages of the reduction technique are listed below: (i.a. from [10])

- Speeds up computation of eigensolutions significantly. Specifically profitable when multiple eigensolution computations are required, like in model updating algorithms or when many load cases have to be analysed
- Smaller models are faster and easier exchanged between engineers
- Easy reuse of components
- Hides the details of a component (confidentiality)

2.2.4.1 CRAIG-BAMPTON COMPONENT MODE SYNTHESIS

Although originally developed as a component mode synthesis method, the method can be considered to be a general model reduction method. Here two different sets of degrees of freedom are introduced; retained *r* and condensed *c* degrees of freedom. Hence, the equations of motion for a substructure could be written as (assuming no forces apply on condensed DOFs and no damping):

$$\begin{bmatrix} \mathbf{M}_{rr}^{(s)} & \mathbf{M}_{rc}^{(s)} \\ \mathbf{M}_{cr}^{(s)} & \mathbf{M}_{cc}^{(s)} \end{bmatrix} \begin{bmatrix} \ddot{\mathbf{q}}_r^{(s)} \\ \ddot{\mathbf{q}}_c^{(s)} \end{bmatrix} + \begin{bmatrix} \mathbf{K}_{rr}^{(s)} & \mathbf{K}_{rc}^{(s)} \\ \mathbf{K}_{cr}^{(s)} & \mathbf{K}_{cc}^{(s)} \end{bmatrix} \begin{bmatrix} \mathbf{q}_r^{(s)} \\ \mathbf{q}_c^{(s)} \end{bmatrix} = \begin{bmatrix} \mathbf{f}_r^{(s)} \\ \mathbf{0}_c^{(s)} \end{bmatrix} + \begin{bmatrix} \mathbf{g}_r^{(s)} \\ \mathbf{0}_c^{(s)} \end{bmatrix} \tag{52}$$

The Craig-Bampton reduction matrix is:

$$\mathbf{R}^{(s)} = \begin{bmatrix} \mathbf{I}_{rr}^{(s)} & \mathbf{0}_{rm}^{(s)} \\ \mathbf{\Phi}_{cr}^{(s)} & \mathbf{\Phi}_{cm}^{(s)} \end{bmatrix} \in \mathbb{R}^{n^{(s)} \times \left(n_r^{(s)} + n_m^{(s)}\right)} \tag{53}$$

$\mathbf{\Phi}_{cm}$ Fixed boundary modes
$\mathbf{\Phi}_{cr}$ Static modes

The number of fixed boundary modes kept in the reduction matrix *m,* determines the accuracy of the reduced FEM model when it comes to the eigensolutions. More fixed boundary modes result in a broader frequency bandwidth of acceptable accuracy. The static modes can be determined with:

$$\mathbf{\Phi}_{cr}^{(s)} = -\mathbf{K}_{cc}^{(s)}\mathbf{K}_{cr}^{(s)} \tag{54}$$

The fixed boundary modes $i = 1 \ldots m \leq c$ are computed from the following characteristic equation:

$$\left(\mathbf{K}_{cc}^{(s)} - \lambda_i \mathbf{M}_{cc}^{(s)}\right)\boldsymbol{\varphi}_i^{(s)} = \mathbf{0} \tag{55}$$

Hence, typical properties of this method are:

- Fixed interface method; includes fixed interface vibration modes next to all static modes
- Intensity and physical parameters, thus a hybrid reduction method
- With an additional transformation matrix, this method can be used to build a Test-analysis-model (TAM). [13] Such a model makes a wider collection of correlation functions applicable. However, this is only useful in case the dynamics of a single component is of interest.

2.2.5 ASSEMBLY OF REDUCED SUBSTRUCTURES

The assembly of reduced substructures is a similar process as the assembly of normal substructures. Nevertheless, the details are explained in the following subsections, since this will end up into the final results of the analytical approach, the assembled and reduced finite element model.

2.2.5.1 BLOCK-DIAGONAL ASSEMBLED REDUCED SUBSTRUCTURES

Again, the assembly starts with a block-diagonal assembly of the reduced substructures, so the number of degrees of freedom in this step becomes:

$$\hat{\tilde{n}} = \sum_{s=1}^{N_s} \hat{n}^{(s)} \tag{56}$$

Once more, the equations of motion are written with the connection forces separated from the applied forces. The constraint equations are reduced as well, the Boolean and the Localization matrix are reduced as illustrated:

$$\hat{\tilde{\mathbf{M}}}\ddot{\hat{\tilde{\mathbf{q}}}} + \hat{\tilde{\mathbf{C}}}\dot{\hat{\tilde{\mathbf{q}}}} + \hat{\tilde{\mathbf{K}}}\hat{\tilde{\mathbf{q}}} = \hat{\tilde{\mathbf{f}}} + \hat{\tilde{\mathbf{g}}} \tag{57}$$

$$\hat{\mathbf{B}}\hat{\tilde{\mathbf{q}}} = \mathbf{B}\mathbf{R}\hat{\tilde{\mathbf{q}}} = \mathbf{0} \tag{58}$$

$$\hat{\mathbf{L}}^T\hat{\tilde{\mathbf{g}}} = null\left(\hat{\mathbf{B}}\right)\hat{\tilde{\mathbf{g}}} = \mathbf{0} \tag{59}$$

$$\hat{\mathbf{B}} \in \mathbb{R}^{n_b \times \hat{\tilde{n}}}$$

$$\hat{\mathbf{L}} \in \mathbb{R}^{\hat{\tilde{n}} \times \hat{n}}$$

The individual reduction matrices of the substructures are block-diagonally assembled to form the global reduction matrix of the entire system.

$$\mathbf{R} = diag\left(\mathbf{R}^{(1)}, \ldots, \mathbf{R}^{(N_s)}\right) \in \mathbb{R}^{\bar{n} \times \hat{\bar{n}}} \tag{60}$$

$$\hat{\bar{\mathbf{q}}} = \left[\hat{\mathbf{q}}^{(1)T} \ \ldots \ \hat{\mathbf{q}}^{(N_s)T}\right]^T \in \mathbb{R}^{\hat{\bar{n}}} \tag{61}$$

The matrices of the block-diagonally assembled and reduced equations of motion can be calculated with the global reduction matrix by transforming the previously block-diagonally assembled matrices.

$$\hat{\bar{\mathbf{M}}} = \mathbf{R}^T \bar{\mathbf{M}} \mathbf{R} \in \mathbb{R}^{\hat{\bar{n}} \times \hat{\bar{n}}} \tag{62}$$

$$\hat{\bar{\mathbf{C}}} = \mathbf{R}^T \bar{\mathbf{C}} \mathbf{R} \in \mathbb{R}^{\hat{\bar{n}} \times \hat{\bar{n}}} \tag{63}$$

$$\hat{\bar{\mathbf{K}}} = \mathbf{R}^T \bar{\mathbf{K}} \mathbf{R} \in \mathbb{R}^{\hat{\bar{n}} \times \hat{\bar{n}}} \tag{64}$$

$$\hat{\bar{\mathbf{f}}} = \mathbf{R}^T \bar{\mathbf{f}} \in \mathbb{R}^{\hat{\bar{n}}} \tag{65}$$

$$\hat{\bar{\mathbf{g}}} = \mathbf{R}^T \bar{\mathbf{g}} \in \mathbb{R}^{\hat{\bar{n}}} \tag{66}$$

The block-diagonal assembly is illustrated graphically in Figure 10. Besides the substructure boundary nodes, also other degrees of freedom could be retained: nodes of interest. For example, these could be the measurement degrees of freedom.

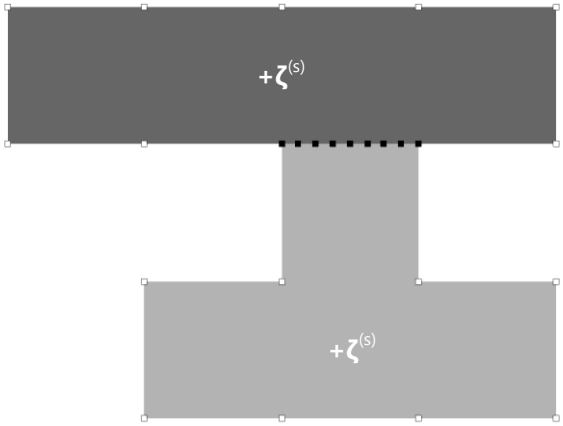

Figure 10: Block-diagonal assembled and reduced FEM model of example structure

2.2.5.2 PRIMAL ASSEMBLED REDUCED SUBSTRUCTURES

The last step is assembling the whole system by using the primal assembled formulation. This means that the constrained equations are again substituted into the equations of motion. The mathematical formulation in matrix notation of the assembled and reduced analytical finite element model is:

$$\hat{\mathbf{M}}\ddot{\hat{\mathbf{q}}} + \hat{\mathbf{C}}\dot{\hat{\mathbf{q}}} + \hat{\mathbf{K}}\hat{\mathbf{q}} = \hat{\mathbf{f}} \tag{67}$$

With its matrices defined as:

$$\hat{\mathbf{M}} = \hat{\mathbf{L}}^T\hat{\bar{\mathbf{M}}}\hat{\mathbf{L}} \in \mathbb{R}^{\hat{n}\times\hat{n}} \tag{68}$$

$$\hat{\mathbf{C}} = \hat{\mathbf{L}}^T\hat{\bar{\mathbf{C}}}\hat{\mathbf{L}} \in \mathbb{R}^{\hat{n}\times\hat{n}} \tag{69}$$

$$\hat{\mathbf{K}} = \hat{\mathbf{L}}^T\hat{\bar{\mathbf{K}}}\hat{\mathbf{L}} \in \mathbb{R}^{\hat{n}\times\hat{n}} \tag{70}$$

$$\hat{\mathbf{f}} = \hat{\mathbf{L}}^T\hat{\bar{\mathbf{f}}} \in \mathbb{R}^{\hat{n}} \tag{71}$$

In short, the large structure proposed in section 2.2.1 has been modelled with the commonly used finite element method in section 2.2.2. The more flexible model, presented in this section, is an approximation and reduction of that model. The advantages of this model are advantages of the substructuring and reduction technique combined. Below these are recapitulated:

The advantages of the substructuring technique are: (i.a. from [7], [8])

- Allows parallel engineering to increase development speed
- Natural approach if model is already decomposed
- Allows evaluating dynamic behaviour of structures that are too large or complex to be analysed as a whole
- By analysing substructures: local dynamic behaviour can be recognized more easily than when the entire structure is analysed
- Gives the possibility of combining analytical and experimental models in an assembly
- Enables the possibility of correcting the model parameters of an assembly locally during model updating

The advantages of the reduction technique are: (i.a. from [10])

- Speeds up computation of eigensolutions significantly. Specifically profitable when multiple eigensolution computations are required as in model updating algorithms or when many load cases have to be analysed
- Smaller models are faster and easier exchanged between engineers
- Easy reuse of components
- Hides the details of a component (confidentiality)

The analytical modelling part has been finished in this section; the result of the analytical approach is illustrated in Figure 11. Further reduction is possible; the interfaces can be reduced as well. An overview of all reduction techniques, including interface reduction, is presented by P.L.C. van der Valk. He also compares the performances of each technique [14].

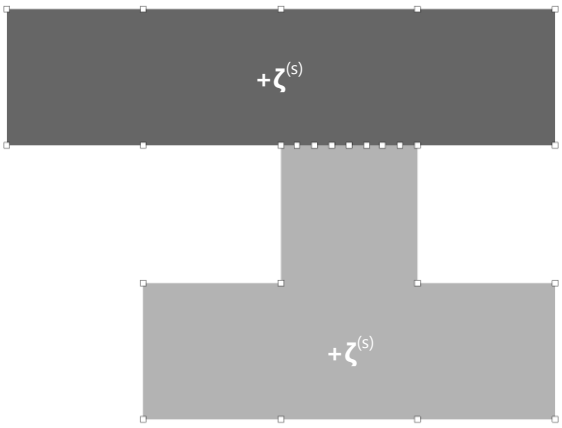

Figure 11: Primal assembled and reduced FEM model of example structure

2.3 EXPERIMENTAL MODEL

The experimental model is based on the 'real' structure, which has an infinite amount of degrees of freedom. However, the experimental model has a finite number of degrees of freedom, typically a few orders less than the number of degrees of freedom of the full finite element method structure. Also, for several reasons (mentioned later on in the discussion section) these are not always equally distributed over the analytical substructures. This is illustrated in Figure 12.

Figure 12: Experimental model of example structure

In many situations, only unidirectional accelerometers are used for the measurement. Here, in the example structure only the vertical direction is measured. (Nodes have two degrees of freedom, since the example is two dimensional.)

So far, the concept of the analytical and experimental approach and the analytical and experimental models for large assembled structures has been explained. The focus was on the degrees of freedom present in the models. Natural differences were illustrated by representative example figures. Now it is time to analyse the typical results of the models with the validation of the analytical model as the ultimate goal. In this report this analysis is called the post analysis.

2.4 POST ANALYSIS

The validation of an analytical model is usually done in three main steps. All the steps are explained in this section in more detail. In short, the steps are: [2]

- Comparison and correlation of specific dynamic properties, often predicted versus measured values
- Verification and reconciliation of the model to estimate whether updating the model is useful or not and to judge on the possible cause(s) of the differences found
- Localization of errors and correction of the analytical model in order to bring the results of both models closer together

In general these steps can be visualized in a scheme as: (see Figure 13)

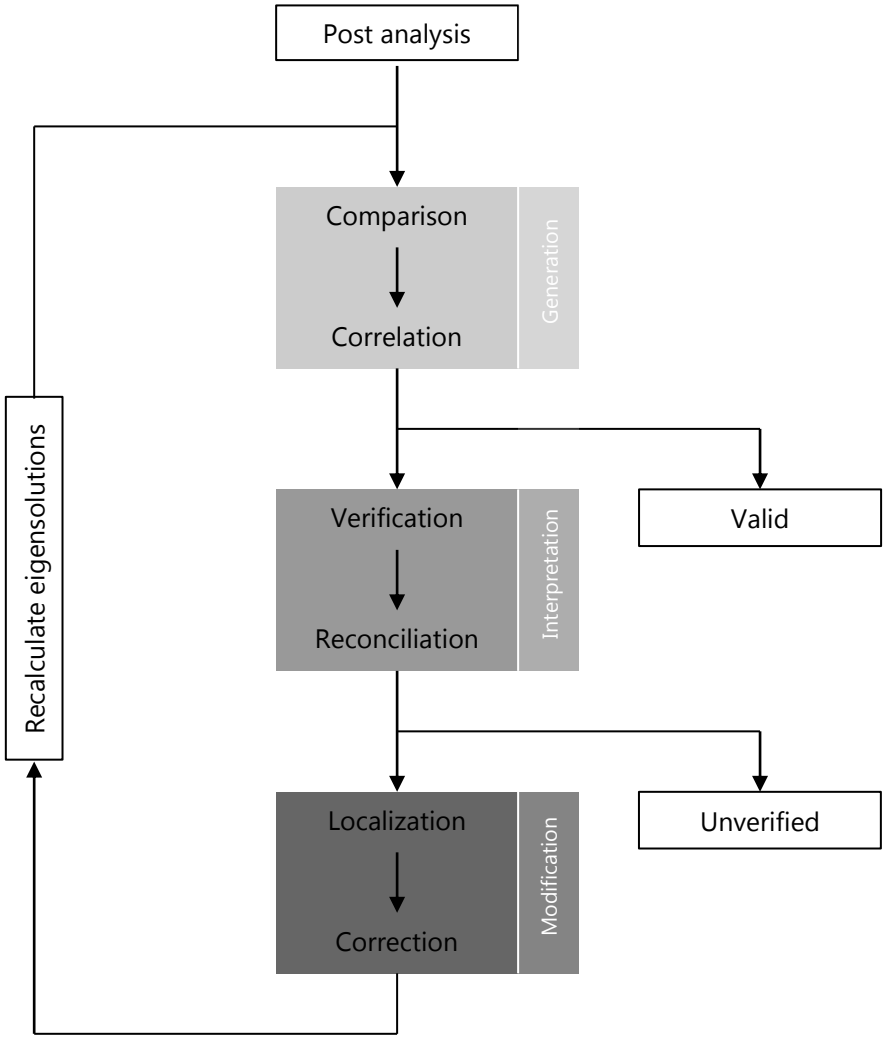

Figure 13: General validation process

Note that this process has to be repeated for every new load case or set of boundary conditions, when validation is required. The post analysis only makes sense if both models are compatible.

Here, this means that both models should have corresponding degrees of freedom. However, this situation is not the case when the experimental setup is an assembly. (Assumed the Craig Bampton reduction method is applied on the analytical model and the experimental model is not similarly substructured.)

In the first place, the analytical model has both modal and physical degrees of freedom, while the experimental model only has the latter. Secondly, the physical degrees of freedom of both models do not have to be similar. Think of the boundary degrees of freedom connecting two substructures. These are not always in the experimental model, since this model may not be substructured.

That is why you either need to expand the analytical results or incorporate the measured degrees of freedom in the retained degrees of freedom from the reduced model. Either solution creates the possibility to observe the physical degrees of freedom that are similar to those of the experimental model.

The expansion option is performed with the following mathematical operations, starting with the reduced model degrees of freedom. The goal is to obtain the analytical degrees of freedom that are compatible with the experimental degrees of freedom.

To obtain the block diagonal reduced degrees of freedom from the reduced degrees of freedom; apply the reduced localization matrix:

$$\hat{\bar{\mathbf{q}}} = \hat{\mathbf{L}}\hat{\mathbf{q}} \tag{72}$$

To obtain the unreduced block diagonal degrees of freedom hereafter; apply the global reduction matrix:

$$\bar{\mathbf{q}} = \mathbf{R}\hat{\bar{\mathbf{q}}} \tag{73}$$

To obtain the full degrees of freedom hereafter; apply the pseudo inverse of the localization matrix.

$$\mathbf{q} = \mathbf{L}^{+}\bar{\mathbf{q}} \tag{74}$$

Note, that this step is not necessary since from the block diagonal degrees of freedom, the experimental equivalent degrees of freedom can already be observed.

Finally, to obtain the analytical degrees of freedom, which are compatible with the experimental degrees of freedom; an observation matrix should be applied. The observation matrix is a simple Boolean matrix to localize required degrees of freedom.

$$\tilde{\mathbf{q}} = \mathbf{O}\mathbf{q} \tag{75}$$

$\mathbf{O}$ Observation matrix

The second option, including the measurement degrees of freedom in the reduced degrees of freedom, would result into Figure 14 when applied at the example structure.

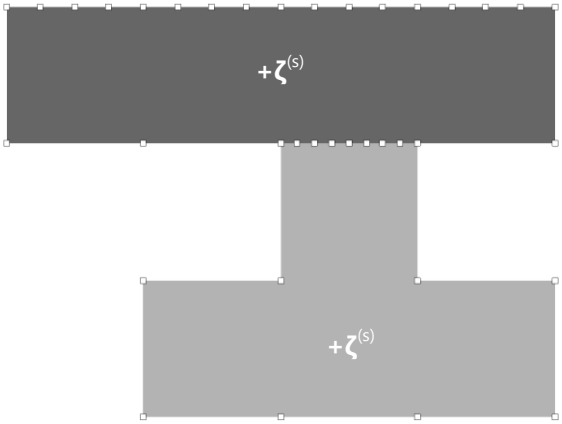

Figure 14: Primal assembled and reduced FEM model of example structure with measurement degrees of freedom included

Note that in many publications it is assumed that a test-analysis model reduction (TAM) is possible. (i.a. [15], [16]) However, this is not the case for models of large structures assembled as in section 2.2. This is a significant difference, which makes direct use of several existing correlation tools and model updating methods impossible.

In summary: due to the application of analytical expansion or including the experimental degrees of freedom in the reduced master structure, these two modal models are of equal size, which makes them convenient for further correlation purposes. Since many correlation functions and model updating algorithms are developed for a test-analysis model and are not constructed in the natural approach for large structural assemblies, these procedures cannot be applied directly.

In the next section the remaining correlation tools and algorithms are explained. Use is made of the following compatible results from this section.

ANALYTICAL MODAL ANALYSIS RESULTS

$$\tilde{\boldsymbol{\Phi}} = \left[\tilde{\boldsymbol{\varphi}}_1 \,, \ldots, \tilde{\boldsymbol{\varphi}}_m\right] \tag{76}$$

$$\tilde{\boldsymbol{\Lambda}} = diag\left(\tilde{\lambda}_1 \,, \ldots, \tilde{\lambda}_m\right) \tag{77}$$

EXPERIMENTAL MODAL ANALYSIS RESULTS

$$\underset{\sim}{\boldsymbol{\Phi}} = \left[\underset{\sim}{\boldsymbol{\varphi}}_1 \,, \ldots, \underset{\sim}{\boldsymbol{\varphi}}_m\right] \tag{78}$$

$$\underset{\sim}{\boldsymbol{\Lambda}} = diag\left(\underset{\sim}{\lambda}_1 \,, \ldots, \underset{\sim}{\lambda}_m\right) \tag{79}$$

2.4.1 COMPARISON

The comparison of results is a qualitative analysis. The goal is to recognize the major deviations of independently obtained results, just by observation. This can be done by comparing a list of numbers or by plotting the numbers in a graph.

The results of the analytical and experimental modal analysis are often compared by listing two columns of eigenfrequencies and plotting two columns of mode shapes (deformed structure plots). The comparison of the eigenfrequencies is meaningful when the compared modes are matching. This match could be confirmed by calculating the modal correlation value (*MAC*) [17], often seen as an essential step. These correlation calculations are part of a quantitative analysis and will be explained in the next subsection. Other modal domain comparisons are:

- Mode shape plot
- Nodal patterns of mode shapes
- Compass diagram of complex mode shapes

Comparison in the frequency domain is also done. Some typical comparison plots in this domain are:

- Frequency response functions
  - Real / Imaginary
  - Magnitude / Phase
  - Nyquist plot

These representations, together with several variations, are explained in more detail in literature, written by M. Radeş. [18] Some of these comparison methods are applied on a real test case in section 3.

2.4.2 CORRELATION

The following four correlation categories are discussed in this section; correlation of:

- Modal frequencies
- Mode shapes
- Degrees of freedom
- Frequency response functions

Correlation of damping is not discussed here, since in this study damping is neglected. Also correlation in the spatial domain is not discussed, because an experimental model is hardly ever transformed to this domain.

For scalars, such as eigenfrequencies, only cross-correlation is meaningful. For vectors, such as mode shapes, also correlation criteria exist, which mutually compare vectors coming from the same model. This gives information about how distinguishable each result of a particular model is. Only when these criteria give satisfactory results, it makes sense to perform a cross-correlation.

2.4.2.1 MODAL FREQUENCY CORRELATION

The formula for relative modal frequency discrepancy is:

$$\varepsilon_{\omega_r} = \frac{\underset{\sim}{\omega}_r - \tilde{\omega}_r}{\underset{\sim}{\omega}_r} \cdot 100\% \tag{80}$$

As mentioned before, this is only a meaningful correlation tool when the mode shapes are paired. For good correlation purposes: this difference should be less than 5%. [16]

2.4.2.2 MODE SHAPE CORRELATION

Mode shape correlation provides a global indicator of the level of correlation achieved. The simple formula for the relative mode shape norm difference is illustrated below. For good correlation purposes this difference should be lower than 10%. [16]

$$\varepsilon_{\boldsymbol{\varphi}_r} = abs \frac{\left|\underset{\sim}{\boldsymbol{\varphi}}_r^T \underset{\sim}{\boldsymbol{\varphi}}_r\right| - \left|\tilde{\boldsymbol{\varphi}}_r^T \tilde{\boldsymbol{\varphi}}_r\right|}{\left|\underset{\sim}{\boldsymbol{\varphi}}_r^T \underset{\sim}{\boldsymbol{\varphi}}_r\right|} \cdot 100\% \tag{81}$$

If this is not the case, it may be due to badly scaled experimental mode shapes. Recalling from the comparison section: each element of an experimental mode shape could be plotted against the corresponding element of the analytical mode shape in a two dimensional plot. For consistent correspondence, all points should lie close to a straight line passing through the origin. If both mode shape vectors are of a similar norm due to the modal scale factor, then the approximating line has a slope of one. The modal scale factor (*MSF*) is defined as:

$$\tilde{\boldsymbol{\varphi}}_r = MSF_{rr} \underset{\sim}{\boldsymbol{\varphi}}_r \tag{82}$$

$$MSF_{rr} = \frac{\tilde{\boldsymbol{\varphi}}_r^T \underset{\sim}{\boldsymbol{\varphi}}_r}{\underset{\sim}{\boldsymbol{\varphi}}_r^T \underset{\sim}{\boldsymbol{\varphi}}_r} \tag{83}$$

Like the frequency and vector correlation of eq. (80) and (81), the modal scale factor does not say anything useful about two uncorrelated mode pairs.

These days, the modal assurance criterion (*MAC*) matrix is used to identify corresponding mode pairs, but was originally introduced to quantify the accuracy of identified mode shapes. [17] The *MAC* value is 'one' for parallel and 'zero' for orthogonal vectors. It is a simple dot product and independent of mass weighting and vector scaling. The criteria is formulated as: (for real vectors)

$$MAC_{rs} = \frac{\left(\tilde{\boldsymbol{\varphi}}_r^T \underset{\sim}{\boldsymbol{\varphi}}_s\right)^2}{\left(\tilde{\boldsymbol{\varphi}}_r^T \tilde{\boldsymbol{\varphi}}_r\right)\left(\underset{\sim}{\boldsymbol{\varphi}}_s^T \underset{\sim}{\boldsymbol{\varphi}}_s\right)} \tag{84}$$

Note that the ideal *MAC* matrix cannot be a unity matrix because the modal vectors are not directly orthogonal, but mass-orthogonal. [19] However, perfect correspondence of *m* mode shapes results in *m* unit values in the *MAC* matrix.

Auto-MAC matrices are used to address the spatial incompleteness problem of the model. Spatial aliasing, a limiting factor when it comes to observability of mode shapes, is occurring when the *Auto-MAC* matrix shows larger-than-usual off-diagonal elements. [16] Here, the *Auto-MAC* of the analytical ($\tilde{M}AC$) and experimental ($\underset{\sim}{M}AC$) model are formulated:

$$\tilde{M}AC_{rs} = \frac{\left(\tilde{\boldsymbol{\varphi}}_r^T \tilde{\boldsymbol{\varphi}}_s\right)^2}{\left(\tilde{\boldsymbol{\varphi}}_r^T \tilde{\boldsymbol{\varphi}}_r\right)\left(\tilde{\boldsymbol{\varphi}}_s^T \tilde{\boldsymbol{\varphi}}_s\right)} \tag{85}$$

$$\underset{\sim}{M}AC_{rs} = \frac{\left(\underset{\sim}{\boldsymbol{\varphi}}_r^T \underset{\sim}{\boldsymbol{\varphi}}_s\right)^2}{\left(\underset{\sim}{\boldsymbol{\varphi}}_r^T \underset{\sim}{\boldsymbol{\varphi}}_r\right)\left(\underset{\sim}{\boldsymbol{\varphi}}_s^T \underset{\sim}{\boldsymbol{\varphi}}_s\right)} \tag{86}$$

Several variations on the *MAC* exist (mostly weighted or normalized variations). However, these do not give much additional information and are not always applicable, especially in the case when no test-analysis model (TAM) format is available. Further notes on *MAC*: [20]

- It is no orthogonality check
- Wild points could dominate the *MAC*-value
- Since this computation was originally a statistical computation, it is a sensitive value when the mode shape has a limited number of degrees of freedom

The *FMAC* is a way of displaying the *MAC*, the *Auto-MAC* and the natural frequency comparison in a single plot [21], such that the mode shape correlation, the degree of spatial aliasing and the natural frequency comparison can be plotted simultaneously. This is obtained by drawing a circle with a radius proportional to the *MAC* or *Auto-MAC* value at the coordinates of each modal frequency pair.

2.4.2.3 DEGREE OF FREEDOM CORRELATION

Degree of freedom correlation provides an indicator on how the individual degrees of freedom contribute to the overall modal vector correlation. The coordinate *MAC* (*COMAC*) [22] is a simple dot product, a correlation on degree of freedom basis for correlated mode pairs and independent of mass weighting. The only thing the *COMAC* does is to detect local differences between two sets of modal vectors. It does not identify modelling errors, because their location can be different from the areas where their consequences are felt. Another limitation is the fact that *COMAC* weights all degrees of freedom equally, irrespective of their magnitude in the modal vector. [19]

$$COMAC_i = \frac{\left(\sum_{r=1}^{m} \left|\tilde{\varphi}_{ir} \underset{\sim}{\varphi}_{ir}\right|\right)^2}{\sum_{r=1}^{m} \left(\tilde{\varphi}_{ir}\right)^2 \cdot \sum_{r=1}^{m} \left(\underset{\sim}{\varphi}_{ir}\right)^2} \tag{87}$$

Note that the above formulation assumes that there is a match for every modal vector in the two sets and the modal vectors are renumbered accordingly, so that the matching modal vectors have the same subscript. Only those modes that match between the two sets are included in the computation. [20]
Again, several variations on this formula exist (mostly weighted or normalized variations). However, these do not give much additional information.

2.4.2.4 FREQUENCY RESPONSE FUNCTION CORRELATION

The frequency domain assurance criterion (*FDAC*) [23] is analogous to the *MAC*, however for each frequency. The *FDAC* value is 'one' for parallel and 'zero' for orthogonal vectors.

$$FDAC(\tilde{\omega},\underset{\sim}{\omega},j)=\frac{\left|\tilde{\mathbf{H}}_{.j}^{T}(\tilde{\omega})\underset{\sim}{\mathbf{H}}_{.j}^{*}(\underset{\sim}{\omega})\right|^{2}}{\left(\tilde{\mathbf{H}}_{.j}^{T}(\tilde{\omega})\tilde{\mathbf{H}}_{.j}^{*}(\tilde{\omega})\right)\left(\underset{\sim}{\mathbf{H}}_{.j}^{T}(\underset{\sim}{\omega})\underset{\sim}{\mathbf{H}}_{.j}^{*}(\underset{\sim}{\omega})\right)} \tag{88}$$

A more clean representation is the response vector assurance criterion (*RVAC)* [24]. The *RVAC* can be considered similar as the *MAC*, evaluated only at the eigenfrequencies. $\mathbf{H}_{.j}$ is column vector *j* of receptance matrix **H**.

$$RVAC(\omega,j)=\frac{\left|\tilde{\mathbf{H}}_{.j}^{T}(\omega)\underset{\sim}{\mathbf{H}}_{.j}^{*}(\omega)\right|^{2}}{\left(\tilde{\mathbf{H}}_{.j}^{T}(\omega)\tilde{\mathbf{H}}_{.j}^{*}(\omega)\right)\left(\underset{\sim}{\mathbf{H}}_{.j}^{T}(\omega)\underset{\sim}{\mathbf{H}}_{.j}^{*}(\omega)\right)} \tag{89}$$

The modal frequency response function assurance criterion (*MFAC*) [21] has the combination of the benefits of the *MAC* and the *RVAC*. For this reason, it is the most accurate criterion. (No modal parameter identification and no transformation to the frequency domain needed.)

$$MFAC(\tilde{\omega}_{r},\underset{\sim}{\omega})=\frac{\left|\tilde{\boldsymbol{\varphi}}_{r}^{T}\underset{\sim}{\mathbf{H}}_{.j}^{*}(\underset{\sim}{\omega})\right|^{2}}{\left(\tilde{\boldsymbol{\varphi}}_{r}^{T}\tilde{\boldsymbol{\varphi}}_{r}\right)\left(\underset{\sim}{\mathbf{H}}_{.j}^{T}(\underset{\sim}{\omega})\underset{\sim}{\mathbf{H}}_{.j}^{*}(\underset{\sim}{\omega})\right)} \tag{90}$$

The frequency response assurance criterion (*FRAC*) is comparative to the *COMAC*. [25] $\mathbf{H}_{ij}$ is a vector with values for each frequency.

$$FRAC_{ij}=\frac{\left|\tilde{\mathbf{H}}_{ij}^{T}\underset{\sim}{\mathbf{H}}_{ij}^{*}\right|^{2}}{\left(\tilde{\mathbf{H}}_{ij}^{T}\tilde{\mathbf{H}}_{ij}^{*}\right)\left(\underset{\sim}{\mathbf{H}}_{ij}^{T}\underset{\sim}{\mathbf{H}}_{ij}^{*}\right)} \tag{91}$$

2.4.2.5 INAPPLICABLE CORRELATION TOOLS

Due to no M_{TAM} (test-analysis mass matrix):

- Test orthogonality matrix (TOR)
- Generalized mass matrix (GM)
- Cross-orthogonality matrix (XOR)
- Normalized cross-orthogonality matrix (NCO)
- Coordinate orthogonality check (CORTHOG)
- Force unbalance

2.4.3 VERIFICATION

The third step in the general process of model validation is the model verification. A model is said to be verified if it contains the correct features (model parameters), most importantly the appropriate number and choice of degrees of freedom, to represent the behaviour of the structure. This means: the primary load paths, the mass and stiffness distribution, the boundary conditions and the material properties must be properly represented in the equations of motion. [16]

When the model is not valid but verified, the significantly deviating model parameter settings should be localized and corrected in order to end up with a validated model. In case the model cannot be verified, the model itself has to be modified. Maybe some features were forgotten, unjustly neglected or ignored.

2.4.4 RECONCILIATION

Modelling errors are due to system properties which are not fully understood, such as: nonlinearities, hysteresis, model dimensions, truncation errors, and a general lack of the full characterization of structural materials. These errors could be in the analytical model, the experimental model or both. Reconciliation refers to the sometimes delicate task of establishing reasons for the observed differences between measurement and prediction. [16]

Fortunately many errors are recognized because they have occurred before in a similar situation, thus the experience of the engineer plays an important role here. All other errors need to be found by reviewing the complete analysis, mainly focussed on the used parameters, assumptions, the models, and of course, the calculations.

2.4.5 LOCALIZATION

The last two steps of the post analysis cycle are localization and correction. The purpose the localization step is to find the incorrect model parameters. Most localization methods are based on the determination of parameter sensitivity with respect to a arbitrarily chosen error function.

Sensitivity studies allow one to distinguish between more and less sensitive elements. They are therefore a relative measure. It may be argued that more sensitive regions are indeed the elements in error, but this will only hold true if the level of perturbation is relatively small, i.e. if the initial model parameters are close to the correct model. Although this is indeed a frequently-expressed pre-requisite for the validity of many model updating techniques, it is often not a realistic assumption to make. This is particularly true if the finite element model representation is very coarse and some characteristic features of the structure are not captured. In this case, the physical cause of the error is not represented in the finite element model and the sensitivity study will eventually lead to flawed conclusions. [26]

An illustration of this characteristic is the presence of joints or grounded coordinates in a structure. It is known that in these cases, the rigid finite element representation must be replaced by a less-than-rigid model. This is conveniently done by modelling a joint, using simple (and linear) spring-mass-damper systems. The initial estimation of these lumped parameters, however, is difficult and usually the magnitudes of the spring-mass-damper properties are guessed. [26]

For a general localization procedure the typical updating parameters that are analysed are:

- Parameters associated with individual elements
  - Element stiffness or density
- Parameters associated with of groups of elements
  - Global stiffness or density (e.g. Young's-modulus)
  - Local stiffnesses such as connections
  - Local mass distribution (mass loading)

Because remeshing is unwanted, not very often used model parameters are dimensions like: lengths, diameters and thicknesses.

2.4.6 CORRECTION

Correction is the final step in the complete validation process; it is the computation of the necessary changes to be introduced to the parameters which have been identified or guessed as containing the errors. After this step, the whole validation process repeats itself until validation of the model has been achieved.

There have been many methods proposed for the task of correcting an experimental model. They can all be split in two categories

- Direct techniques
- Indirect techniques

The direct techniques correct the elements of the finite element method mass and stiffness matrices so that they accurately predict the experimentally derived modes and frequencies. Indirect techniques are based on determining corrections for the input parameters of the finite element model, in order to reduce the model differences.

The applicability of direct techniques is limited, especially for assemblies, since a limited number of measured eigenvectors is employed and the measurements are wrongly assumed to be complete. [26] Both Berman [1] and Dascotte [27] concluded that in many cases it is impossible to identify a physical meaningful model by using a direct approach, making it less effective.

Hereby, the indirect techniques have become the most popular ones; it gave the engineers the possibility to optimize incomplete and truncated models. Also the choice of updating parameters had become more flexible. The indirect techniques however have their own disadvantages. The main disadvantage is that the optimum has to be found iteratively with an:

- Algorithm
- Design of experiments

In this report, both are not explained in detail, but the major lesson is that both could still give suboptimal results. Algorithms can get stuck in local minima or the solution is not in the scope of the design of experiments. Success of the indirect methods also greatly depends on the chosen objective parameter(s) and function(s), and the results may not be unique (e.g. there are more updating parameters than measurements).

2.4.6.1 OBJECTIVE FUNCTION

The purpose of an objective function is to compare two differently parameterized models and judge on the degree of optimization. In this case a minimization means a best possible correlation of the analytical and experimental model with the current model characteristics. Note this does not mean that the correlation is always satisfactory. Also the objective function is often an arbitrarily chosen function. However, there exist objective functions, which are used by many, since for many engineers the purpose of the optimization is comparable.

One objective function is commonly used is an eigenfrequency based objective function, the squared error function J_1: [11]

$$J_1 = \sum_{r=1}^{m} \frac{\left(\tilde{\lambda}_r - \underset{\sim}{\lambda}_r\right)^2}{\underset{\sim}{\lambda}_r^2} \tag{92}$$

A second commonly used objective function is a mode shape based objective function, specifically based on the modal assurance criteria for the modes $r = 1,\ldots,m$. [11]

$$J_2 = \sum_{r=1}^{m} (1 - MAC_{rr}) \tag{93}$$

These two functions could also be combined into one objective function. This is done with a weighting function w, again an arbitrarily chosen function.

$$J = wJ_1 + J_2 \tag{94}$$

Of course, many other existing objective functions are applicable. For example: you could design a similar objective function based on frequency response data. Most important: the function should give a minimum value for perfectly compatible models; otherwise this function does not perform as required.

Some objective functions might be more sensitive to certain parameter variations than others. Also, it would be favourable if it is most sensitive to the parameters you can control, instead of to the ones you cannot control.

General problems with the objective function field could be:

- Many local minima; algorithm might converge in a local minimum
- Slow convergence of the algorithm due to shallowness of the field
- Stability of result depending on initial values

2.5 DISCUSSION

To start with, assume a large structural assembly, containing one hundred slave components. According to the theory explained in section two, all these components have to be modelled using the finite element method (substructuring) and reduced to a super element. Thereafter, all the super elements are assembled and the eigensolutions of the assembly are calculated.

In practice, engineers have three important constraints that may influence this process. The first two restraints are: the software to use and the time to spend, regarding finite element modelling and eigensolution computation. For instance, mesh convergence checks are often skipped to save time. The third restraint is the complexity; it is hard to predict the direct consequences of your choices on component level with respect to the dynamic behaviour of the assembly. General assumptions on structural assembly level are (thus assumptions on component level excluded):

- Omission of components, because their mass is less than one per cent of the master structure
- Omission of structural dynamics of components, because it is assumed that it only has a neglectable influence on the dynamics of the assembly. In this case, the component is often modelled as a point mass, also called mass loading
- Simplification of connections, because connections are often difficult interfaces to model

With the differences for the theoretical and the practical process in mind the attention on improving the general process could either be focussed at

- Troubleshooting, to locate mistakes
- Modelling, to prevent mistakes

In this report the attention is paid to troubleshooting instead of modelling, for several reasons; firstly, many engineers have more experience in the latter. Secondly, errors as discussed above could still occur, with or without an improved modelling technique. Thirdly, for troubleshooting additional information is known, namely the experimental model. This information could be used to identify parts of the construction which were not well understood during modelling.

The company's engineering environment brings along some additional practical issues with this approach. For the sake of troubleshooting; the following boundary conditions are making it very difficult or time-consuming to determine the exact cause of the differences found:

- Many components and connections in one assembly that might cause the differences found
- Unreachable components, built-in due to the assembly, cannot be measured
- Not removable components making experimental setup variations impossible
- Roving hammer testing preferred in many situations because of the speed and flexibility of the procedure, but some components are vulnerable and cannot bear any impact
- Short measurement time schedule, making frequently re-measuring unwanted and costly

A lot can be found on troubleshooting in literature, especially about model updating of lumped models, or solid parts. However, much less examples in literature are about (large) structural assemblies.

When assemblies are discussed, typically all components deliver measuring points during the experiment. In this case the measured degrees of freedom might already be sufficient for the identification of unexpected dynamic behaviour, like uncoupled components.

Also, the geometric aspect ratios of the components are commonly not much different from one and thus each component is often modelled with the finite element method. In case a broken beam element of a civil structure has to be identified, the stiffness of each beam element is multiplied with an updating parameter.

The properties of assemblies that remain and occur in typical structural dynamic models from companies like ASML are:

- Many components
- Aspect ratios that are much larger or smaller than one
- Only measurement points on the master structure

Looking at all these issues and differences, several interesting questions come to mind. All of these had little or no attention in literature yet:

- What is the influence of a relatively lightweight resonating component (typically smaller than one per cent of assembly) on the global structural dynamic behaviour of the master structure? Is its influence significant? Could the dynamics of this component be ignored?
- How could we find the location of a resonating component analytically, when multiple components are suspicious? Is this possible by using existing tools, methods and procedures?
- Which lumped model of a relatively small slave structure satisfactorily represents the components behaviour and properties, when the global structural dynamic behaviour of the assembly is of concern?

2.5.1 FINAL RESEARCH QUESTION

Initially, the first two points have the main interest. When these two questions have been answered, additional reasons are created for the investigation of the third question. The final research question is formulated:

What is the influence of a relatively lightweight resonating slave structure on the global structural dynamic behaviour of the master structure? How could you find the location of an unmeasured resonating slave structure with existing correlation tools and validation procedures, when multiple components are suspicious?

3 METHODOLOGY

This study concerns the dynamic behaviour of large structures with several small components attached to it. The dynamic behaviour of such a structural assembly is altered when one of the small components is not properly attached. This is typically observed in a modal measurement. The current section addresses the question whether it is possible to identify which component causes the disturbance in dynamics. A post analysis procedure is proposed to find this component. It uses finite element method (FEM) calculations and requires no additional measurements. The procedure is described in section 3.1.

A simple structural assembly was designed to test the feasibility of the procedure. This simplified assembly consisted of a plate representing a large master structure and of several small masses (slave structures) that can be attached on different locations on the master structure. One of these smaller masses is attached via a leaf spring. This mass represents the component that is not properly attached and therefore alters the dynamic behaviour of the assembly. The design of the test assembly is described in detail in section 3.2

A FEM model of the structural assembly is required for the diagnostics procedure. Such an FEM model is developed. It is described in section 3.2.3.

The test assembly was actually made by the ASML model-shop. The actual hardware for the experiment and deviations to the intended design are described in section 3.2.4.

The application of both models, FEM model versus experimental model, in the procedure to find the loose component is described in the results section 3.3

3.1 POST ANALYSIS PROCEDURE

For the proposed component localization procedure, the general post analysis cycle of Figure 13 has been modified such that the final goal becomes the localization of the loose slave structure instead of model validation. The new process is illustrated in Figure 16. The last step has been inverted (localization is now after correction) and a new iteration loop has been created.

The large loop is normally performed by an algorithm. It can be replaced by two smaller loops that are independently performed when a design of experiments process is preferred. For this study, the latter has been chosen. The reasons are:

- Controllability of the process
- Create insight into process
- Simplicity of process

Since this procedure is still a quite general representation, a more practical implementation is shown in Figure 15.

	Comparison and Correlation
-	The starting point is a modal measurement of an assembly. Measurement data shows an unexpected additional eigenmode relative to the intended design (the FEM model)
-	The current FEM model is judged to be invalid to describe the current hardware assembly
	Verification and Reconciliation
-	It is reasonable to assume that one component is not properly attached
-	Isolate the FEM model of the master structure (preferably as a super element). Retain the degrees of freedom that couple the master structure with the slave structures which are potentially causing the resonance
-	Add small mass spring systems to represent the suspicious components
-	Initially fix components with high stiffness
	First loop: Correction and Recalculation Eigensolutions
-	The value of the extra frequency and the mass of the respective slave structure provide an estimate of its actual connection stiffness
-	Vary the connection stiffness of the suspicious slave structures one by one around the respective estimated stiffness
-	Recalculate the eigenfrequencies and eigenmodes for all FEM model variations
	Second loop: Comparison and Correlation
-	Correlate each FEM model variation to the experimental modal analysis results by means of objective functions
	Localization
-	The slave structure with lowest value for all objective functions is the most likely cause for the unexpected change in dynamics

Figure 15: Practical implementation of the modified post analysis process from Figure 16.
The colours in the table are similar to the referred figure.

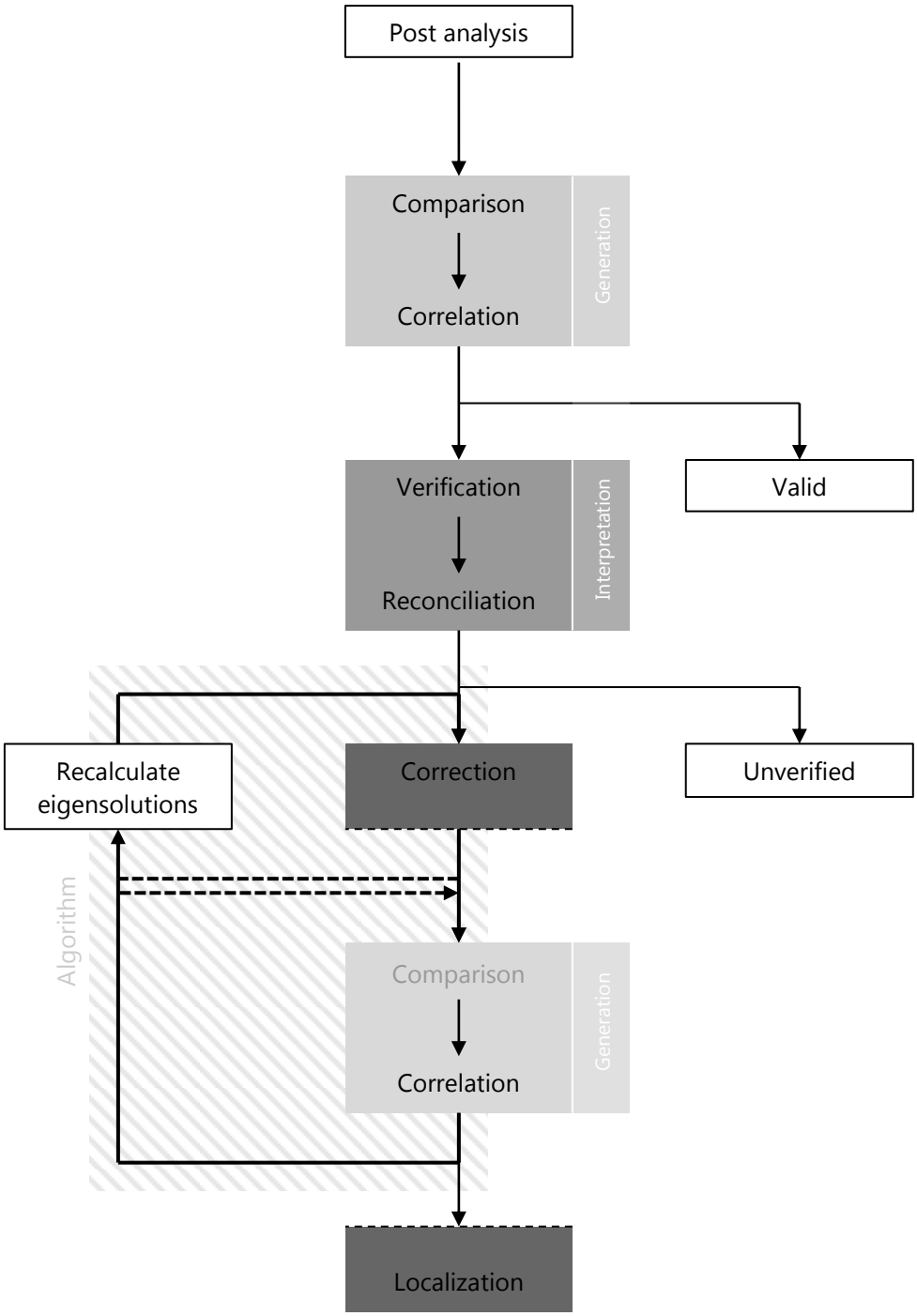

Figure 16: Modified post analysis process with localization as the last step

3.2 APPLICATION ON STRUCTURAL ASSEMBLY

To test the proposed procedure: a structural assembly and both its analytical and experimental model are required. These are designed and built in the next subsections. To increase controllability of the results with respect to a complex structure as used in the lithography industry, the design is kept as simple as possible.

The design requirements are set up in section 3.2.1. The actual design of the master and slave structures is explained in section 3.2.2. After the design of the individual components, the structural assembly model is made analytically as well as experimentally, in section 3.2.3 and 3.2.4 respectively.

3.2.1 REQUIREMENTS

For the design of this structure a requirements list has been set up for both the master and the slave structures. Most of the requirements are supported with arguments and hand calculations in the design phase. The general requirements are:

- Multiple locations with similar masses to make the location identification process of the erroneous connection flexibility independent of other parameters
- Linear elastic material
- Simple property validation
  - Control measurements of the masses, stiffnesses and the geometries
  - Analytical convergence and experimental validation

3.2.1.1 REQUIREMENTS MASTER STRUCTURE

- First eigenfrequency around 200 Hz, to make the low support stiffness neglectable
- Reduce dynamic dimensions of interest if possible, uniaxial sensors preferred
- Asymmetric, prevent having double eigenfrequencies and mode shapes
- Avoid damping as much as possible in model or suspension
  - Obtain clear resonances in frequency response functions
  - No phase delay between coordinates, real valued modes preferred
- Global and local modes

3.2.1.2 REQUIREMENTS SLAVE STRUCTURES

- Push higher order resonances to frequencies outside the interesting frequency bandwidth, hence, the first eigenfrequency around 500 Hz, second around 2500 Hz
- Stiff and flexible connections (bolted or leaf spring)
  - Possibility to change the flexibility of a connection by changing components or spring parts
  - Flexible connections only in out of plane direction
  - A single, easy mountable and well determined connection per slave structure
- Similar mass ratio as in reality (mass of a sensor or small component)

3.2.2 DESIGN

The simplified structural assembly is designed as a master structure: a rectangular plate, with several slave structures, sprung and unsprung masses, mounted on top of that plate. The size of the plate is arbitrarily chosen. Each mass, however, is around hundred times lighter than the plate. Because of this weight ratio, these masses are often neglected in a model or their dynamics is assumed to be of no interest. This assumption could be significantly wrong; therefore, these mass ratios are of main interest in this study.

3.2.2.1 MASTER STRUCTURE

The main reason for choosing a plate as the master structure is to simplify the structural dynamics to out-of-plane dynamics. The deformation in this direction is a few orders of magnitude larger than in the two in-plane directions. In this situation uniaxial accelerometers, relatively lightweight and inexpensive, are sufficient to represent the structures mode shapes in a meaningful way.

Other reasons for the choice of this simplified structure are that its production is fast, cheap and accurately. The shape is relatively easy to model in ANSYS and it is suitable for estimations by hand calculations. Simple production steps, as milling and drilling, are sufficient to build the complete physical model in a short time, for a good price.

By milling out a rectangular hole in one of the corners of the plate, such that the plate becomes asymmetric, well separated eigenfrequencies are obtained. Also, no multiplicity of mode shapes will be found. When the structure has this property, the fitted mode shapes could be determined more accurately. Another feature that the plate obtains through this modification is the presence of local modes. These make the decision to neglect relatively small masses more complex, since their effective mass is smaller.

A pattern of holes spanning the entire plate creates the possibility to put the masses at later determined locations. As a consequence, the design of the setup can be performed parallel to the creation of both the analytical model and the experimental model.

The plate is made from aluminium, because this linear elastic material has an approximately three times lower density than steel. As a result, the pattern of holes could be more densely designed when the masses are made from steel and a certain mass ratio (m_{slave}/m_{master}) is required.

As mentioned before, the controllability of the setup is important. The components of the simplified structure have to be made with sufficient precision and accuracy. Milling, drilling and turning are suitable production methods for fulfilling these requirements. The fact that the structure is a plate with holes, makes it relatively easy to control lengths, widths, thicknesses, diameters and locations.

The first eigenfrequency, required to be around the target frequency f_t of 200 *Hz*, of a solid aluminium plate (3.8 *kg*) could be estimated by the following formula: [28]

$$f_1 = \frac{20.13}{2\pi l^2}\left[\frac{Et^2}{12\rho\left(1-\upsilon^2\right)}\right]^{\frac{1}{2}} = 243\ Hz \tag{95}$$

This eigenfrequency is a good starting point for the plate, since from here all the modifications will influence its stiffness and mass. The components mounted on top of the plate will lower its first eigenfrequency, as they will add mass, but no stiffness. Controlling the thickness *t* of the plate was done by milling the top of the plate. The thickness is the most important parameter, since this dimension is more than one order of magnitude smaller than the length *l*. The dimensions and tolerances of the plate are illustrated in the engineering drawing of Figure 17.

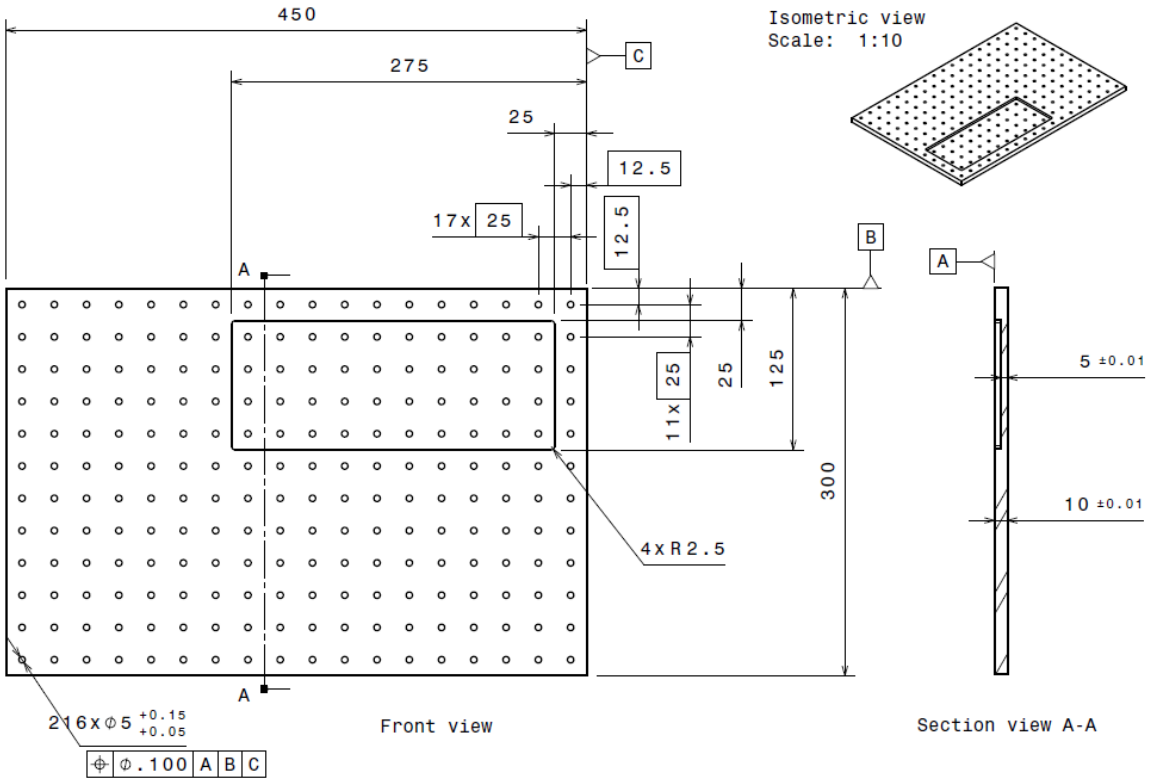

Figure 17: Engineering drawing of asymmetric aluminium plate with holes

SPECIFICATIONS AND RESULTS

The material parameters used for the calculation are (Al 7075) [29]

$$E = 71.7\ GPa \tag{96}$$

$$\rho = 2810\ kgm^{-3} \tag{97}$$

$$\upsilon = 0.33 \tag{98}$$

Discretization is a quad mesh with mid-side nodes. The converged mesh is illustrated in Figure 18.

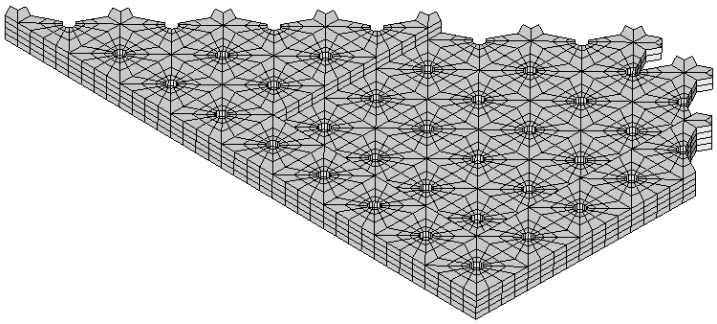

Figure 18: Zoom in on mesh of plate

First eigenfrequency is 207 *Hz*; the comprehensive torsion mode shape is illustrated in Figure 19.

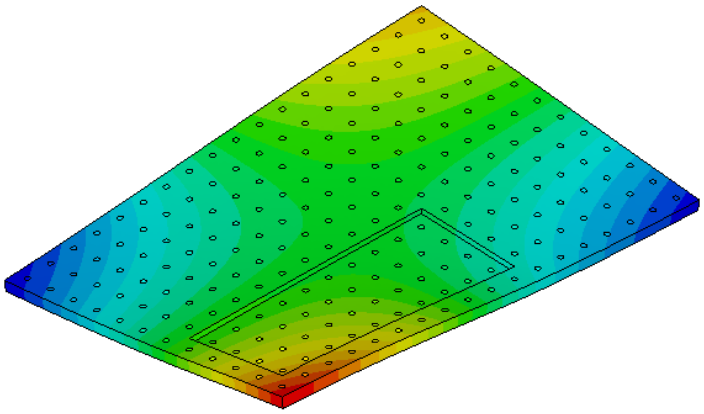

Figure 19: First flexible mode shape (207 *Hz*)

All other eigenfrequencies and mode shapes are listed in the appendix 5.2. All the eigenfrequencies are well separated and the first eigenfrequency is just above 200 *Hz* as preferred.

The driving point frequency response functions of all the theoretical measurement locations are plotted in Figure 20. In this figure you can see the separation of the eigenfrequencies. Preferably these could have been separated a bit more, however these frequency response functions will change significantly when the slave structures are mounted on the plate.

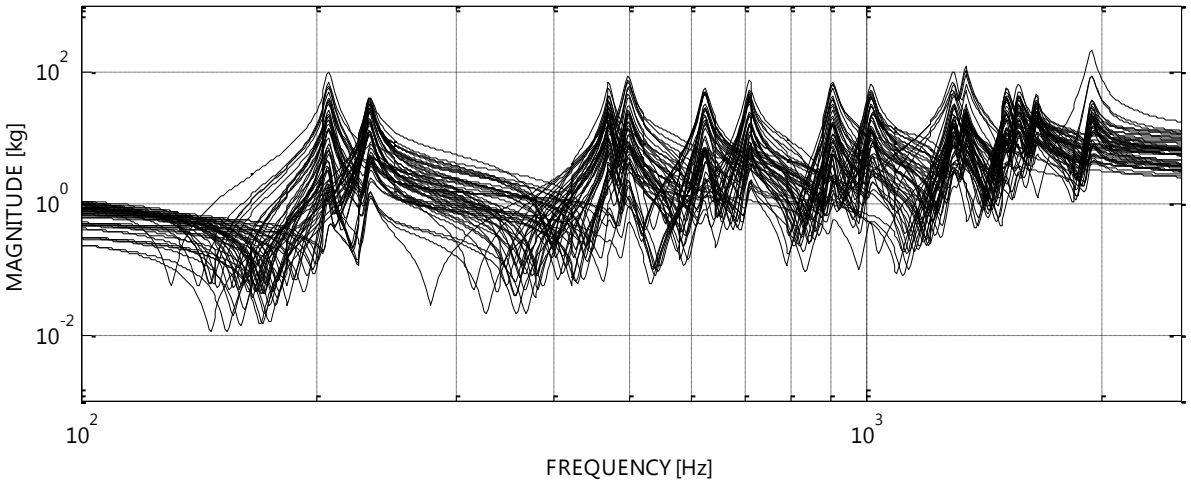

Figure 20: Driving point frequency response functions of the plate

3.2.2.2 SLAVE STRUCTURES

For the representation of rigid and compliant slave structures, two different parts are designed. The relatively flexible component will be referred as the sprung mass. Its design is explained in the next subsection. The rigid component will be referred as the unsprung mass. The design should be very similar to the sprung mass design regarding its mass and inertia properties felt by the master structure. Its design is explained, in the second subsection.

3.2.2.2.1 SPRUNG MASS

Creating a component like a sprung mass is simple; just design a mass that is supported by a flexible structure, like a leaf spring. However, it becomes more complex when the second mode is preferably at a relatively high eigenfrequency. This requirement has arisen due to the effect that other modes will also be excited by the deformation of the mode shapes of the plate.

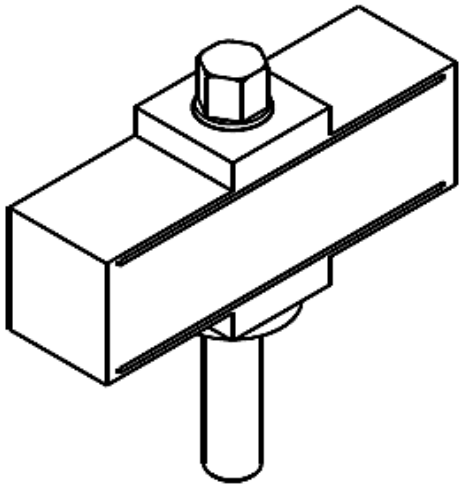

Figure 21: Sprung mass concept with two parallel leaf springs

An analytical model will become less accurate for higher frequencies. To reduce the chance of creating a bad model, possible disturbances, like inaccurately modelled higher order modes, are preferably pushed outside the frequency bandwidth of interest. Here, one way to achieve this, is by using two parallel leaf springs on a relatively large distance with respect to each other; preferably above and below the mass. The design process eventually resulted into the concept of Figure 21.

The next step is to determine the dimensions of these leaf springs and the sprung mass by hand for a rough estimation of the shape. The two leaf springs could also be assumed as four smaller leaf springs, all being rotationally constraint at both ends. The next assumption: each of these could be modelled as two cantilever beams, joined in series at their free ends. For each cantilever beam, the stiffness formula is:

$$k_{BEAM} = \frac{3EI}{L^3} \tag{99}$$

Here E is the Young's modulus, I is the area moment of inertia and L is the length of the beam. When you make all these assumptions, the stiffness of the total suspension of the mass could be seen as eight equal cantilever beams organised, like:

$$k_{LEAFS} = \underbrace{\underbrace{\underbrace{\left(k_{BEAM}^{-1} + k_{BEAM}^{-1}\right)^{-1}}_{SERIES} + \underbrace{\left(k_{BEAM}^{-1} + k_{BEAM}^{-1}\right)^{-1}}_{SERIES}}_{PARALLEL} + \underbrace{\underbrace{\left(k_{BEAM}^{-1} + k_{BEAM}^{-1}\right)^{-1}}_{SERIES} + \underbrace{\left(k_{BEAM}^{-1} + k_{BEAM}^{-1}\right)^{-1}}_{SERIES}}_{PARALLEL}}_{PARALLEL} = 2k_{BEAM} \tag{100}$$

Besides this relation, there are also some other constraints:

- High stiffness over inertia ratio for all remaining degrees of freedom
- Minimum center pin diameter, fixing the minimum sizes for the center
- Manufacturability
  - Minimum thickness of the beam
  - Minimal slit width
  - Made of steel
- Mountable with required force at plate

Knowing the required first eigenfrequency, the required sprung mass and all other constraints, the dimensions could be determined with several manual design iterations. The result is illustrated in the engineering drawing of Figure 22.

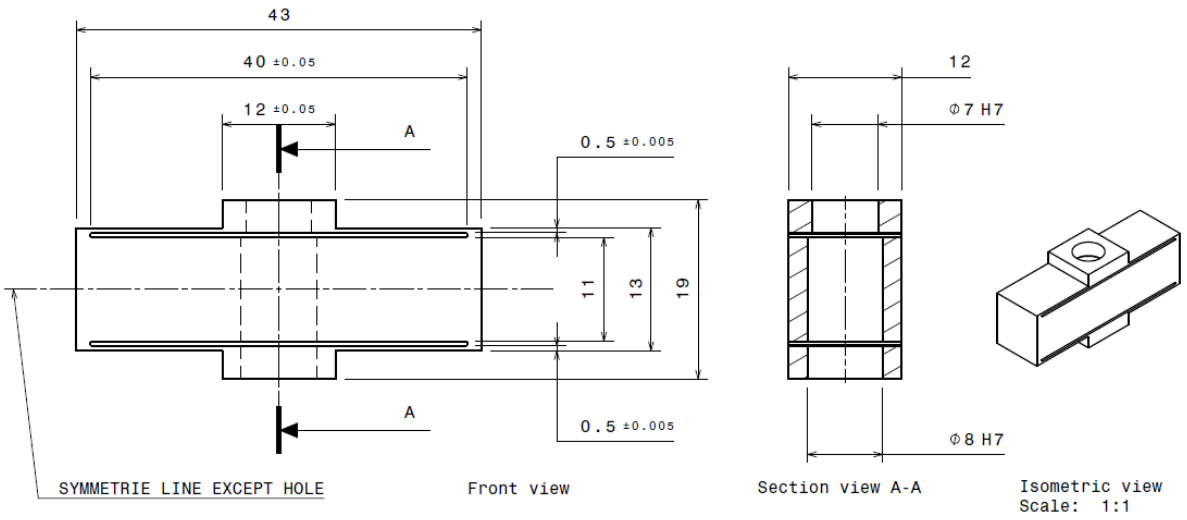

Figure 22: Engineering drawing of the sprung mass

SPECIFICATIONS AND RESULTS

The material parameters used for the calculation are (SS 304) [30]

$$E = 200\ GPa \tag{101}$$

$$\rho = 8000\ kgm^{-3} \tag{102}$$

$$\upsilon = 0.29 \tag{103}$$

The majority of the discretization is a quad mesh. All elements are with mid-side nodes. The converged mesh is illustrated in Figure 23.

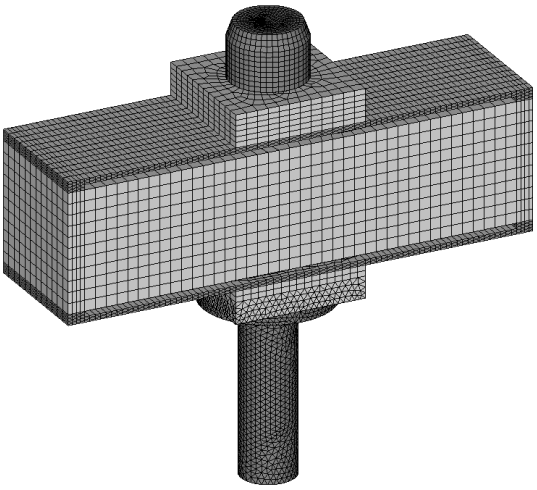

Figure 23: Mesh of sprung mass

The first two modes shapes are illustrated in Figure 24. Since the second mode was designed to be outside the frequency range of interest, higher modes are not of interest.

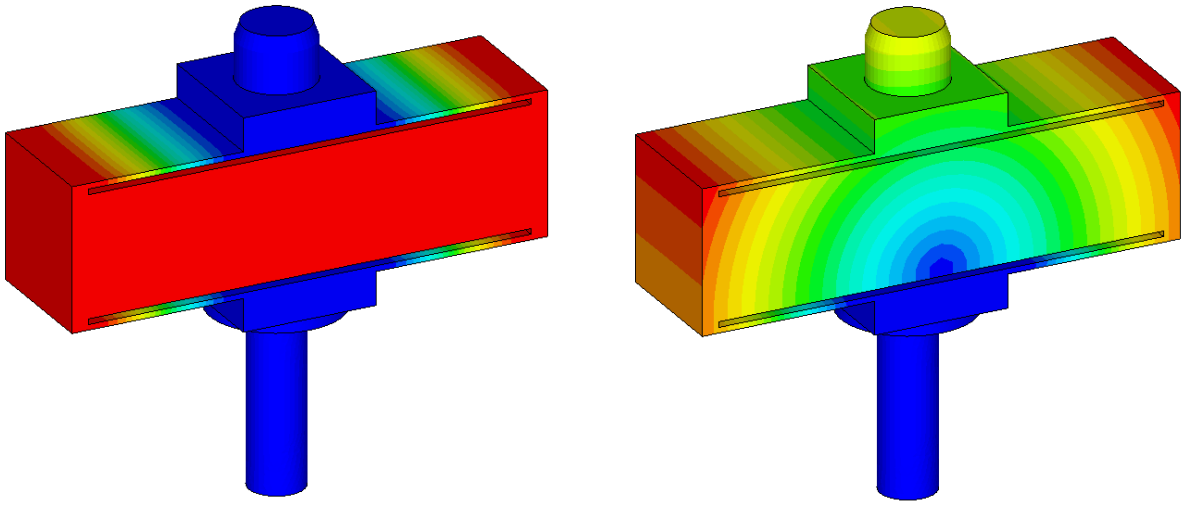

Figure 24: Summed deformation contour plots of the first (left) and second (right) mode shape of the sprung mass. The eigenfrequencies are 496 *Hz* and 2315 *Hz* respectively. No (blue) and large (red) deformation. Hence, the first mode is a mass motion in axial direction; the second mode is a rotational motion of the mass around the blue spot-axis

In the second mode shape, the center pin is deforming with the block. This means that the eigenfrequency is also depending on the stiffness, thus the diameter of this pin. There is a gap between the pin and the block, such that it is free to move.

For manufacturability reasons the sprung mass assembly is glued together at the connecting interfaces. (This change resulted in a small and therefore allowable reduction of the first two eigenfrequencies.)

Another issue is the accuracy and precision of the production of the leaf spring thickness, since the stiffness values of each leaf spring are mostly depending on that dimension. The preferred process for the production of this spring is spark erosion, because the material will not be deformed during the process.

3.2.2.2.2 UNSPRUNG MASS

The unsprung mass should have a comparative mass and inertia as the sprung mass, in order to reduce the number of variables that change when one is swapped with a sprung mass. Thus, it should also have a comparative shape and material properties.

The result is a solid block with a M5 tapped hole to mount the block on the plate. With a 12 *mm* washer, the interface with the plate also becomes similar. The resulting geometry is illustrated in the engineering drawing of Figure 25.

The modal results of this slave structure are not computed, because these would be even higher than the second eigenfrequency of the sprung mass. In this way, the resulting influence of the first mode on the global dynamic behaviour in the interesting frequency bandwidth will be neglectable.

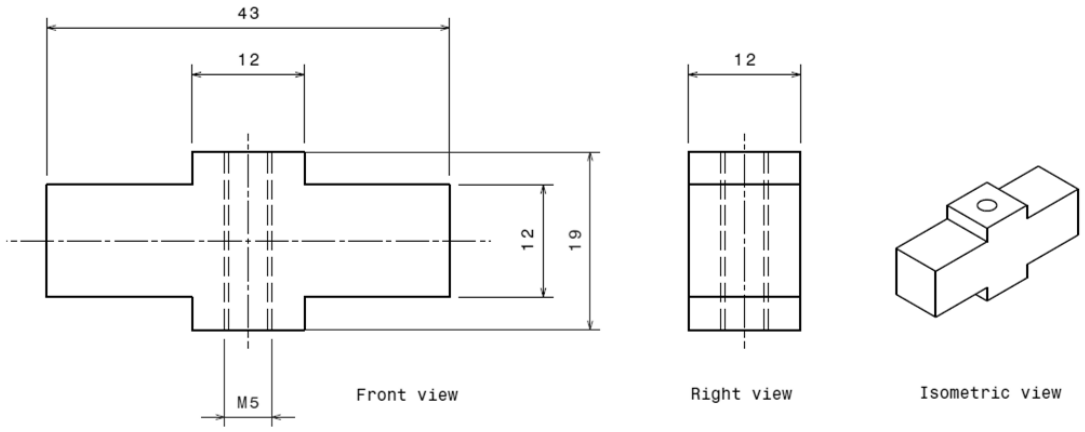

Figure 25: Engineering drawing unsprung mass

3.2.3 ANALYTICAL MODEL

For many applications small slave structures are neglected or simplified to point masses. In this study, the slave structures, the sprung and unsprung mass, are also simplified to a double mass spring system. In Figure 26 the schematic assembly of these point masses is illustrated.

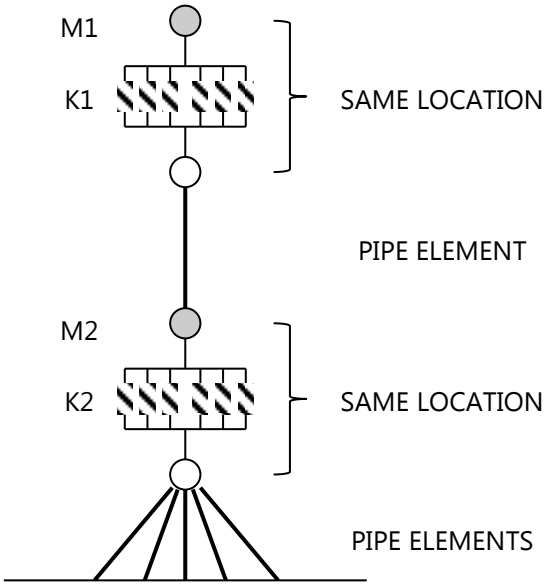

Figure 26: Lumped model of a slave structure

Shown are two masses, M1 and M2, and two sets of springs, K1 and K2. Both are defined by six degrees of freedom, three translational and three rotational coefficients. The pipe elements are ‘massless’ elements with ‘infinite’ stiffness. In the initial finite element model both sets of springs are set to an ‘infinite’ stiffness. The position of the center of mass and the inertia around it, are the only things that have to be determined, which could be done with a computer aided design (CAD) program.

For the confirmation of this simplification, both models: the full finite element model and the lumped model are mounted on top of the plate. By making use of the general validation procedure, the simplified model has been verified until 2000 *Hz*. Additional advantages of the simplified models are:

- Simple stiffness variation
- Simple programming
- Far less nodes

The positions of the slave structures on the plate are arbitrarily chosen. However, physics tells us that mass loading on a distance of the center of gravity, changes the global inertia properties of a structure quadratically over that same distance. This means: if the masses are mounted towards the edge of the plate they have relatively 'more' impact on the dynamics of the assembly than when they are mounted close to the center of gravity. This effect has to be taken into account when the slave structures will be positioned on the plate.

Equivalent points of interest are more compliant parts of the structure, because they are often more sensitive to mass loading as well.

Eventually, an arbitrary number of ten slave structures are positioned on the plate. Four of them are placed on the edge; six of them are placed in the middle and none on the thin area. The resulting analytical model used for the simulation and the experiment is illustrated in Figure 27.

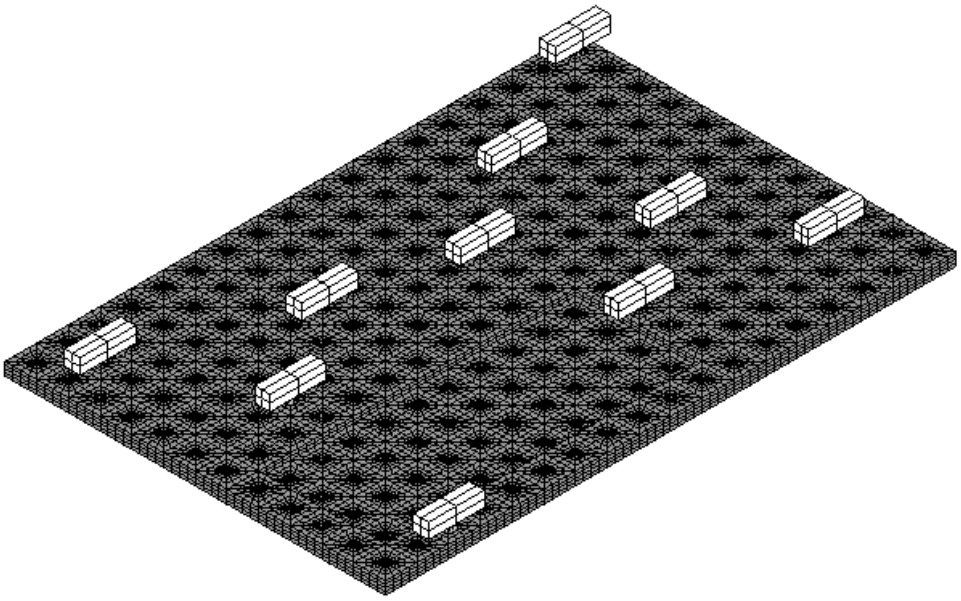

Figure 27: Analytical model of assembly

The slave structures are visualized with dummy elements with no inertia properties and an 'infinite' stiffness. They do not influence the dynamics of the assembly.

The locations of the holes in the plate and the measurement points are numbered as in Figure 28. The location of the slave structures are then represented by bordered numbers. For this assembly with all slave structures firmly fixed, the first 20 eigensolutions were determined. The computation time was approximately three minutes. See appendix 5.3 for the eigenmode figures.

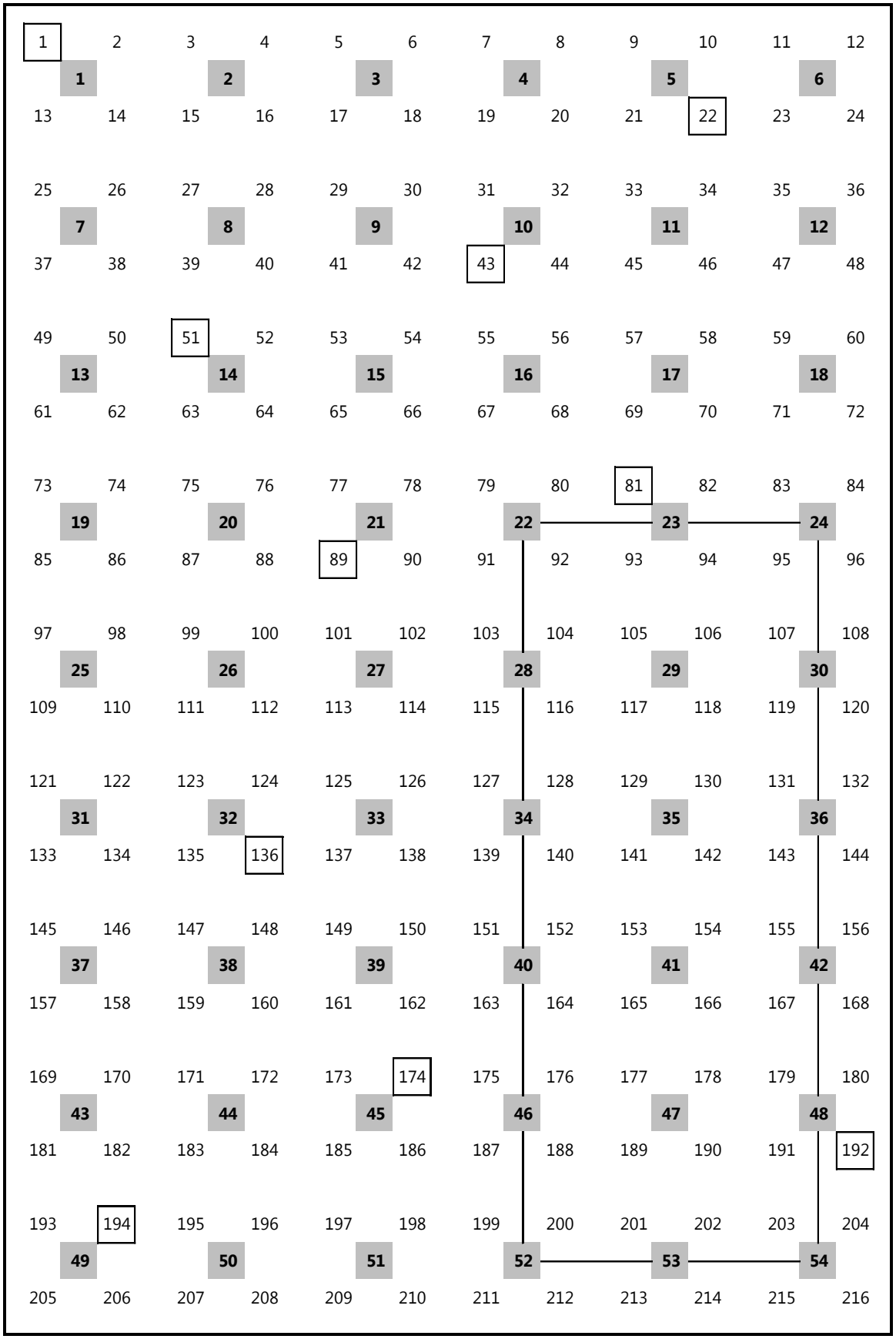

Figure 28: Measurement point (bold and shaded) and hole position numbers; bordered numbers are slave structure positions

The Auto-MAC matrix (of the first 20 modes; all measured in out-of-plane direction; up to a frequency bandwidth of approximately two kHz, see Figure 29) is determined to judge on the spatial aliasing of the mode shapes, with the arbitrarily chosen measurement locations. All the grey colours are representing a value on a linear scale from white to black, from 'zero' to 'one' respectively.

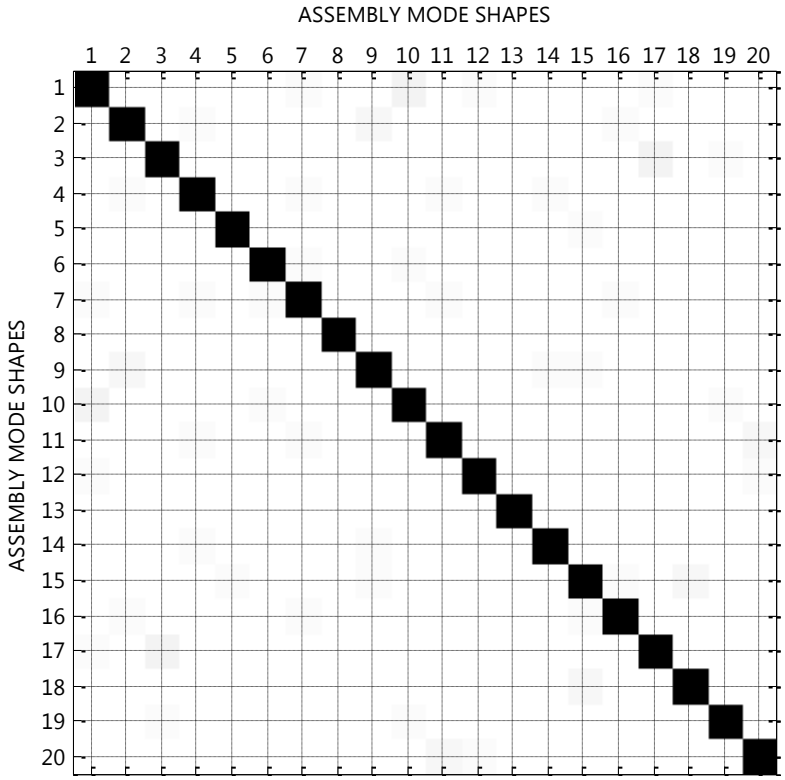

Figure 29: Auto-MAC matrix; assembly's mode shapes (in z-direction); no rigid body modes included

The values on the diagonal are all ones, simply because the vectors correlated are identical. The off-diagonal values are very low, around zero (the highest off-diagonal value is 0.06). This means: all the flexible modes are well identifiable with the chosen measurement points.

3.2.4 EXPERIMENTAL MODEL

After delivery, the first thing to do was checking the mass, the dimensions and associated tolerances of each individual part. The plate was well made except one minor thing; the pattern itself was accurately made, but its location with respect to the plate was shifted around 0.5 *mm* in one direction. This deviation will be neglected when the analytical and experimental model show satisfactory results. All the other tolerances were fine. The plate is illustrated in Figure 30.

The mass of the plate, however, was significantly lower than assumed. The manufacturer had the room to choose the type of aluminium he had available, but for the calculations the material parameters of Al 7075 were used. Thus apparently the manufacturer did use different aluminium. The solution to this: the analytical density was modified such that the mass became identical. The density that fitted was 2650 kgm^{-3}.

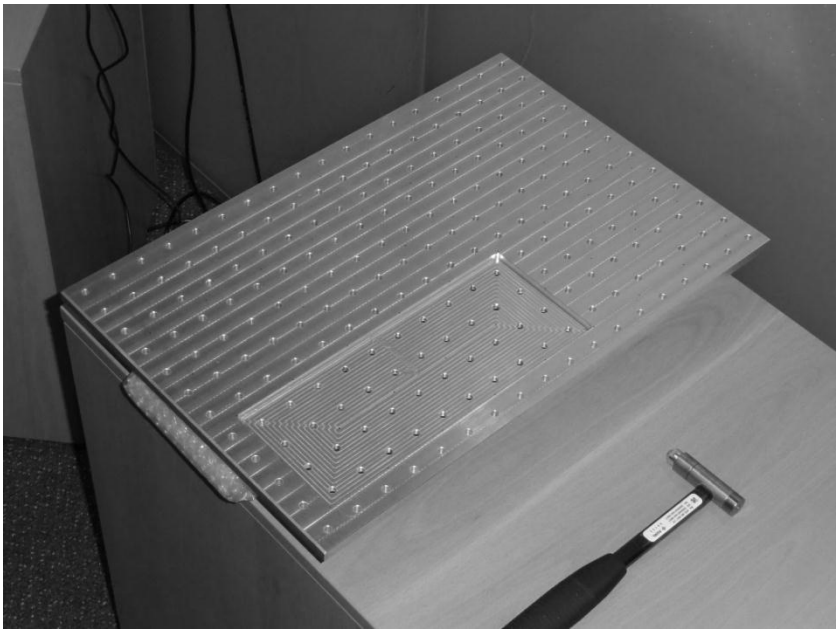

Figure 30: Photo of the plate, the hammer with load cell, the bubble foil (suspension) and the accelerometer attached with bee wax (not visible; on the back side of measurement position one)

The consequence of the previous conclusion is that the Young's-modulus will also not be as assumed, since these are often paired. To find the real value, first an experimental model of only the plate was generated with a complete roving hammer method measurement (for setup see Figure 3). These results were analysed and eventually the Young's-modulus was modified to 70 *GPa*. The results of this comparison and correlation are shown in the next section.

Next, the sprung mass; this part was made within the tolerances and its mass was similar to its mass in the analytical model. The only tolerance that could not be verified was the leaf spring thickness. The main goal of these leaf springs is creating an additional resonance frequency around 500 *Hz* when the sprung mass is mounted on the plate. This dynamic effect was checked by mounting it on position 'one', and compare and correlate the results of the associated experimental and analytical model. These results were satisfactorily; the first 14 eigenfrequencies were modelled within 1% accuracy. The physical model of the sprung mass is illustrated in Figure 31, visualizing the leaf springs.

The unsprung mass was not made as requested. The manufacturer apparently did not notice that the height of the block needed to be 12 *mm* instead of the realized 13 *mm*. Due to this error, all these unsprung masses are 3 grams (5%) heavier than intended. Since returning these parts would take too much project development time and the consequences are expected to be of minor significance for the frequency bandwidth, the error has been accepted. Another reason is that, if necessary, also the analytical model could be adapted to this difference.

Until here, all the individual parts are analysed and the information gathered could be used later on during the discussion of the results. Since all the individual parts are acceptably modelled and manufactured, the final structure to be researched could be assembled. An important factor is the rigidity of the connections to prevent occurrence of unexpected behaviour; thus the bolts and nuts are firmly fastened. The result is illustrated in Figure 32, comparative to its FEM peer of Figure 27.

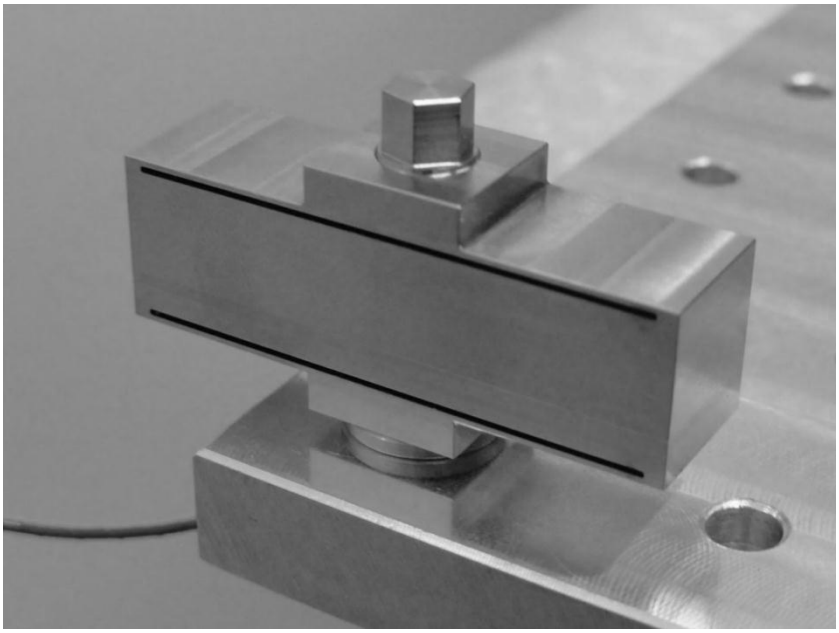

Figure 31: Slave structure - sprung mass

For the measurements a hard hammer tip was used to obtain reliable results for the required frequency bandwidth. Just three averages were taken for each measurement, since the coherence values were close to one and did not change much after each measurement. [28] This was a comfortable property which kept the total measurement time for all points to approximately two hours. The sampling frequency was set to 8192 *Hz*, the measurement block time was set to around 2 seconds. The result is a relatively fine frequency resolution of 0.5 *Hz*.

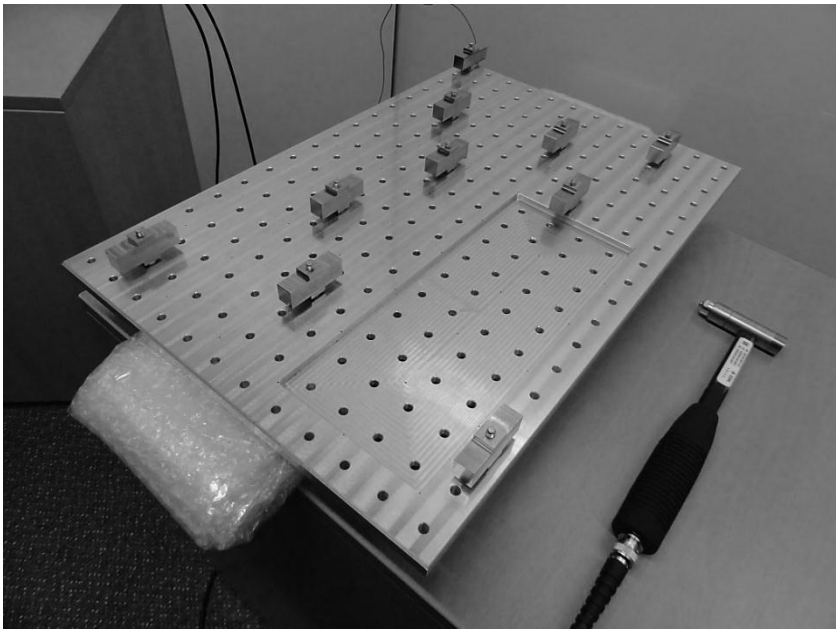

Figure 32: Experimental setup; plate with nine unsprung masses and one sprung mass; the latter located here at hole-position one [P001]

3.3 RESULTS

The procedure was tested on the structural assembly FEM model. This simulation showed that the proposed procedure was able to find the component that altered the dynamics and led to an additional mode, see appendix 5.5. (This was also true when artificial noise was added.)

In this section, the procedure was applied to an actual dynamic measurement on the test assembly with real measurement data and realistic noise. Two different configurations for the assembly were analysed. Both with the same distribution of slave structures, though in configuration I the sprung mass is located at position one [P001] and in configuration II at position eighty-nine [P089] (see Figure 28 for positions). These two assemblies represent deviating behaviour due to the sprung mass, relative to the intended design, where all slave structures are firmly fixed to the master structure. The comparison and correlation of the experimental model from the first configuration with the intended design is described in section 3.3.1. In section 3.3.2 the same procedure is applied to the second configuration in order to test whether the procedure also works for a different case.

The procedure of Figure 15 is explained in two steps. First only the connection stiffness of one component is varied. Here the actual resonating component is selected in order to obtain insight in the presented objective values (section 3.3.1.1). Subsequently the connection stiffnesses of all the slave structures are varied one by one (section 3.3.1.2). This step represents the actual correction, eigensolution recalculation and correlation procedure as proposed in section 3.1. The process and its results are discussed in section 3.3.1.3.

3.3.1 ASSEMBLY CONFIGURATION I

After satisfactory simulation results the proposed procedure was applied to an actual dynamic measurement on the test assembly, with real measurement data and realistic noise. Two different configurations for the assembly were analysed, both with the same distribution of slave structures, though a different position for the sprung mass.

In assembly configuration I: the sprung mass is located at position 'one' [P001], the results of the localization procedure are presented in this section (hence, assuming the location is unknown). To start with, the measurement data of experimental model configuration I is compared and correlated to the computed data of the intended design with the following four post analysis tools:

- FRF figures
- Eigenfrequency listing
- Mode shape plots
- *MAC*-matrix

The frequency response functions from the first row of the accelerance matrix of both models are illustrated in Figure 33. The difference between these two graphs starts around 500 *Hz* (red area). In this case, the disturbance is caused by the sprung mass at position 'one' [P001].

The differences can also be found in the listed eigenfrequencies from Figure 34. All frequencies are correlated following the highest correlation values of the *MAC* matrix. Besides the additional resonance, the frequencies of three other modes changed significantly (more than a few per cent).

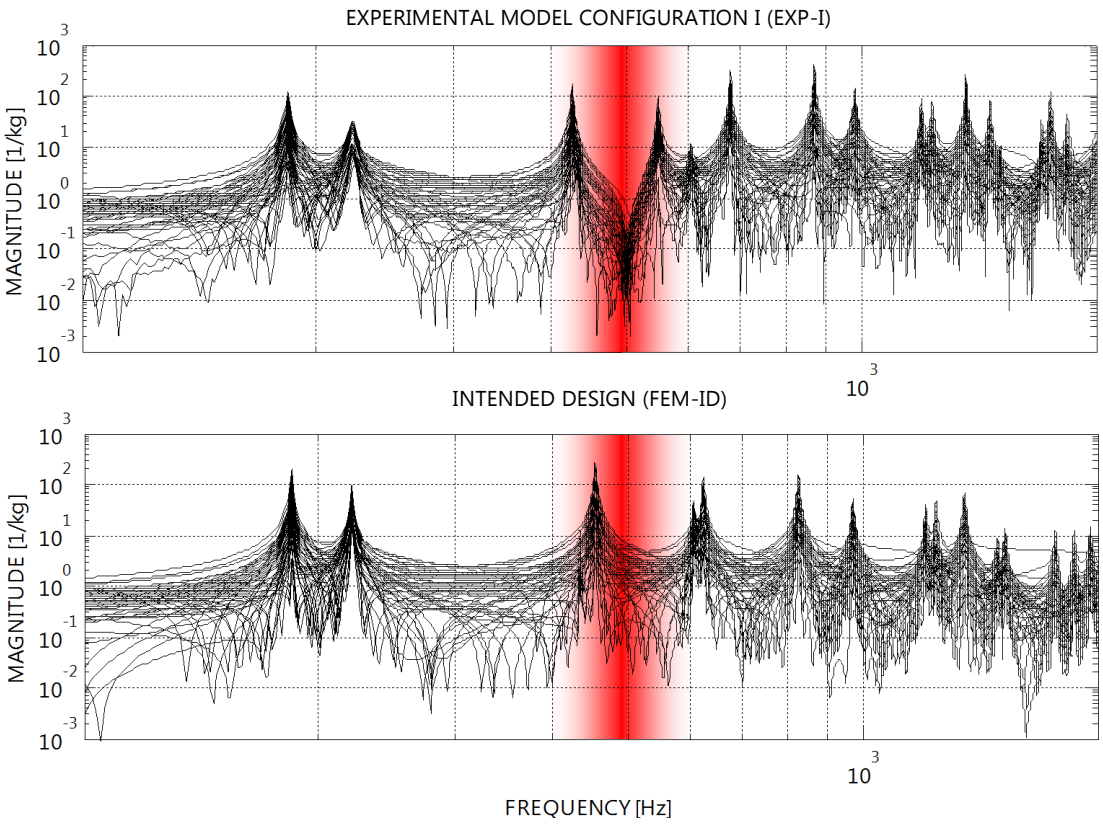

Figure 33: FRF plots; (top) experimental model configuration I (EXP-I) versus (bottom) the intended design (FEM-ID); the resonating component leads to an additional peak around 500 *Hz* in the responses of the experimental model (see red area)

MODE	FREQUENCY [*Hz*] EXP-I	FREQUENCY [*Hz*] FEM-ID	Δ FREQUENCY [%]
1	184	185	0.5
2	222	220	-0.8
3	425	433	0.3
4	432	454	8.3
5	549	607	0.4
6	605	624	-8.0
7	679	827	-5.0
8	870	971	-1.1
9	982	1203	0.7
10	1194	1242	0.7
11	1233	1350	-0.9
12	1362	1488	1.7
13	1463	1522	1.0
14	1507	1766	

Figure 34: Eigenfrequency listing; experimental model configuration I (EXP-I) versus the intended design (FEM-ID); the resonating component leads to an additional eigenfrequency around 500 *Hz* in the experimental model

A third way to see that an additional mode is present in the model with the unsprung mass, is by analysing the *MAC* matrix of these two models (see Figure 35). The diagonal has shifted (see red trend-lines) after four modes. This means that the experimental model with the unsprung mass has a mode which the analytical model does not have. To show that this is not a unique situation, you can observe a second shift (near mode 15) when the second mode starts to influence the assembly dynamics.

Note that the resonating component also created a mode order shift after two modes, however it did not change the shapes much (*MAC* values are still close to 'one').

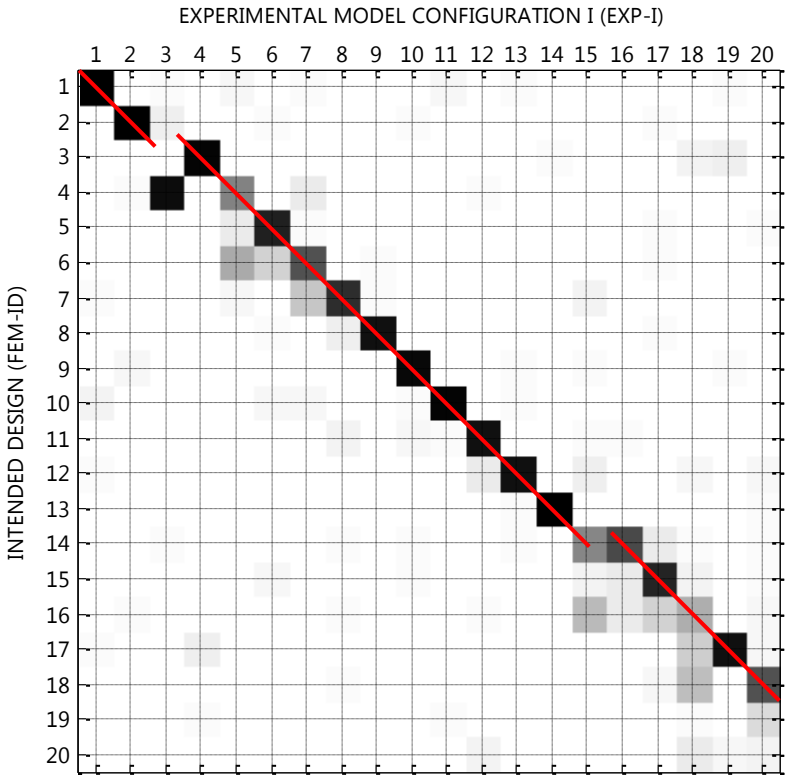

Figure 35: *MAC*-matrix; experimental model configuration I (EXP-I) versus the intended design (FEM-ID); the mode shapes only contain deformation in z-direction; also no rigid body mode correlations are included here; the red lines are trend lines

To give an indication of what the *MAC* values actually represent, the following mode pairs are illustrated in Figure 36. The experimentally identified mode shapes and the analytically computed mode shapes are plotted respectively on the left (red) and on the right (blue) side. The two mode shapes at the top represent a *MAC* value of 1.0 (resulting from the cross correlation of either model's second mode). Those at the bottom represent a *MAC* value of 0.48 (resulting from the cross correlation of the fifth mode from the experimental model, versus the fourth mode from the finite element model).

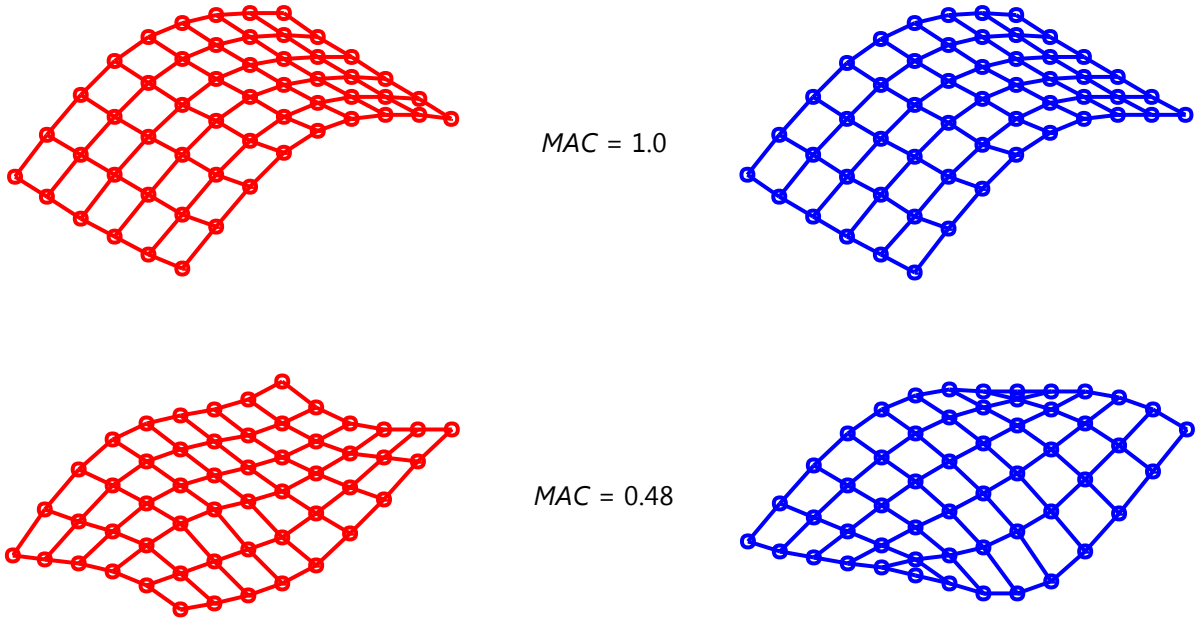

Figure 36: Mode shape plots; experimental model configuration I (EXP-I) on the left (red) versus the intended design (FEM-ID) on the right (blue); EXP-I mode shapes number two and five versus the FEM-ID mode shapes number two and four.

3.3.1.1 VARIATIONS ON INTENDED DESIGN AT SLAVE STRUCTURE [P001]

After comparing and correlating the two starting models in the previous section, it is reasonable to assume that a resonating slave structure is present (reconciliation step). In this case, the model was built up such that the model can be verified and it is thus suitable for updating purposes. (Note that this was done by including mass spring systems for small components in the FEM model.)

The next step is to modify the intended FEM design. Since one of the unsprung masses must be the disturbing sprung mass (hence, we assumed that the location of the sprung mass is unknown) the connection stiffness of each slave structure is modified with a range of connection stiffnesses, all one by one. The value around which the connection stiffnesses of the sprung masses are varied is determined with:

$$k_{sm} = 2\pi f^{2} m_{sm} \tag{104}$$

The frequency f of 500 Hz is chosen, because this is the frequency where the first disturbances were encountered, see Figure 33. The sprung mass m_{sm} of 0,042 kg could be approximated by hand calculations or more accurately estimated by the modal analysis of the sprung mass. In case of the latter, the effective mass of the first mode in vibration direction gives you the desired value. In reality, you will probably not know this mass and it might differ for each slave structure. The way to deal with this, will be explained in the final discussion.

Now pick one component and assume it causes the change. Here, the unsprung mass located at position 'one' [P001] is chosen but another mass could be picked as well.

In this study, the connection stiffness is varied by 21 stiffness variations (*k* variations) to create a range of models wherein a best fit is assumed to be found. The stiffness step is chosen here such that the covered frequency domain ranges from 300 to 700 *Hz*, by steps of 20 *Hz*. From all these FEM model variations the eigensolutions are computed. The results are subsequently processed by the following two objective functions

$$J_1 = \sqrt{\frac{1}{m}\sum_{r=1}^{m}\frac{\left(\tilde{\omega}_r - \underset{\sim}{\omega}_r\right)^2}{\underset{\sim}{\omega}_r^2}} \tag{105}$$

$$J_2 = \frac{1}{m}\sum_{r=1}^{m}\left(1 - MAC_{rr}\right) \tag{106}$$

Here J_1 and J_2 are modifications of the objective functions presented in section 2.4.6.1. The scaling is adjusted, such that it becomes independent of the number of modes included. This improves the interpretability of the results. The square root in function J_1 is introduced to plot its values on a linear scale with respect to the frequency discrepancy. Hence, it becomes equal to the dimensionless root-mean-square (RMS) value of the relative modal frequency discrepancy. In addition: the objective functions are combined to one value *J* with a weighted summation, as described with the following formulation:

$$w = \frac{1}{\omega_{accuracy} m} \tag{107}$$

$$J = wJ_1 + J_2 \tag{108}$$

Here $\omega_{accuracy}$ is an arbitrary chosen reference value representing an absolute relative modal frequency discrepancy. The weighting function *w* is used here to, get a better understanding of the objective values when you interpret the figures. Namely, it goes along with a reference line *R* with which has a certain meaning. The reference line which is taken for the second objective function, is the 1/*m*-line. This line tells you that the objective values of J_2 close to this line are originating from a correlation with one zero *MAC* value on the diagonal, and all other MAC values equal to 'one' (or multiple MAC-values that have a summed deviation of 'one').

Subsequently, the eigenfrequency based objective function is weighted such that wJ_1 shares the same reference line *R*. In this case, the line has to be interpreted as the line where the dimensionless RMS value (objective value J_1) of the relative modal frequency discrepancy is equal to the arbitrarily chosen absolute relative modal frequency discrepancy $\omega_{accuracy}$.

In this study $\omega_{accuracy}$ is chosen to be 0.01 and the number of modes m = 14. The average was taken over the first 14 modes to avoid the effects of the disturbances, created by the second mode. The resulting objective values and the reference line R = 1/14 are illustrated in Figure 37. Twenty-two models are visible, the initial model on the far left and the twenty-one finite element model variations.

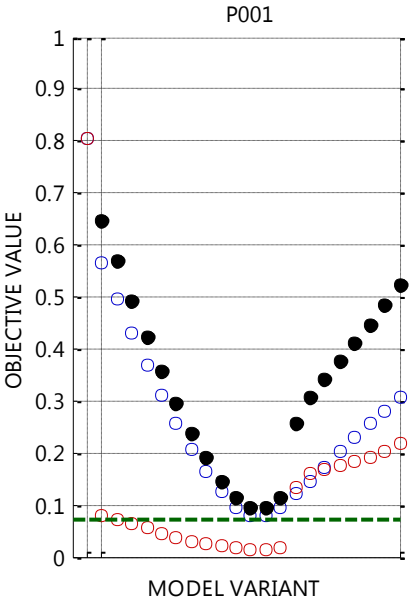

Figure 37: Objective values; experimental model configuration I (EXP-I) versus the intended design (FEM-ID) and its 21 variations at slave structure [P001]; Legend: wJ_1 (blue), J_2 (red), J (black), R (dashed green)

The following can be observed:

- Each objective function has a minimum
- Minima are all located near the same FEM model variant
- The objective values of the initial model are much higher than the minimum values of the model variations
- The lowest objective values corresponding with the best fitted model variation are created with a stiffness k = 415 kNm^{-1}, corresponding with a sprung mass with a first eigenfrequency of 500 Hz
- The minimum value for wJ_1 is close to the reference line, which means that the RMS frequency discrepancy is near one per cent
- The minimum value for J_2 = 0.01; this means that the average MAC value is approximately 0.99 for the first 14 modes
- The objective functions are nonlinear with respect to the stiffness variations
- Step in second objective function values due to mode order switching

Hereby, the post analysis process for one slave structure is explained. The same process will be applied to all the suspicious slave structures, explained in the next section.

3.3.1.2 VARIATIONS ON INTENDED DESIGN AT ALL SLAVE STRUCTURES

Since the procedure has been explained for one slave structure, it will now be applied to all slave structures. This means: for each slave structure the eigensolutions are calculated for 21 connection stiffness modifications. Hence, the total number of finite element method variations is (including the reference model)

$$n_{FEM\,variations} = n_{slaves} \cdot n_{samples} = 10 \cdot 21 = 210 \tag{109}$$

All models are automatically created with a script in ANSYS. Total computation time for all models is nine hours (less than 3 minutes per model). The modal analysis results have been treated as discussed in the previous section, resulting into Figure 38.

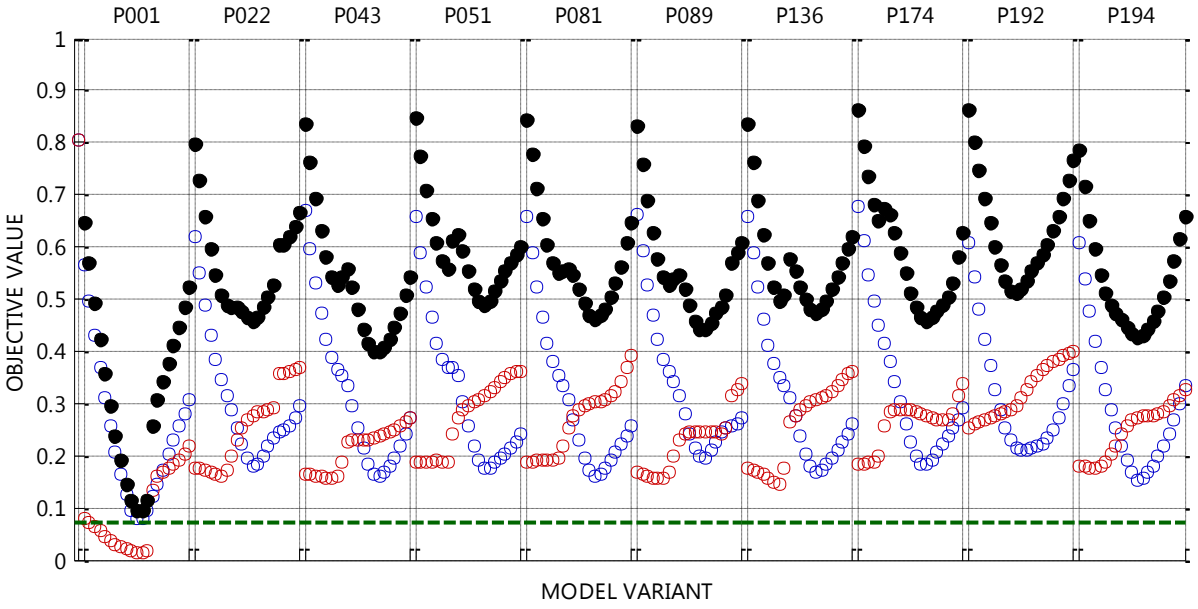

Figure 38: Objective values; experimental model configuration I (EXP-I) versus the intended design (FEM-ID) and its 21 variations at all slave structures; Location of resonating slave structure is indicated by minima for all three objective functions; Legend: wJ_1 (blue), J_2 (red), J (black), R (dashed green)

The following additional observations could be done:

- For almost all slave structures each objective function has a minimum, but the minima of wJ_1 and J_2 are not obtained with the same model variant, except for the slave structure at [P001]
- Significant difference between the minima of the sprung mass, with respect to the minima of the fixed slave structures
- Objective values are nonlinear with stiffness variations
- Clear global minimum for all objective functions at position one, hence the procedure adequately predicts that the component at position one [P001] causes the disturbance in the structural assembly dynamics

To show the resulting correlations of the procedure, below the *MAC* values and frequency discrepancies of four typical results from the objective value figure (Figure 38) are compared. Notice the differences highlighted by the red circles. Firstly the experimental model configuration I (EXP-I) is correlated with the intended design (FEM-ID): the typical observation here is the diagonal shift. Secondly, the *Auto-MAC* of (EXP-I) is shown to see where a perfect FEM model update would lead to. From the third plot could be observed that an acceptable correlation is obtained by updating the connection stiffness of slave structure [P001]. To give an indication of the differences in objective values between the best and second best fit, slave structure [P043], *MAC* values of the latter are shown in the last matrix. Here, relative chaos could be observed with respect to the third matrix. Similar conclusions could be drawn from the frequency listing (Figure 40).

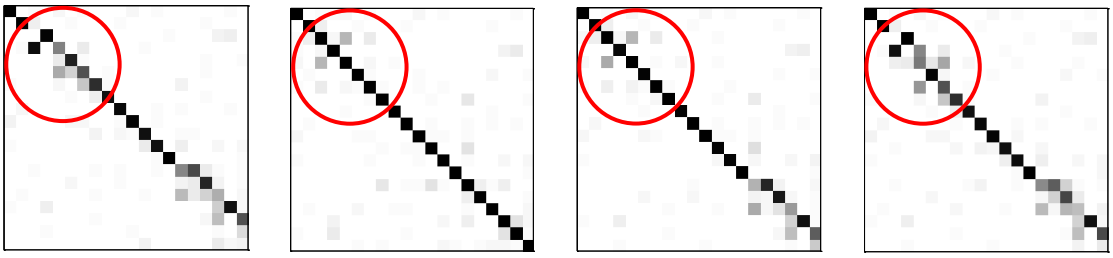

Figure 39: *MAC* tables; (a) experimental model configuration I (EXP-I) versus the intended design (FEM-ID), (b) EXP-I versus EXP-I (*Auto-MAC*), (c) EXP-I versus best fitted slave structure (see [P001]), (d) EXP-I versus second best fitted slave structure (see [P043])

MODE	Δ FREQUENCY [%] FEM-ID (a)	Δ FREQUENCY [%] FEM-P001 (c)	Δ FREQUENCY [%] FEM-P043 (d)
1	0,5	0,2	0,5
2	-0,8	-1,0	-0,8
3	1,9	-0,4	1,7
4	5,0	0,3	4,8
5	10,6	-0,9	-1,0
6	3,2	0,7	1,1
7	21,8	-0,4	-3,7
8	11,6	0,1	-5,0
9	22,5	0,2	-0,9
10	4,0	1,3	1,2
11	9,5	1,2	0,8
12	9,3	2,5	-0,4
13	4,0	1,9	1,9
14	17,2	1,0	1,0

Figure 40: Frequency listing; (a) experimental model configuration I (EXP-I) versus the intended design (FEM-ID), (c) EXP-I versus best fitted slave structure (see [P001] in Figure 38), (d) EXP-I versus second best fitted slave structure (see [P043] in Figure 38)

3.3.2 ASSEMBLY CONFIGURATION II

The proposed procedure is supposed to work for a different configuration as well. In this section, the results of configuration II are illustrated. Here, the sprung mass was mounted at position eighty-one [P089]. This location was chosen, because it is much closer to the center of gravity of the plate. Therefore, the changes in eigensolutions are expected to be less than before.

The same analysis as in section 3.3.1 will be applied to this case. Hence, the measurement data of experimental model configuration II is compared and correlated to the computed data of the intended design (FEM model with all masses firmly fixed), by the same post analysis tools.

The frequency response functions from the first row of the accelerance matrix of both models are illustrated in Figure 41. Again: the differences start around 500 *Hz* (red area).

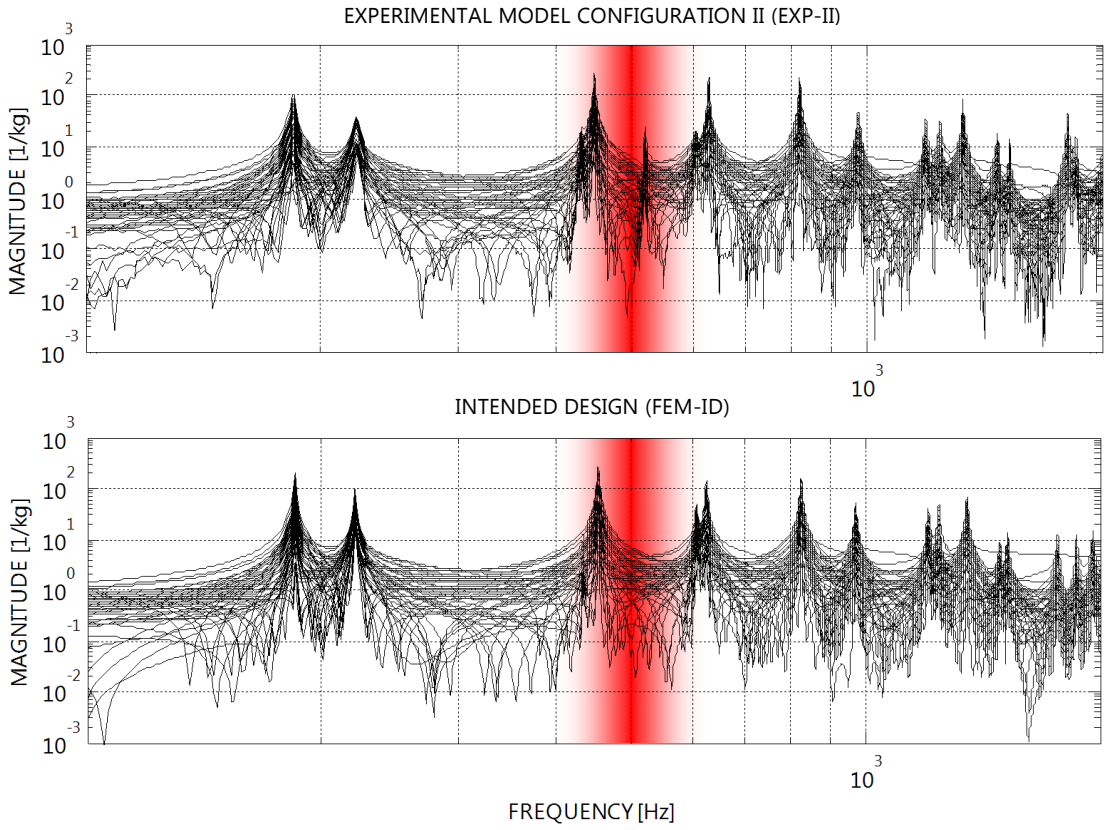

Figure 41: FRF plots; experimental model configuration II (EXP-II) versus the intended design (FEM-ID); the resonating component leads to an additional peak around 500 *Hz* in the responses of the experimental model (see red area)

Once more, the differences are also clear when the eigenfrequencies are listed (see Figure 42). All frequencies are correlated following the highest correlation values of the *MAC* table.

A third way to see that an additional mode is present in the experimental model is by analysing the *MAC* matrix of these two models (see Figure 43). Again, the diagonal has shifted (see red trend-lines) after four modes.

MODE	FREQUENCY [*Hz*] EXP-II	FREQUENCY [*Hz*] FEM-ID	Δ FREQUENCY [%]
1	184	185	0.2
2	222	220	-0.6
3	431	433	0.6
4	449	454	1.1
5	520	607	0.5
6	604	624	-0.5
7	628	827	0.7
8	821	971	-0.4
9	976	1203	1.1
10	1190	1242	0.1
11	1241	1350	1.7
12	1328	1488	1.3
13	1469	1522	-0.1
14	1523	1766	

Figure 42: Eigenfrequency listing; experimental model configuration II (EXP-II) versus the intended design (FEM-ID); the resonating component leads to an additional eigenfrequency around 500 *Hz* in the experimental model

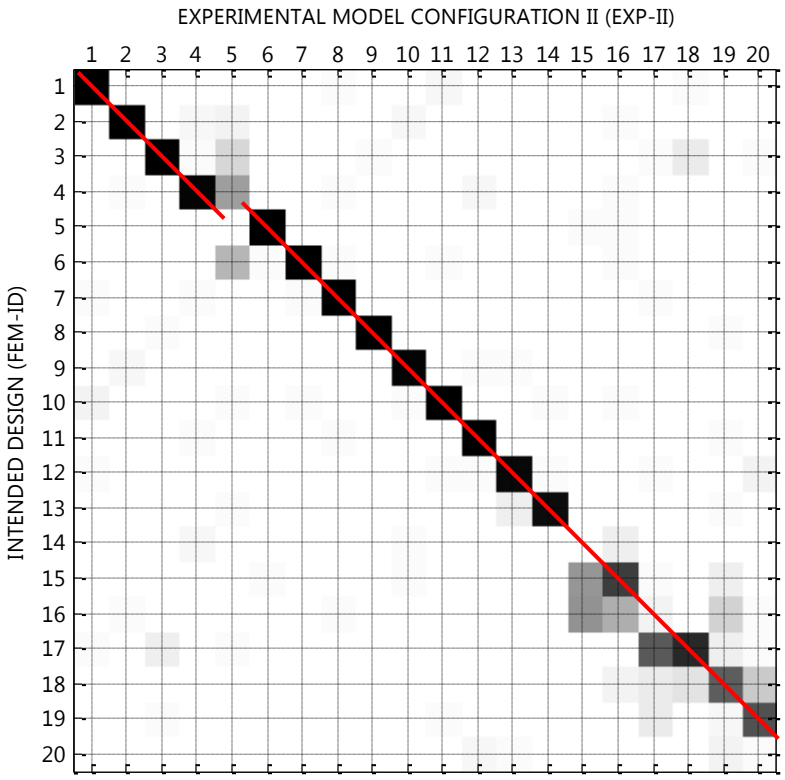

Figure 43: *MAC*-matrix; experimental model configuration II (EXP-II) versus the intended design (FEM-ID); the mode shapes only contain deformation in z-direction; also no rigid body mode correlations are included here; the red lines are trend lines

3.3.2.1 VARIATIONS ON INTENDED DESIGN AT SLAVE STRUCTURE [P089]

Almost identical conclusions can be drawn from the comparison and correlation figures from the previous section, as those from section 3.3.1. Therefore, in this section the same process has been followed as in section 3.3.1.1, applied to the second configuration. This means that the connection stiffness variations are again performed near the estimated stiffness for the actual resonating slave structure. (Thus, this time for the slave structure located at position eighty-nine [P089].) The recomputed eigensolutions are subsequently processed by the objective functions (105) and (106), resulting in Figure 44.

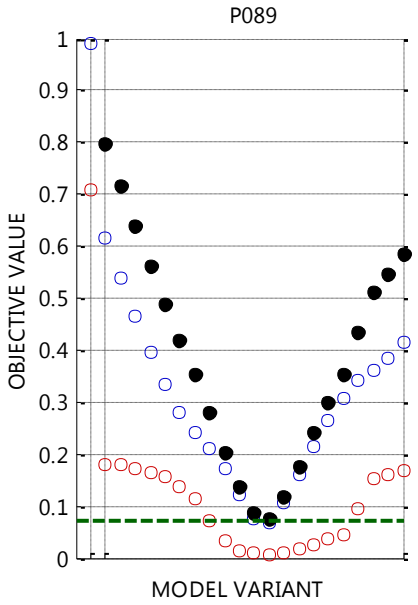

Figure 44: Objective values; experimental model configuration II (EXP-II) versus the intended design (FEM-ID) and its 21 variations at slave structure [P089]; Legend: wJ_1 (blue), J_2 (red), J (black), R (dashed green)

Similar phenomena can be observed as those described in section 3.3.1.1. Hence, in the second configuration the lowest objective values corresponding with the best fitted model variation are created with a stiffness k = 448 kNm-1, corresponding with a sprung mass with a first eigenfrequency of 520 Hz. The minimum value for J2 = 0.01; this means that the average MAC value is approximately 0.99 for the first 14 modes. Again, the RMS frequency discrepancy is near one per cent.

The best fitted model has been created with a different connection stiffness value than in the previous configuration. However, if you look at the best two fitted models, the results of both configurations included, are based on the same stiffness values. The small differences are caused by external influences (small variations in measurement setup, measurement noise). The small differences also show that the chosen stiffness resolution is sufficient.

Hereby, the post analysis process for one slave structure is explained. The same process will again be applied to all the suspicious slave structures, explained in section 3.3.2.2

3.3.2.2 (EXP) SPRUNG MASS [P089] VS. (FEM) SPRUNG MASS [P###] K-VARIATIONS

The connection stiffness is varied (k-variations) for each slave structure and all eigensolutions are calculated. All models are automatically created with a script in ANSYS. Total computation time for all models is nine hours (less than 3 minutes per model). Again, the modal analysis results are processed by the objective functions, resulting in Figure 45.

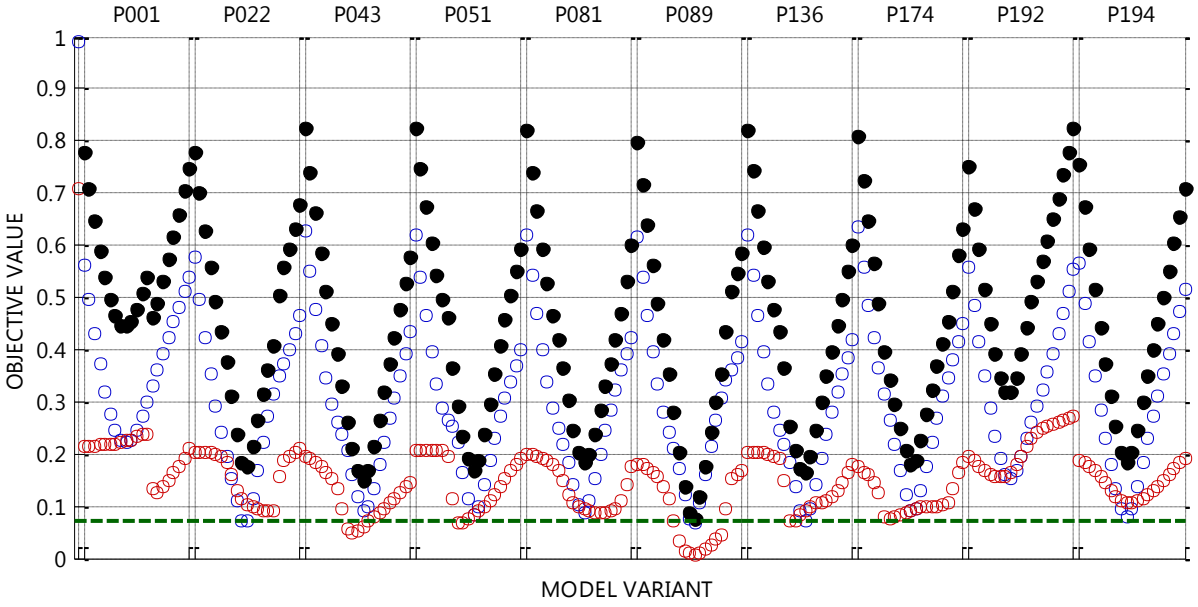

Figure 45: Objective values; experimental model configuration II (EXP-II) versus the intended design (FEM-ID) and its 21 variations at all slave structures; Location of resonating slave structure is indicated by minima for all three objective functions; Legend: wJ_1 (blue), J_2 (red), J (black), R (dashed green)

The following additional observations could be done:

- All other slave structure variants show a closer correlation with the experimental model, as in the previous configuration
- The values of objective function wJ_1 show almost no difference with these of the neighbouring slave structures, especially contrary to the values of objective function J_2
- Based on the values of objective function J_2 and J the procedure adequately predicts that the component at position eighty-nine [P089] causes the disturbance in the structural assembly dynamics

4 DISCUSSION

A procedure is proposed to localize small resonating components in a large structural assembly. It is applied to different configurations of a test setup which was specially designed and manufactured. The results illustrate a successful localization; the proposed objective function based on eigenfrequencies and MAC values proved to be a useful indicator.

A major advantage of the proposed procedure: no additional measurements are required. The entire procedure can be performed with ANSYS (or any other FEM software) in combination with MATLAB. It requires a validated FEM model of the master structure as a starting point.

For the performed tests, the positions of the slave structures were arbitrarily chosen. During the simulation, other assemblies lead to similar results. This indicates that the procedure seems robust and applicable to a wide range of assemblies.

The objective values of the sprung mass on the edge of the assembly distinguished themselves relatively more, with respect to the remaining objective values, like those near the center of gravity. This was expected since the inertia around the center of mass changes more in the first configuration, when the component resonates.

In this analysis the resonating mass was assumed to be known. In practice only the total mass of the component is known. This can be solved by a well educated guess of the sprung/unsprung mass ratio. An estimate is probably sufficient because two different masses lead to similar changes in mode shapes. The change of the assembly dynamics seems more sensitive to variations in the location, rather than the mass of the resonating component (see appendix 5.5). In principle: it is also possible to include an optimization parameter for this ratio.

During the design of the assembly, specific attention was paid to the design of the sprung mass. The goal was to isolate the effect of one additional resonance on the dynamics of the assembly. This was achieved and successfully demonstrated by the tests.

In practice, the component modes are likely to be closer together, making the reconciliation step more complex. In that case, the changes are expected to be less discrete. Though, the procedure should still work, since a partial validation of the model should be sufficient; hence, updating the model to describe the effects of the first mode from the resonating component. Therefore, only a limited number of modes have to be included.

For this study, the disturbing component is assumed to only resonate in one direction. For that reason, it is sufficient to modify only the connection stiffness in that direction. In general, the component could resonate in any direction (x, y, z, R_x, R_y, or R_z). The procedure could be extended to stiffness (and inertia) variations in multiple directions, but this would dramatically increase the number of calculations to be done. Three options exist to reduce computation time to acceptable levels.

First of all, it is possible to apply a reduction method. In this study no reduction method was applied to the master structure, because the model had an acceptable amount of nodes. For larger models reduction techniques can reduce computation time with orders of magnitude, see section 2.2.4.

Secondly, the number of variation directions per component can be reduced (to less than six), either by reasoning or by a sensitivity study. For example, in case of a component attached to a local plate structure, the out-of-plane direction will probably be dominant and may be representative for other directions as well.

A third solution would be to apply an optimization algorithm that searches the minimum of the objective function. However, this may be difficult since the objective functions are nonlinear with respect to the connection stiffness.

In literature, comparable studies can be found focussing on localizing structural deficiencies in large structures. These aimed to find structural weaknesses in the master structure, for example broken bridge elements. In this study, it is assumed that the master structure is intact and the disturbances are caused by relatively small slave structures which are mounted on top. An alternative procedure is proposed. It seems promising, since it proved to be successful when applied to a simplified structure. Several options have been proposed to further improve the procedure and to make it applicable for high tech industry. The procedure may help during troubleshooting, if structural dynamic issues are encountered when assembly steps of prototypes are monitored. Thus, it may contribute in the development of complex machines like the lithography machines at ASML.

4.1 RECOMMENDATIONS

The complexity of the investigated structural assembly could be increased in further researches, since the procedure proved to be robust. Two interesting follow-up researches are proposed:

In the first place, the extension of the research for multiple resonance directions; hence, what lumped model is a sufficient general representation for a resonating component.

Secondly, the application of the procedure in case multiple components disturb the dynamics of the assembly. Hence, describe typical properties of this phenomenon and discuss the differences with one resonating component containing multiple disturbing modes.

5 APPENDIX

The appendix provides additional information and explanation to the main text.

5.1 CONSTRUCTION OF BOOLEAN MATRICES

This appendix illustrates the construction of the Boolean matrices **B** and **L**. [10] To this end, the general system shown in Figure 46 is considered: this figure schematically shows the coupling of two general substructures.

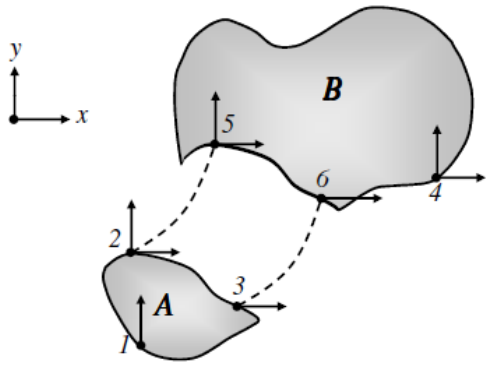

Figure 46: Coupling of two general substructures A and B

Both substructures consist of three nodes; substructure *A* has 4 DOF, whereas substructure *B* holds 5 DOF. In this example, nodes 2 and 3 of substructure *B* are coupled to nodes 5 and 6 of substructure *B*, respectively. And so, three compatibility conditions should be satisfied:

$$\begin{cases} u_{2x} = u_{5x} \\ u_{2y} = u_{5y} \\ u_{3x} = u_{6x} \end{cases} \tag{110}$$

To express this condition as in **Bu** = **0**, the signed Boolean matrix **B** must be constructed. The total vector of degrees of freedom **u** is:

$$\mathbf{u} = \begin{bmatrix} u_{1y} & u_{2x} & u_{2y} & u_{3x} & u_{4x} & u_{4y} & u_{5x} & u_{5y} & u_{6x} \end{bmatrix}^T \tag{111}$$

The signed Boolean matrix **B** is now found as:

$$\mathbf{B} = \begin{array}{c} \begin{matrix} u_{1y} & u_{2x} & u_{2y} & u_{3x} & u_{4x} & u_{4y} & u_{5x} & u_{5y} & u_{6x} \end{matrix} \\ \begin{bmatrix} 0 & 1 & 0 & 0 & 0 & 0 & -1 & 0 & 0 \\ 0 & 0 & 1 & 0 & 0 & 0 & 0 & -1 & 0 \\ 0 & 0 & 0 & 1 & 0 & 0 & 0 & 0 & -1 \end{bmatrix} \end{array} \tag{112}$$

Every coupling term or, equivalently, every compatibility condition corresponds to a line in the Boolean matrix **B**. Therefore, in the general case where the coupled substructures comprise *n*

degrees of freedom of which *m* are coupled interface DOF, the matrix **B** has size *m* x *n*. In this example, *n* = 9 and *m* = 3; the size of B is *3* x *9*. It can easily be seen that the condition **Bu** = **0** is equivalent to the three compatibility equations in (111).

From this signed Boolean matrix, the Boolean localization matrix **L** is found by computing its null space. In this example, this gives

$$\mathbf{L} = \begin{bmatrix} 1 & 0 & 0 & 0 & 0 & 0 \\ 0 & 0 & 0 & 1 & 0 & 0 \\ 0 & 0 & 0 & 0 & 1 & 0 \\ 0 & 0 & 0 & 0 & 0 & 1 \\ 0 & 1 & 0 & 0 & 0 & 0 \\ 0 & 0 & 1 & 0 & 0 & 0 \\ 0 & 0 & 0 & 1 & 0 & 0 \\ 0 & 0 & 0 & 0 & 1 & 0 \\ 0 & 0 & 0 & 0 & 0 & 1 \end{bmatrix} \tag{113}$$

The set of unique interface DOF that is chosen for this example, is found as:

$$\mathbf{q} = \begin{bmatrix} u_{1y} & u_{4x} & u_{4y} & u_{5x} & u_{5y} & u_{6x} \end{bmatrix}^T \tag{114}$$

The Boolean matrix **L** transforms this unique set of degrees of freedom to the total set of DOF:

$$\mathbf{u} = \mathbf{L}\mathbf{q} = \begin{bmatrix} u_{1y} \\ u_{5x} = u_{2x} \\ u_{5y} = u_{2y} \\ u_{6x} = u_{3x} \\ u_{4x} \\ u_{4y} \\ u_{5x} \\ u_{5y} \\ u_{6x} \end{bmatrix} = \begin{bmatrix} 1 & 0 & 0 & 0 & 0 & 0 \\ 0 & 0 & 0 & 1 & 0 & 0 \\ 0 & 0 & 0 & 0 & 1 & 0 \\ 0 & 0 & 0 & 0 & 0 & 1 \\ 0 & 1 & 0 & 0 & 0 & 0 \\ 0 & 0 & 1 & 0 & 0 & 0 \\ 0 & 0 & 0 & 1 & 0 & 0 \\ 0 & 0 & 0 & 0 & 1 & 0 \\ 0 & 0 & 0 & 0 & 0 & 1 \end{bmatrix} \cdot \begin{bmatrix} u_{1y} \\ u_{4x} \\ u_{4y} \\ u_{5x} \\ u_{5y} \\ u_{6x} \end{bmatrix} \tag{115}$$

In addition, the Boolean localization matrix **L** describes the force equilibrium naturally as well:

$$\mathbf{L}^T\mathbf{g} = \begin{bmatrix} 1 & 0 & 0 & 0 & 0 & 0 & 0 & 0 & 0 \\ 0 & 0 & 0 & 0 & 1 & 0 & 0 & 0 & 0 \\ 0 & 0 & 0 & 0 & 0 & 1 & 0 & 0 & 0 \\ 0 & 1 & 0 & 0 & 0 & 0 & 1 & 0 & 0 \\ 0 & 0 & 1 & 0 & 0 & 0 & 0 & 1 & 0 \\ 0 & 0 & 0 & 1 & 0 & 0 & 0 & 0 & 1 \end{bmatrix} \begin{bmatrix} 0 \\ g_{2x} \\ g_{2y} \\ g_{3x} \\ 0 \\ 0 \\ g_{5x} \\ g_{5y} \\ g_{6x} \end{bmatrix} = \begin{bmatrix} 0 \\ 0 \\ 0 \\ g_{2x} + g_{5x} \\ g_{2y} + g_{5y} \\ g_{3x} + g_{6x} \end{bmatrix} = \mathbf{0} \tag{116}$$

To satisfy the equilibrium condition, the connection forces on dual degrees of freedom must thus sum to zero. There is another way to obtain the matrix **L** from **B**, see literature. [10]

5.2 PLATE MODES

In this appendix the computed plate modes are visualized. It is clear that no symmetric modes have been found.

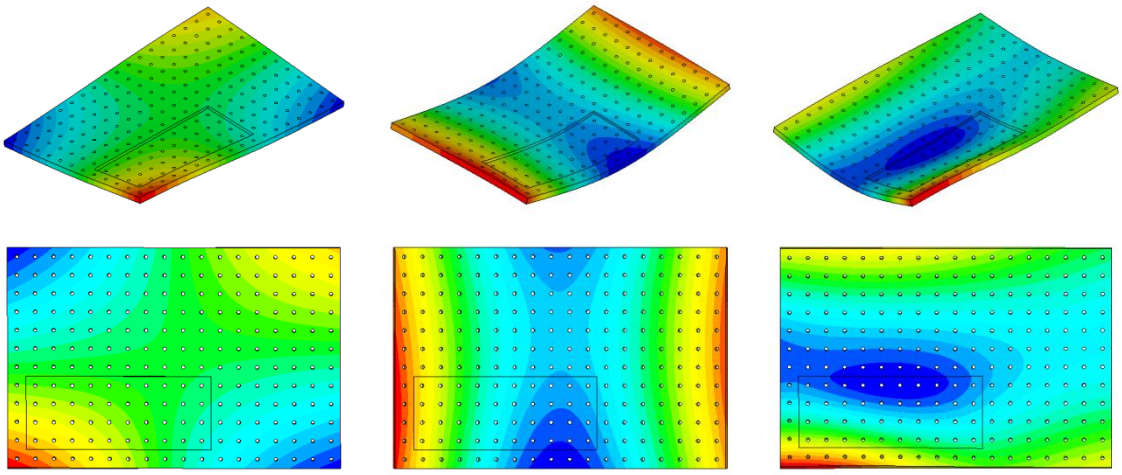

Mode 1 (211 *Hz*) Mode 2 (237 *Hz*) Mode 3 (479 *Hz*)

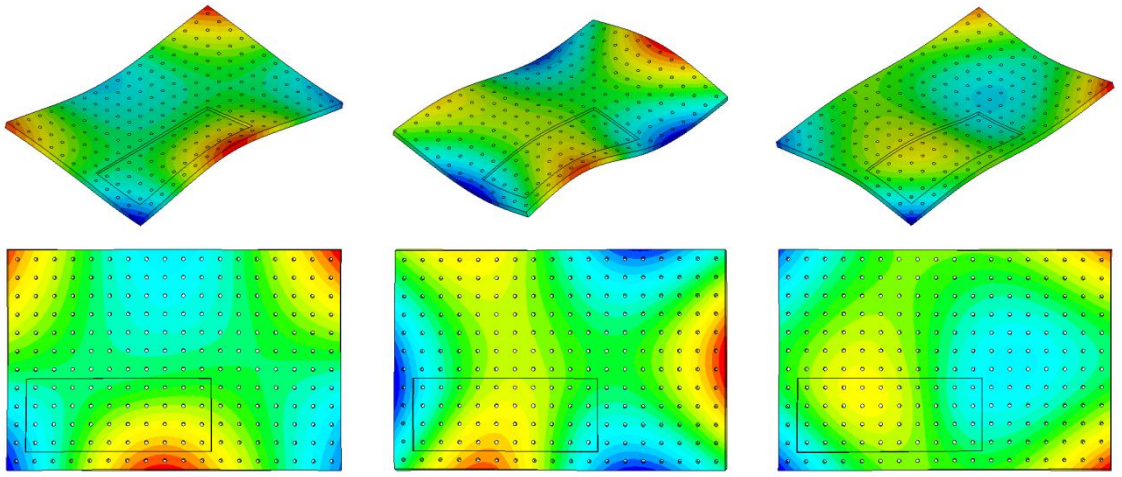

Mode 4 (506 *Hz*) Mode 5 (633 *Hz*) Mode 6 (720 *Hz*)

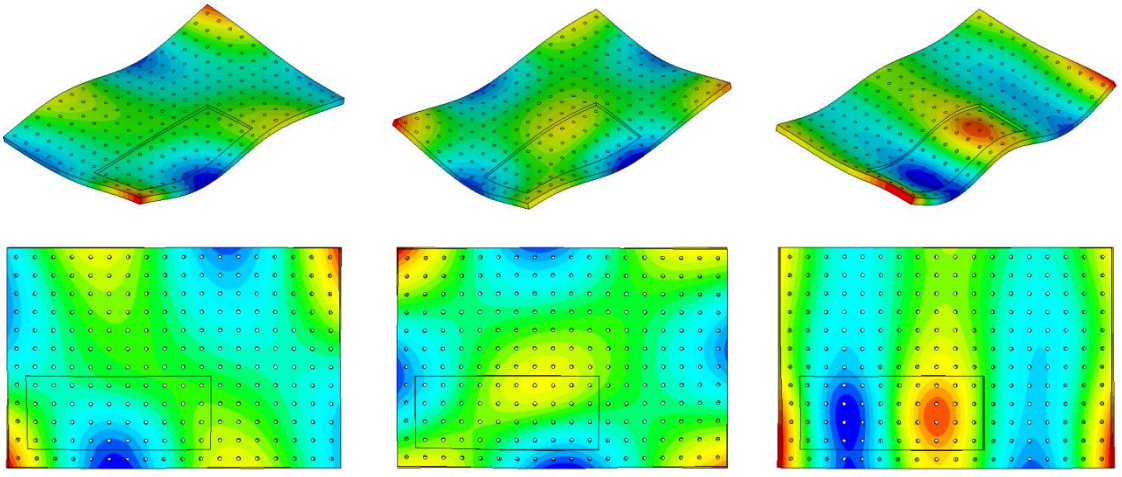

Mode 7 (922 *Hz*) Mode 8 (1032 *Hz*) Mode 9 (1313 *Hz*)

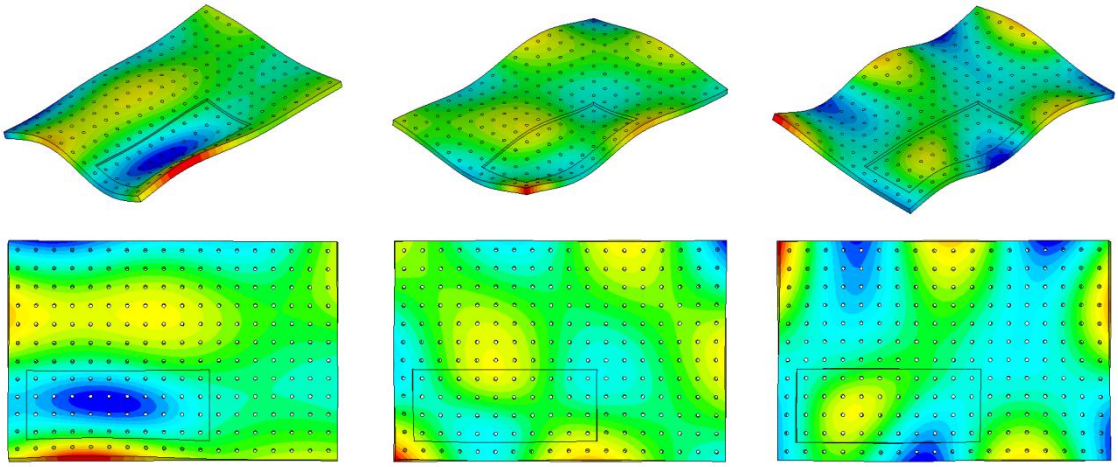

Mode 10 (1360 *Hz*) Mode 11 (1536 *Hz*) Mode 12 (1588 *Hz*)

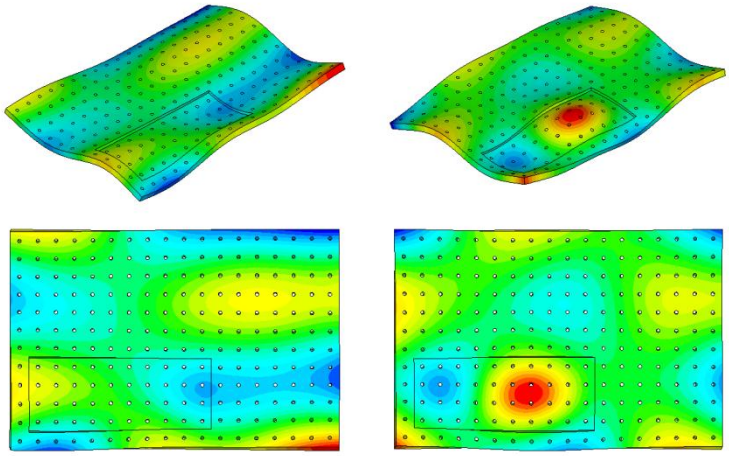

Mode 13 (1669 *Hz*) Mode 14 (1966 *Hz*)

5.3 ASSEMBLY MODES

In this appendix the computed assembly modes are visualized.

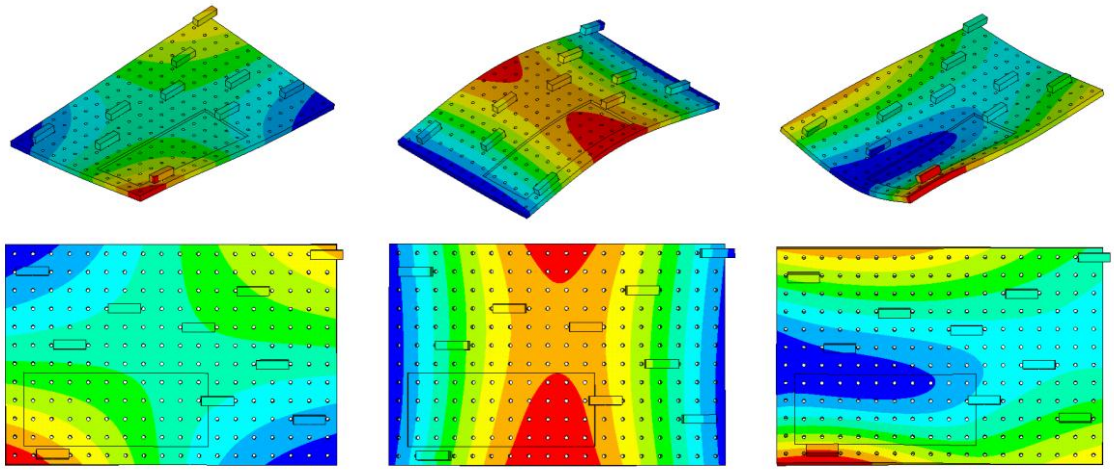

Mode 1 (185 *Hz*) Mode 2 (220 *Hz*) Mode 3 (433 *Hz*)

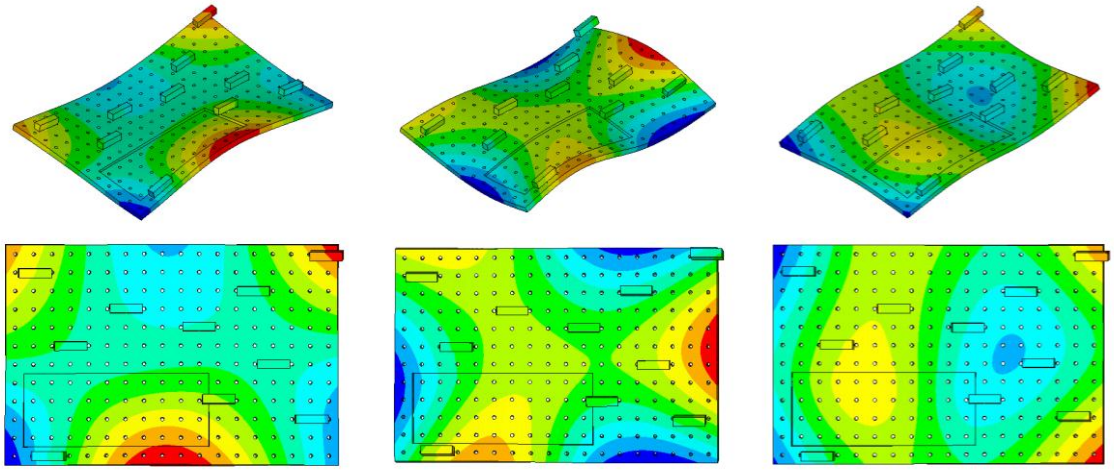

Mode 4 (454 *Hz*) Mode 5 (607 *Hz*) Mode 6 (624 *Hz*)

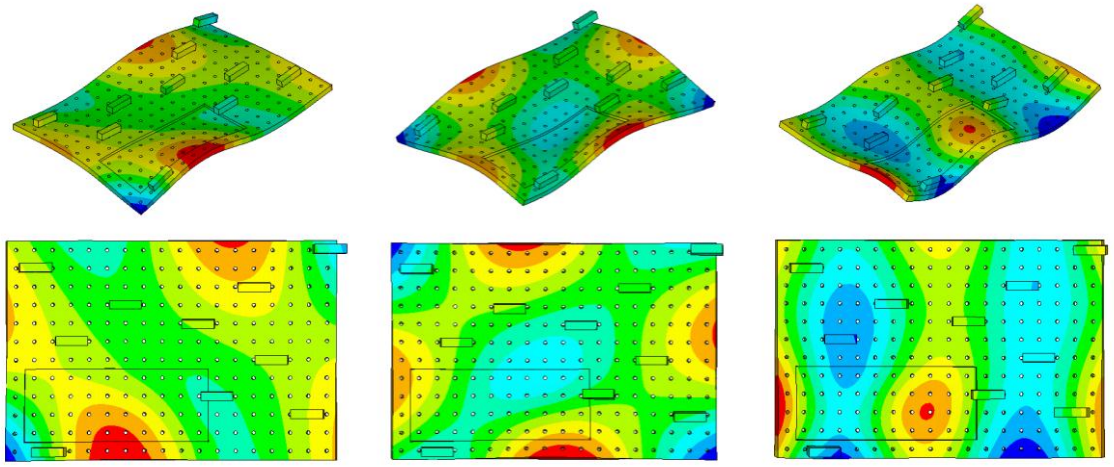

Mode 7 (826 *Hz*) Mode 8 (971 *Hz*) Mode 9 (1203 *Hz*)

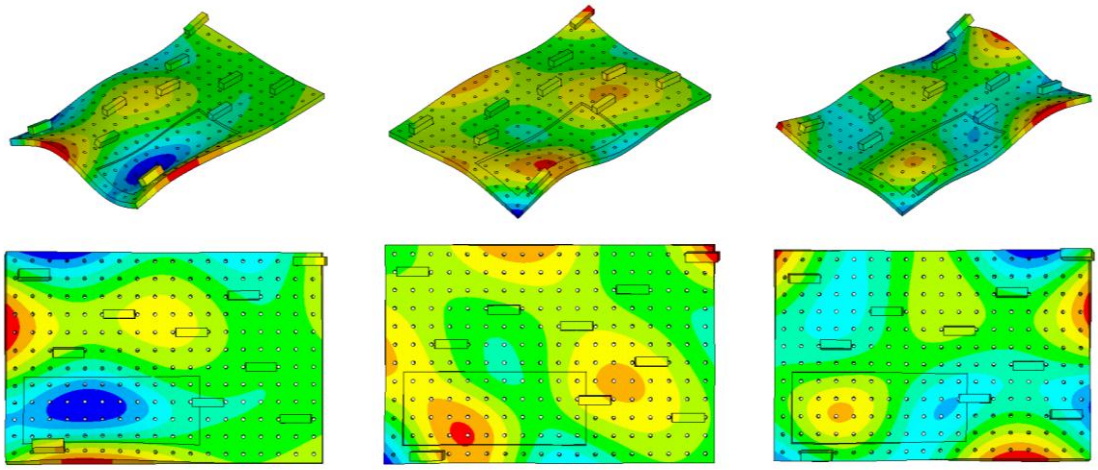

Mode 10 (1242 *Hz*) Mode 11 (1350 *Hz*) Mode 12 (1488 *Hz*)

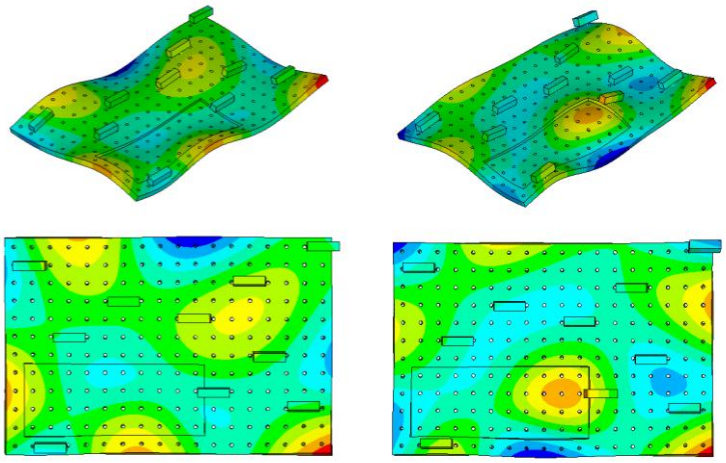

Mode 13 (1522 *Hz*) Mode 14 (1766 *Hz*)

5.4 SUSPENSION

In this appendix, the required suspension stiffness is estimated for a certain maximum measurement error of the eigenfrequencies. The suspension of the plate could be bubble foil or springs, attached to the roof. For example, to achieve an error smaller than 0.1%, the suspension should have a maximum stiffness of around: [31]

$$\Delta f = f_m - f_t = 0.1\ \%$$
$$f_s = \sqrt{\left(f_m^2 - f_t^2\right)} = 9\ Hz$$
$$k_s = \left(2\pi f_s\right)^2 m = 12\ kNm^{-1}$$

Note that for these calculations the mass m and target frequency f_t of the solid plate is used. The measured frequency is denoted by f_m. Hence, the support stiffness k_s should be lower than 10 kNm^{-1} to achieve that accuracy; achievable with both suspension types. However, the experimental support had an eigenfrequency of around 20 *Hz*. Its influence was around 0.5%, still low and therefore acceptable.

5.5 SIMULATION RESULTS

In this appendix, the simulated objective value figures are shown from the plate assembly. The first (Figure 47(a)) and the sixth graph (Figure 49(a)) are, as it should be, similar to Figure 38 and Figure 45 respectively. The simulated experimental model is indicated with SIM-[P###], where the number ### stands for the position of the sprung mass. The locations of the slave structures on the plate are visualized in Figure 28.

Also, the effect of estimating a wrong sprung mass is simulated. The original ratio is 3/2 for the sprung mass/unsprung mass. For the wrong sprung mass assumption, the ratio is assumed to be 2/3. Figure 51 illustrates the results of this simulation. These results can also be compared with Figure 38 and Figure 45. The conclusions are similar, making the analysis more robust.

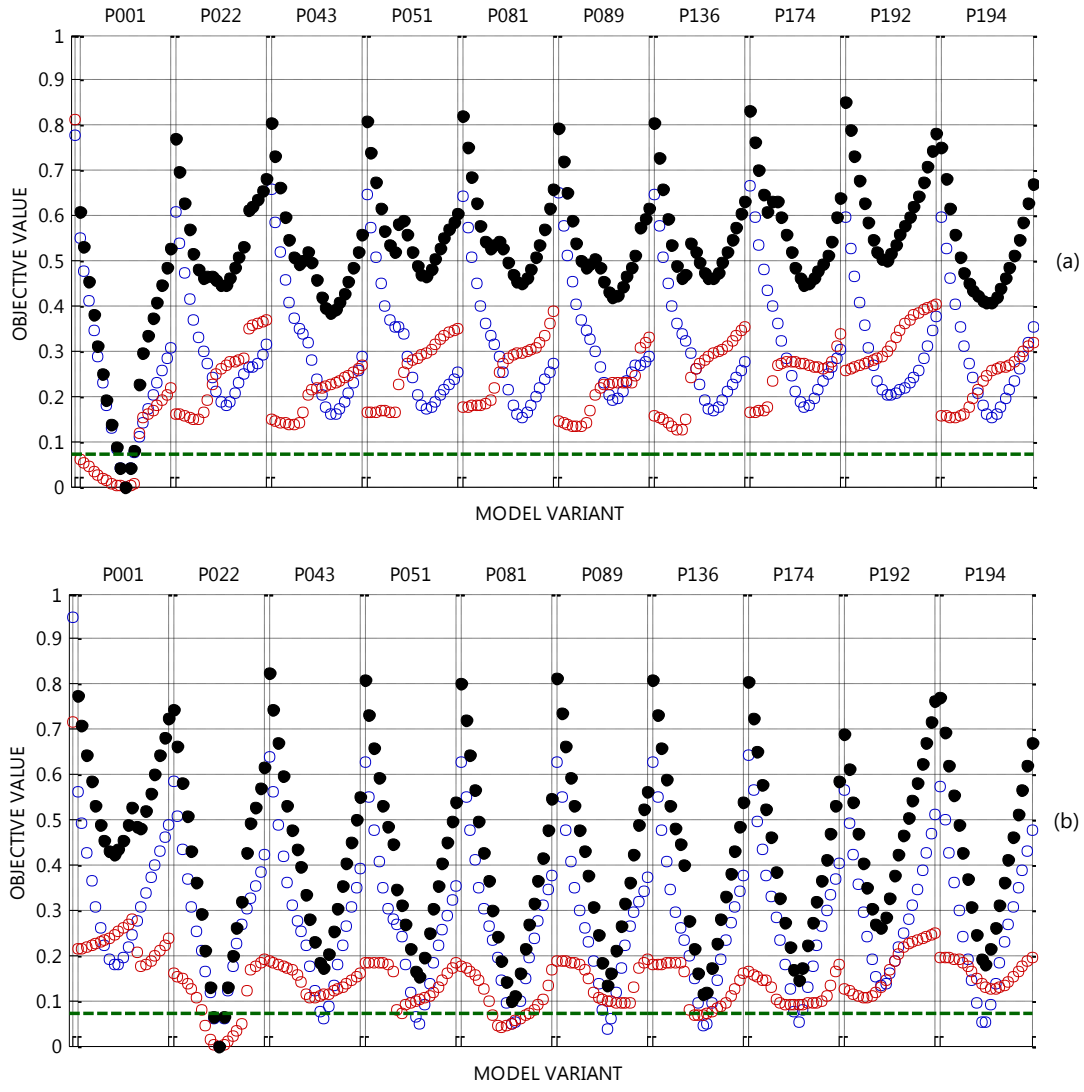

Figure 47: Objective values; (a) SIM-[P001] versus the intended design (FEM-ID) and its 21 variations at all slave structures; (b) SIM-[P022] versus FEM-ID and its 21 variations at all slave structures; Location of resonating slave structure is indicated by minima for all three objective functions;
Legend: wJ_1 (blue), J_2 (red), J (black), R (dashed green)

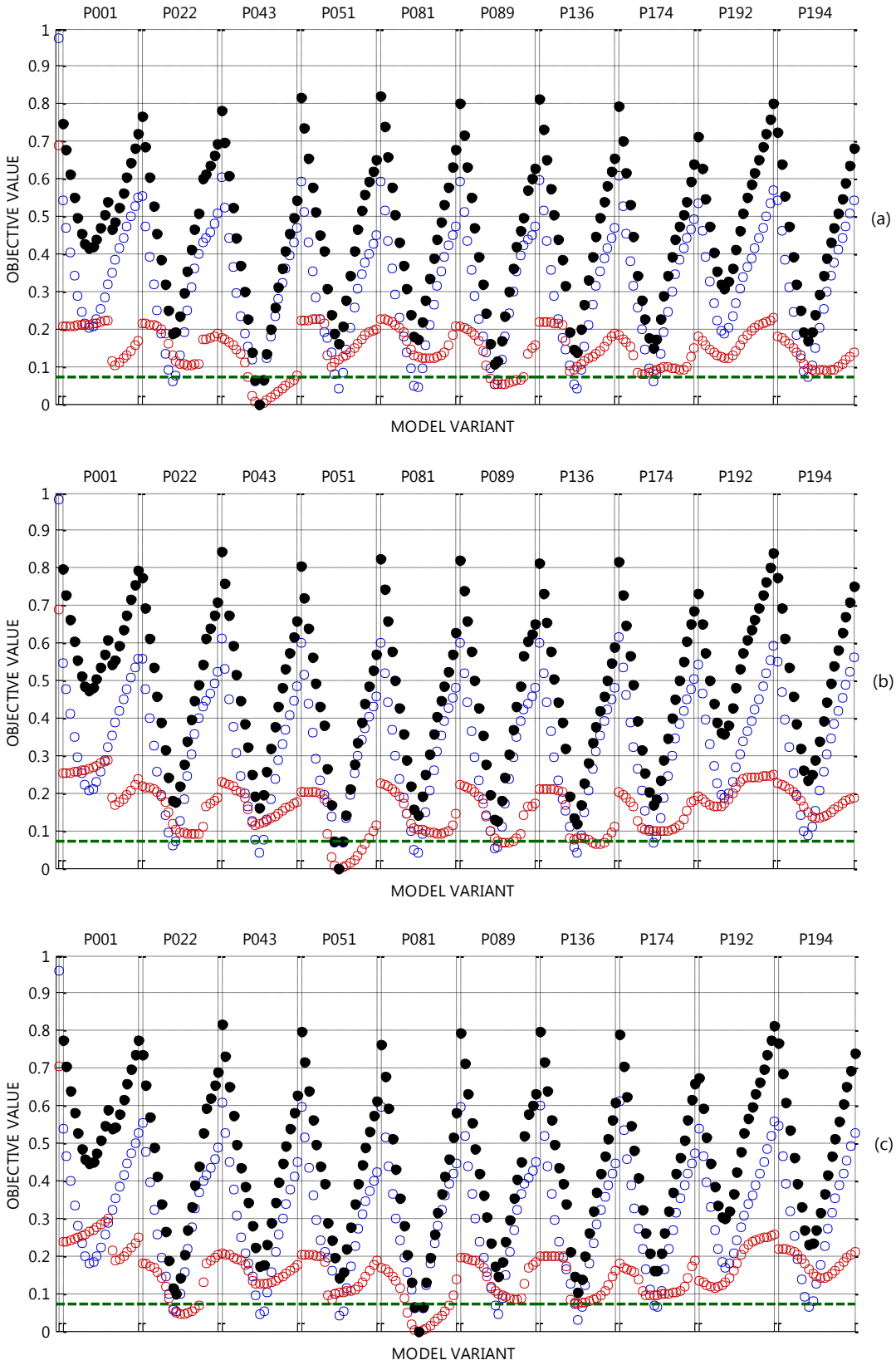

Figure 48: Objective values; (a) SIM-[P043] versus the intended design (FEM-ID) and its 21 variations at all slave structures; (b) SIM-[P051] versus FEM-ID and its 21 variations at all slave structures; (c) SIM-[P081] versus FEM-ID and its 21 variations at all slave structures; Location of resonating slave structure is indicated by minima for all three objective functions;
Legend: wJ_1 (blue), J_2 (red), J (black), R (dashed green)

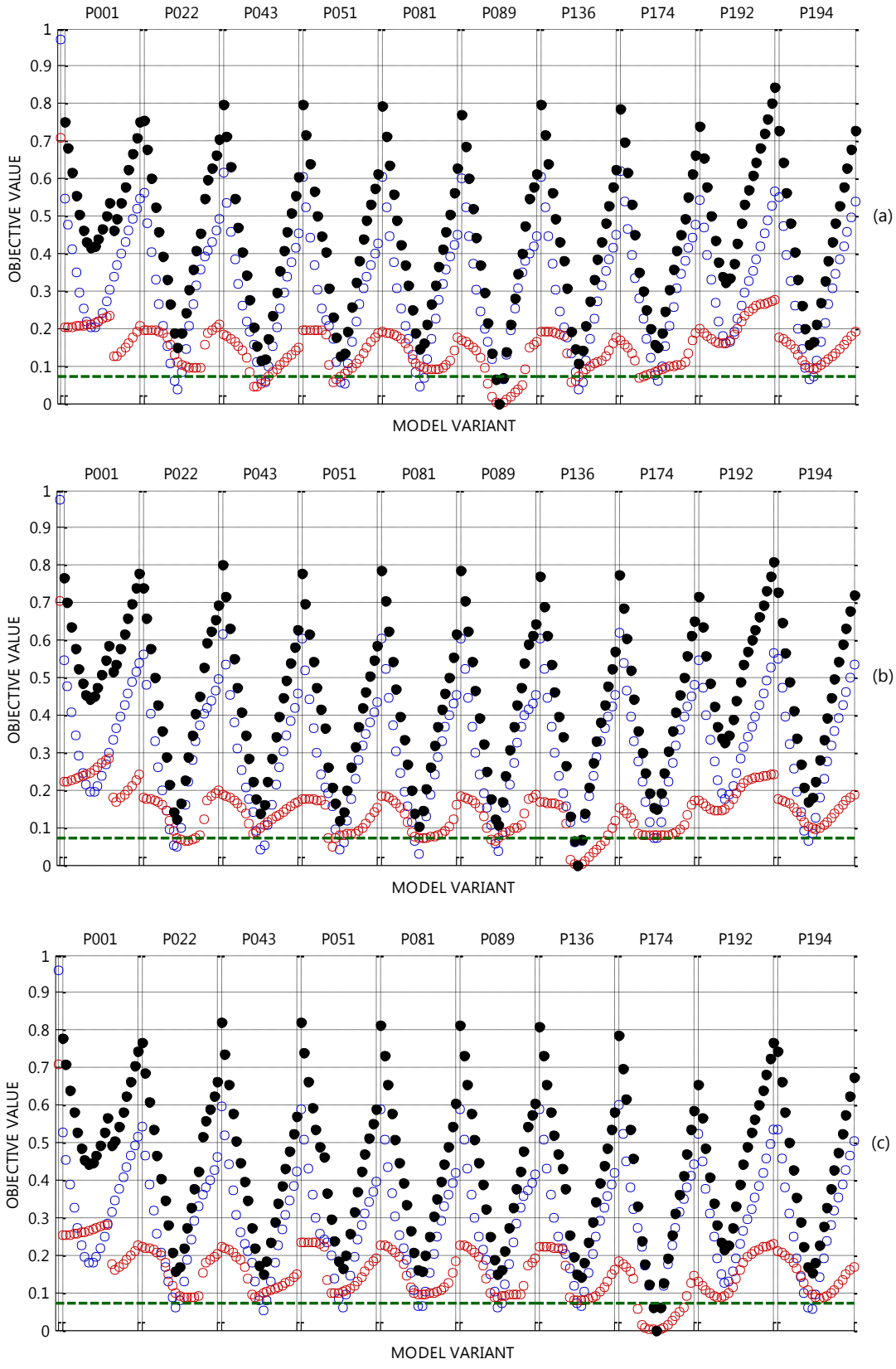

Figure 49: Objective values; (a) SIM-[P089] versus the intended design (FEM-ID) and its 21 variations at all slave structures; (b) SIM-[P136] versus FEM-ID and its 21 variations at all slave structures; (c) SIM-[P174] versus FEM-ID and its 21 variations at all slave structures; Location of resonating slave structure is indicated by minima for all three objective functions;
Legend: wJ_1 (blue), J_2 (red), J (black), R (dashed green)

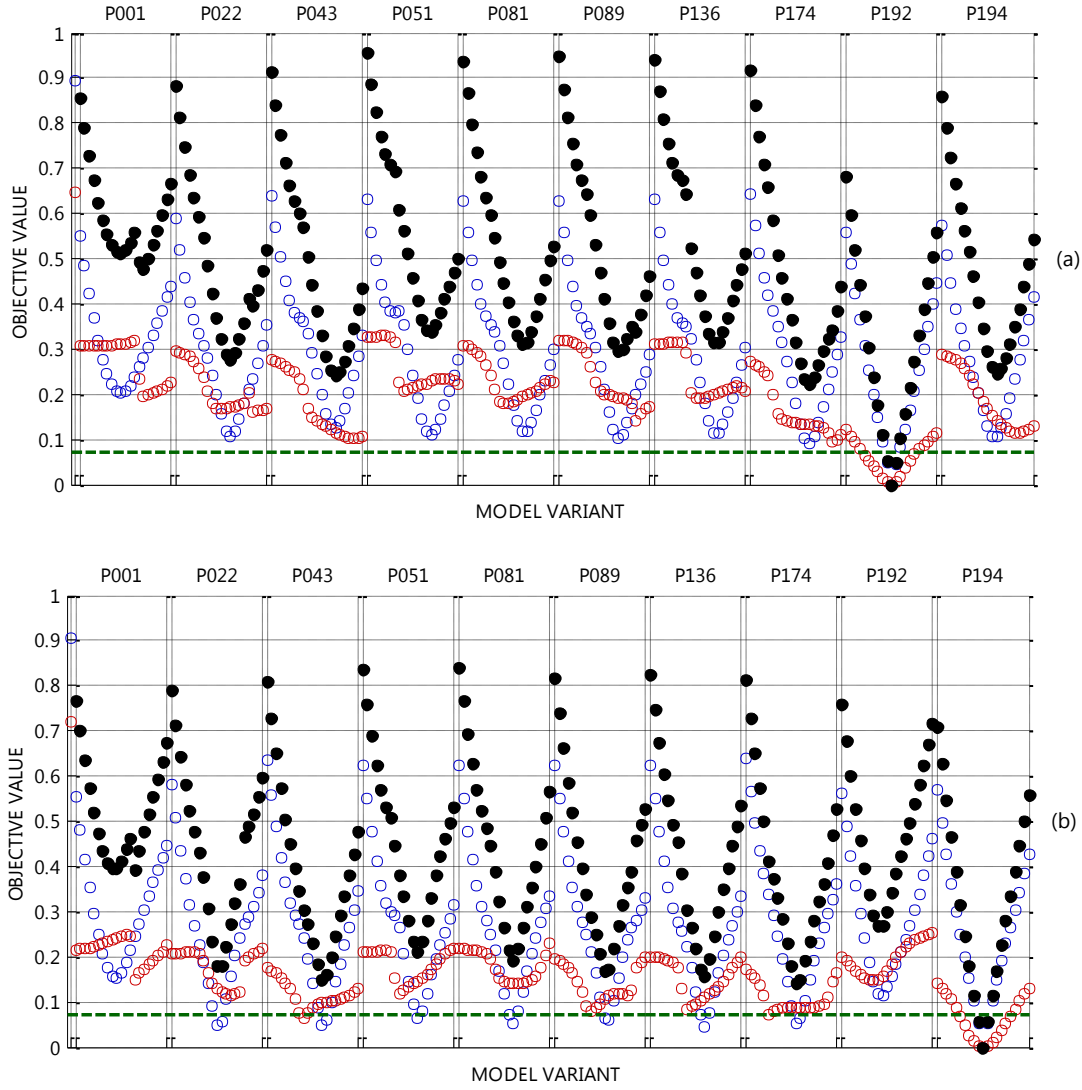

Figure 50: Objective values; (a) SIM-[P192] versus the intended design (FEM-ID) and its 21 variations at all slave structures; (b) SIM-[P194] versus FEM-ID and its 21 variations at all slave structures; Location of resonating slave structure is indicated by minima for all three objective functions;
Legend: wJ_1 (blue), J_2 (red), J (black), R (dashed green)

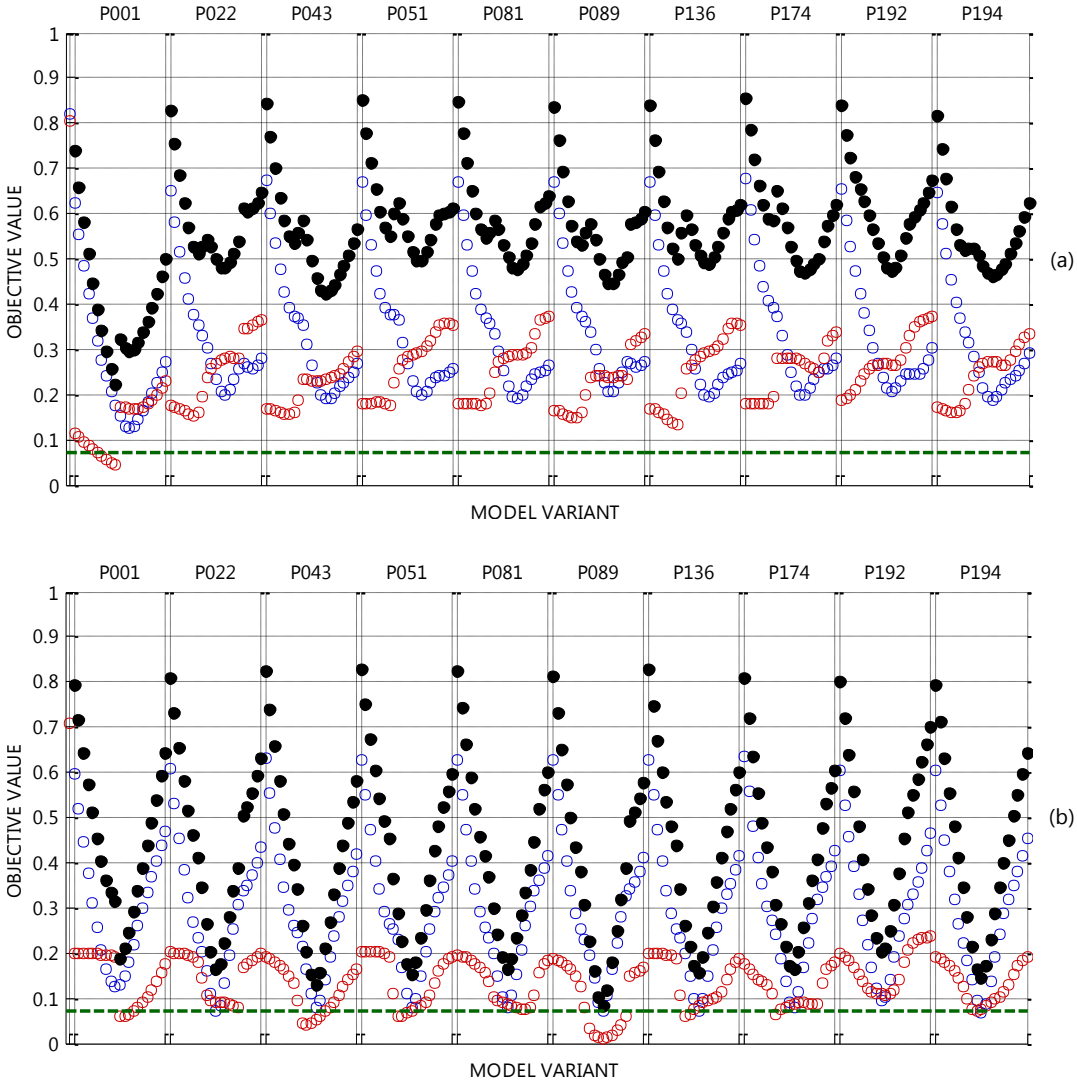

Figure 51: Objective values; (a) experimental model configuration I (EXP-I) versus the intended design with wrong sprung mass assumed (FEM-ID_{wm}) and its 21 variations at all slave structures; (b) EXP-II versus FEM-ID_{wm} and its 21 variations at all slave structures; Location of resonating slave structure is indicated by minima for all three objective functions;
Legend: wJ_1 (blue), J_2 (red), J (black), R (dashed green)

6 REFERENCES

[1] J.E. Mottershead and M.I. Friswell, "Model Updating in Structural Dynamics: A Survey," *Journal of Sound and Vibration,* vol. 2, no. 167, pp. 347-375, 1993.

[2] D.J. Ewins, Modal Testing: Theory, Practice and Application, Research Studies Pre, 2000.

[3] O. Døssing, "Structural Testing Part I: Mechanical Mobility Measurements," Brüel and Kjær, 1988.

[4] O. Døssing, "Structural Testing Part II: Modal Analysis and Simulation," Brüel and Kjær, 1988.

[5] D.J. Ewins and M. Imregun, "On the Reliability of Computational Dynamic Response Prediction Capabilities," *Journal of the Society of Environmental Engineers,* vol. 27, no. 116, 1988.

[6] N.M.M. Maia, "Construction of Models from Tests," in *Encyclopedia of Vibration*, 2001, pp. 824-829.

[7] B.J. Schwarz and M.H. Richardson, "Experimental Modal Analysis," Vibrant Technology, Inc., Jamestown, California, 1999.

[8] *Experimental Modal Analysis,* Brüel and Kjær, 2003.

[9] T.G. Carne and E.C. Stasiunas, *Leassons Learned in Modal Testing Part III: Transient Excitation for Modal Testing, More Than Just Hammer Impacts,* Society for Experimental Mechanics, 2006.

[10] D. de Klerk, D.J. Rixen and S.N. Voormeeren, "General Framework for Dynamic Substructuring: History, Review and Classification of Techniques," *AIAA Journal,* vol. 46, no. 5, pp. 1169-1181, 2008.

[11] C. Papadimitriou and D.C. Papadioti, "Component mode synthesis techniques for finite element model updating," *Elsevier,* 2012.

[12] R.R. Craig Jr. and M.C.C. Bampton, "Coupling of Substructures for Dynamic Analysis," *AIAA Journal,* vol. 6, no. 7, 1968.

[13] E.L. Blades and R.R. Craig Jr., "A Craig-Bampton Test-Analysis Model," in *IMAC 15: International Modal Analysis Conference*, 1997.

[14] P.L.C. van der Valk, "Model reduction and Interface Modelling in Dynamic Substructuring," 2010.

[15] M. Giorelli, "Methodology for Correlating Experimental and Finite Element Modal Analysis on Valve Trains," 2002.

[16] M. Rades, Mechanical Vibrations II: Structural Dynamic Modeling, Editura Printech, 2010.

[17] R. Allemang and D. Brown, "A Correlation Coeffcient for Modal Vector Analysis," in *International Modal Analysis Conference*, 1982.

[18] M. Radeş, "Displays of Vibration Properties," in *Encyclopedia of Vibration*, 2001, pp. 413-431.

[19] M. Radeş, "Comparison of Modal Properties," in *Encyclopedia of Vibration*, 2001, pp. 265-272.

[20] R.J. Allemang, "The Modal Assurance Criterion (MAC): Twenty Years of Use and Abuse," in *IMAC 20: Internationsl Modal Analysis Conference*, 2002.

[21] D. Fotch and D.J. Ewins, "Application of MAC in the Frequency Domain," in *IMAC 18: International Modal Anlysis Conference*, 2000.

[22] N.A. Lieven and D.J. Ewins, "Spatial Correlation of Mode Shapes, the Coordinate Modal Assurance Criterion (COMAC)," *Proceedings of the International Modal Analysis Conference,* vol. 6, pp. 690-695, 1998.

[23] R. Pascual, J.C. Golinval and M. Razeto, "A Frequency Domain Correlation Technique for Model Correlation and Updating," in *IMAC 15: International Modal Analysis Conference*, 1997.

[24] R. Pascual, J.C. Golinval and M. Razeto, "Testing of FRF Based Model Updating Methods Using a General Finite Elements Program," *International Seminar on Modal Analysis,* vol. 21, 1996.

[25] W. Heylen and P. Avitabile, "Correlation Considerations - Part 5," *Proceedings of the International Modal Analysis Conference,* vol. 16, pp. 207-214, 1998.

[26] Henning Grafe, "Model Updating of Large Structural Dynamics Models Using Measured Response Functions," Department of Mechanical Engineering, London, 1998.

[27] E. Dascotte, "Model Updating for Structural Dynamics: Past, Present and Future Outlook," in *International Conference on Engineering Dynamics (ICED)*, 2007.

[28] R.D. Blevins, Formulas for Natural Frequency and Mode Shape, Malabar, Florida: Krieger Publishing Company, 2001.

[29] "http://www.aerospacemetals.com," ASM Aerospace Specification Metals, Inc., [Online]. Available: http://asm.matweb.com/search/SpecificMaterial.asp?bassnum=MA7075T6.

[30] "http://www.aerospacemetals.com," ASM Aerospace Specification Metals, Inc., [Online]. Available: http://asm.matweb.com/search/SpecificMaterial.asp?bassnum=MQ304A.

[31] T.G. Carne, D.T. Griffith an M.E. Casias, "Support Conditions for Free Boundary-Condition Modal Testing," in *IMAC 15: Conference & Exposition on Structural Dynamics* , 2007.